NAVAL POSTGRADUATE SCHOOL

MONTEREY, CALIFORNIA

THESIS

FAILURE OF COMPOSITE PLATES SUBJECTED TO SHOCK LOADING

by

Natalie E. Crow

December 2020

Thesis Advisor:	Young W. Kwon
Second Reader:	Jarema M. Didoszak

THIS PAGE INTENTIONALLY LEFT BLANK

REPORT DOCUMENTATION PAGE	*Form Approved OMB No. 0704-0188*

1. AGENCY USE ONLY *(Leave blank)*	**2. REPORT DATE** December 2020	**3. REPORT TYPE AND DATES COVERED** Master's thesis

4. TITLE AND SUBTITLE FAILURE OF COMPOSITE PLATES SUBJECTED TO SHOCK LOADING	**5. FUNDING NUMBERS** RMP10
6. AUTHOR(S) Natalie E. Crow	
7. PERFORMING ORGANIZATION NAME(S) AND ADDRESS(ES) Naval Postgraduate School Monterey, CA 93943-5000	**8. PERFORMING ORGANIZATION REPORT NUMBER**
9. SPONSORING / MONITORING AGENCY NAME(S) AND ADDRESS(ES) ONR, Washington, DC	**10. SPONSORING / MONITORING AGENCY REPORT NUMBER**

11. SUPPLEMENTARY NOTES The views expressed in this thesis are those of the author and do not reflect the official policy or position of the Department of Defense or the U.S. Government.

12a. DISTRIBUTION / AVAILABILITY STATEMENT Approved for public release. Distribution is unlimited.	**12b. DISTRIBUTION CODE** A

13. ABSTRACT (maximum 200 words)

Underwater explosions and their associated devastating effects are not new to the U.S. Navy. Accurately modeling and scaling them for research and development, however, are areas in need of further study as large explosions are not easily created, accurately repeated, or financially prudent. Smaller models that produce underwater shocks on a reduced scale can mimic the effects of a larger explosive device. This project employed a safe and easily replicated test using liquid nitrogen within a sealed pressure vessel to create an underwater explosion. This test was performed multiple times using the same pressure vessel to produce a baseline explosion. Once a standard was created, the experiment was repeated in close vicinity with strain gages attached to carbon composite plates. Carbon composite plates of varying thicknesses, such as an orthotropic 0/90-degree weave, a unidirectional 0-degree, a cross-ply 0/90/0-degree, and a cross-ply 0/90/90/0-degree laminated plate, were examined. The explosion experiments on the carbon composite material were taken to failure to understand the dynamic response of those composite plates.

14. SUBJECT TERMS composite structure, underwater explosion	**15. NUMBER OF PAGES** 165
	16. PRICE CODE

17. SECURITY CLASSIFICATION OF REPORT	**18. SECURITY CLASSIFICATION OF THIS PAGE**	**19. SECURITY CLASSIFICATION OF ABSTRACT**	**20. LIMITATION OF ABSTRACT**
Unclassified	Unclassified	Unclassified	UU

NSN 7540-01-280-5500 Standard Form 298 (Rev. 2-89) Prescribed by ANSI Std. 239-18

THIS PAGE INTENTIONALLY LEFT BLANK

Approved for public release. Distribution is unlimited.

FAILURE OF COMPOSITE PLATES SUBJECTED TO SHOCK LOADING

Natalie E. Crow
Lieutenant, United States Navy
BS, U.S. Naval Academy, 2013

Submitted in partial fulfillment of the
requirements for the degree of

MASTER OF SCIENCE IN MECHANICAL ENGINEERING

from the

NAVAL POSTGRADUATE SCHOOL
December 2020

Approved by: Young W. Kwon
Advisor

Jarema M. Didoszak
Second Reader

Garth V. Hobson
Chair, Department of Mechanical and Aerospace Engineering

THIS PAGE INTENTIONALLY LEFT BLANK

ABSTRACT

Underwater explosions and their associated devastating effects are not new to the U.S. Navy. Accurately modeling and scaling them for research and development, however, are areas in need of further study as large explosions are not easily created, accurately repeated, or financially prudent. Smaller models that produce underwater shocks on a reduced scale can mimic the effects of a larger explosive device. This project employed a safe and easily replicated test using liquid nitrogen within a sealed pressure vessel to create an underwater explosion. This test was performed multiple times using the same pressure vessel to produce a baseline explosion. Once a standard was created, the experiment was repeated in close vicinity with strain gages attached to carbon composite plates. Carbon composite plates of varying thicknesses, such as an orthotropic 0/90-degree weave, a unidirectional 0-degree, a cross-ply 0/90/0-degree, and a cross-ply 0/90/90/0-degree laminated plate, were examined. The explosion experiments on the carbon composite material were taken to failure to understand the dynamic response of those composite plates.

THIS PAGE INTENTIONALLY LEFT BLANK

TABLE OF CONTENTS

LIST OF FIGURES

THIS PAGE INTENTIONALLY LEFT BLANK

LIST OF TABLES

LIST OF ACRONYMS AND ABBREVIATIONS

DAQ	Data acquisition system
DOD	Department of Defense
FEM	Finite element method
Hz	Hertz
IED	Improvised explosive device
m	Meter
NI	National Instrument
NAVFAC	Naval Facilities Engineering Command
Pa	Pascal
USN	United States Navy

THIS PAGE INTENTIONALLY LEFT BLANK

ACKNOWLEDGMENTS

I would like to thank my thesis advisor, Dr. Young Kwon, for your mentorship and assistance throughout my graduate studies. I would also like to extend my sincere thanks to my second reader, Dr. Jake Didoszak. Any time I hit a stumbling block, you went above and beyond to help me overcome it. Additionally, I would like to thank the team, including Mr. John Mobley and Dr. Chanman Park, that assisted with my rig design and sample preparation.

Lastly, I would like to thank my wife, Carmen Crow, and our son, Carter, for their constant support throughout my graduate studies and thesis research. All my success is attributed to their love and encouragement to pursue my career. Words cannot describe how thankful I am to have you as my family and source of strength.

THIS PAGE INTENTIONALLY LEFT BLANK

I. INTRODUCTION

A. BACKGROUND NAVAL APPLICATION

Extreme loading events, including non-contact underwater explosions, mines, missiles, torpedoes, improvised explosive devices (IED), are an area of high priority research within the United States Navy (USN) due to the being a sizeable threat such events pose to the Naval Surface Fleet [1]. Within the ship building process, hull components, topside equipment, and integrated systems are subject to in-depth testing to verify and certify survivability; one of the major areas of testing for these systems are shock testing trials. The majority of these verification tests are large scale and requiring long preparation times. The experiments themselves are also destructive in nature and result in an inefficiency of one time use parts. Furthermore, the cost of performing these events when using explosive devices to replicate an extreme loading event is extremely high. The ultimate goal of mechanical shock design testing and certification of a ship is to retain a fighting ship [2]. Laboratory tests have changed little over the years. Due to their physical size and weight, many components are only able to be shock designed rather than shock tested [2]. Operational analyses call for further development within the USN and Department of Defense (DOD) of small-scale tests to determine survivability of, not only the ship's hull, but smaller integrated components where internal failure has not historically been measured during full scale shock testing. This operational analysis creates an opportunity to test a multitude of material types utilized in hull design as well as those utilized for minor components. It also allows for testing that will model the failure of these various materials and components under explosive stress.

The USN and DOD are increasingly utilizing composite materials in superstructures, piping, ducting, rudders, propellers, stacks, and ship masts of naval ships [3]. Composite materials have been utilized in aircraft applications for significantly longer than the inception within the USN fleet of ships [4]. Many challenges occur with naval ships that are unique to water vessels and thus not of concern when contemplating materials used to construct aircraft. The material selection of components is dependent on the corrosive marine environment, stressed formed from wave action or an explosive event,

biological fouling, maintenance and repair requirements, cost, manufacturing and machining ease, as well as many other considerations. The ability to manufacture and assemble composites in different sheets and formations allows for the ability to tailor the desired engineering properties [5]. This makes composite research essential for the USN future fleet and for the DOD in order to maintain technological dominance over worldwide adversaries. Numerous types of composites exist with the most common being carbon, silicon carbide, and glass; for this research carbon fiber composites will be the focus.

B. COMPOSITE MATERIAL PROPERTIES

Carbon fiber composites are formed in various sub-categories of designs. The two that will be the focus of this research are a weave formation and a layering method. The specific layering method utilized here combined a varying number of unidirectional sheet plates by stacking them on top of each other to create a crosshatch orientation of the unidirectional pattern. The mechanical properties of strength and rigidity of a carbon fiber component are created by positioning fibers in a specific way in order to maximize effect [6]. The subject carbon material is formed by bonding carbon atoms into a continuous chain. The benefits of such a carbon fiber produced desirable engineering properties to include strength, lightness, and stiffness in material in tension and compression [5]. These properties are beneficial across the numerous applications required of such materials in the naval fleet.

Traditionally, many structural naval applications utilize metal materials due to its relatively low cost in conjunction with its high strength and damage resistance [7]. Stiffness is computed by measuring the modulus of elasticity of a material. Carbon fiber has a modulus of 228 GPa and an ultimate tensile strength of 3.5 GPa [8]. These values both exceed those of commonly used structural metals such as steel and aluminum. In major structural applications, the strength to weight ratio has a substantial impact on material selection. Major benefits, including longer material or system life and signification cost savings, occur from keeping structural weight low while maintaining a high compression and tensile strength. Also, maintaining a low structural weight without losing strength allows for increased weapons loadouts and potential system upgrades. Carbon fiber has a

density almost two times less than aluminum and five times less than steel [8]. Additionally, metals are formed in an isotropic uniform manner, ensuring equal properties in all directions. The benefit of carbon fiber is the ability to decide in advance which direction requires greater strength for the given application and provide this increased strength during the fabrication process.

C. OBJECTIVES

Due to the intense structural demands of naval ship applications, the composite structures must be able to survive harsh external loading conditions. One of the harshest of those conditions is under water explosion and/or implosion. The objective of this study is to understand and predict the failure point of composite structures when subject to underwater explosion(s). The goal of this experiment is to produce an easily replicable, small-scale explosive test to further understand the impact a minor explosion has on a specific subject material. This study will also allow material scientists and engineers to rapidly determine the legitimacy of future composites being considered as hull, structure, and overall shipboard applications.

The general approach of the study will be to begin with an explosion source produced from liquid nitrogen expanding in a closed bottle. This expansion of the liquid nitrogen will eventually detonate the closed bottle underwater, producing an explosion. Using only underwater pressure sensors and the explosion source, a consistent baseline will be determined by obtaining similar maximum pressure peaks from each subject explosion. Following the establishment of a baseline level of consistency, various carbon composite plate types will be tested with the explosion source detonating at different distances placed throughout the tank. The phase of the research in this section will first focus on placing the submerged carbon composite plate parallel to the water surface using a specifically engineered rig to maintain its position relative to the explosion. In the next phase, a second rig will be used to submerge the carbon composite plate perpendicular to the water surface. Comparisons will be made between the various types of carbon composite plates utilized throughout testing, as well as their subsequent failures. Varying the explosion distance from the plate will help to model anticipated failure from an experimental landscape. The

results of these experiments will allow for a better understanding of the utility and weaknesses of carbon composite materials applications when subject to various underwater explosions.

II. EXPERIMENTAL SETUP

A. ANECHOIC WATER TANK

An anechoic water chamber was utilized for all explosive experiments performed within this research. This tank is located at Watkins Hall Room 122A. It measures 2.40 meters in length by 2.40 meters in width and has a depth of 3.03 meters. It holds 1,4498.13 liters of liquid and was filled with tap water from Monterey County. Six aluminum I-beams stretch from side to side at a length of 4.56 meters. Each beam stands at a height of 0.21 meters and 0.21 meters wide. Five plywood platforms attach to the top of the steel beams providing tank coverage for ease of movement and safety. An opening measuring 0.6604 meters by 1.7526 meters was utilized for access and ease of testing. Safety metal chain and posts surround the entirety of the square tank. Figure 1 displays the described tank set-up.

Figure 1. Tank set-up

Figures 2 and 3 show the initial tank design schematics obtained from NAVFAC Monterey. The tank was built into the structure of the building and was attached by a slab of concrete flush with the floor within the laboratory. The tank design features redwood diagonally cut triangles protruding from the tank wall. This design element is shown in Figure 4. Behind the redwood triangle pieces is a cement plaster finish with 5 inches of gunite. Gunite is a mixture of water, sand, and cement with similar application to concrete. This material serves to account for the expansion and contraction of the tank during an explosion event. This feature is required for clear testing results and mimics an open ocean water comparison. The shape of the tank wall allows for wave propagation to almost completely dissipate without reflecting and/or combining, thus minimizing the effect of the reflective wave on the actual model.

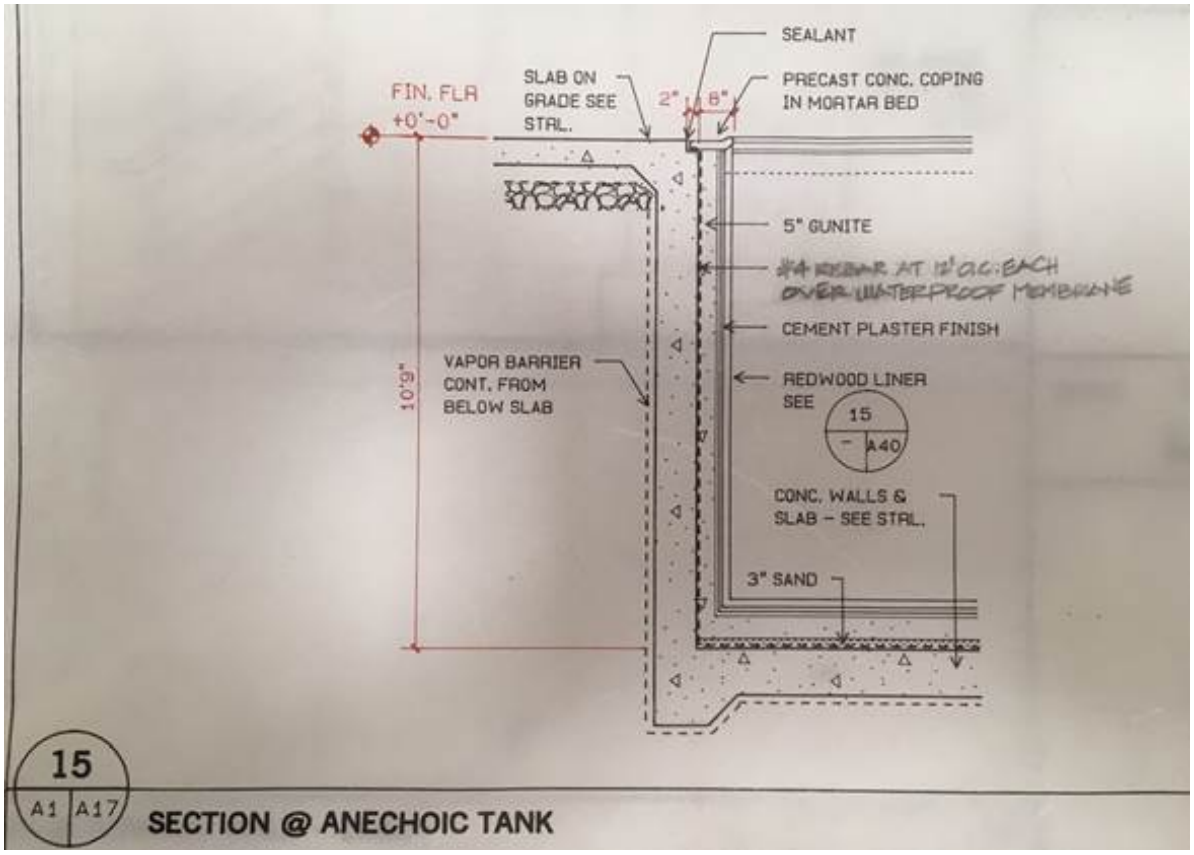

Figure 2. Anechoic tank 1

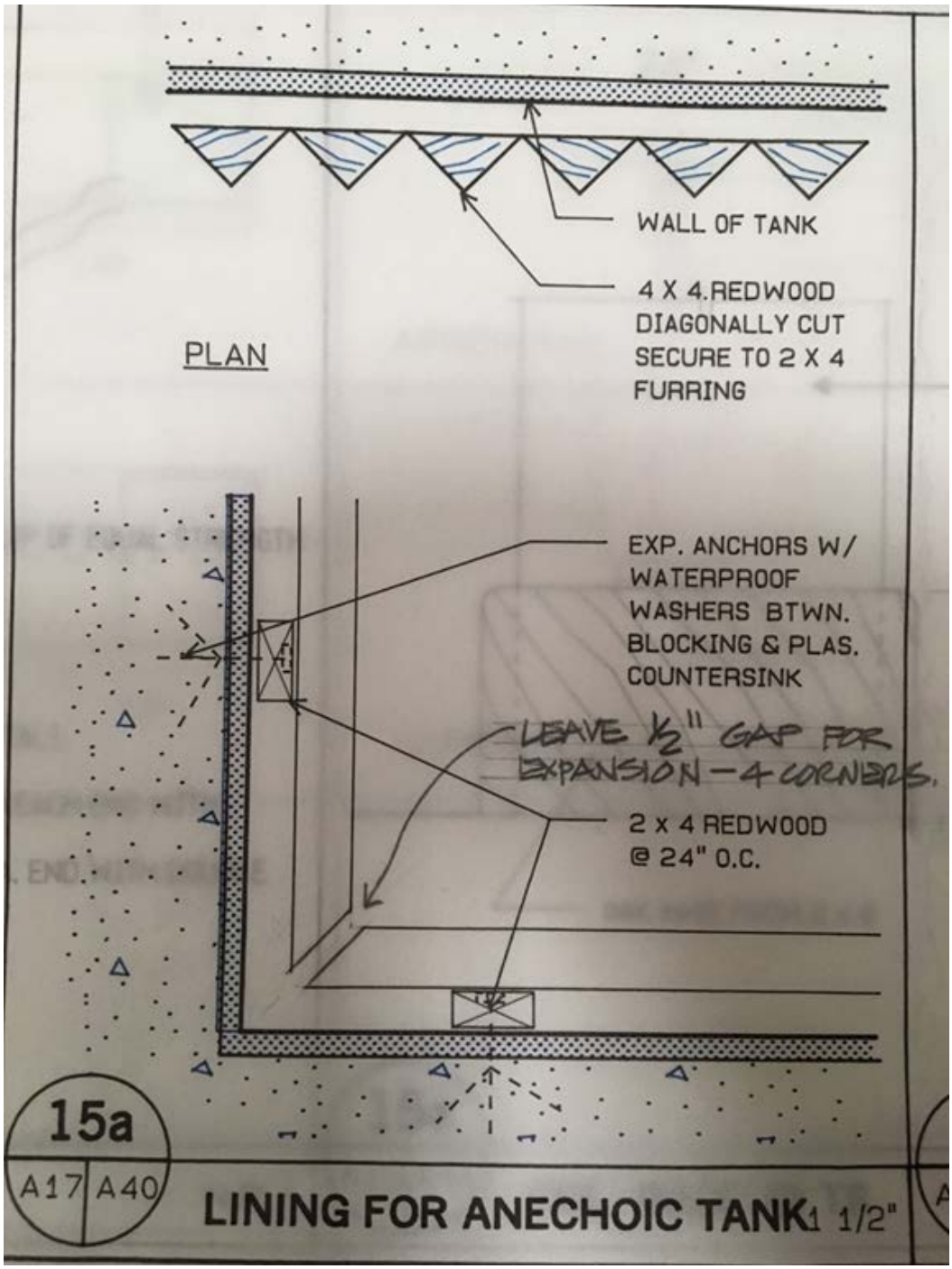

Figure 3. Anechoic tank 2

Figure 4. Non-reflective wall design

B. APPARATUS

1. Rig 1

Experiments within phase 2 utilized rig 1. As shown in Figure 5, the rig was designed to place the carbon composite plate horizontally and at a relatively shallow depth. This rig is composed of one square aluminum piece containing a T-slot. The T-slot allows the rig hardware to secure the connection between pieces. The rig was designed with a beam of sufficient length to make it stable when laid across the aluminum I-beams and plywood tank coverings. In addition, beam reinforcements were used at multiple points throughout the height of the rig in order to add another level of beam rigidity. This rig was designed using the program SolidWorks. The computer model is shown in Figure 6. The dimensions for this rig are shown in Table 1.

Figure 5. Overview rig 1

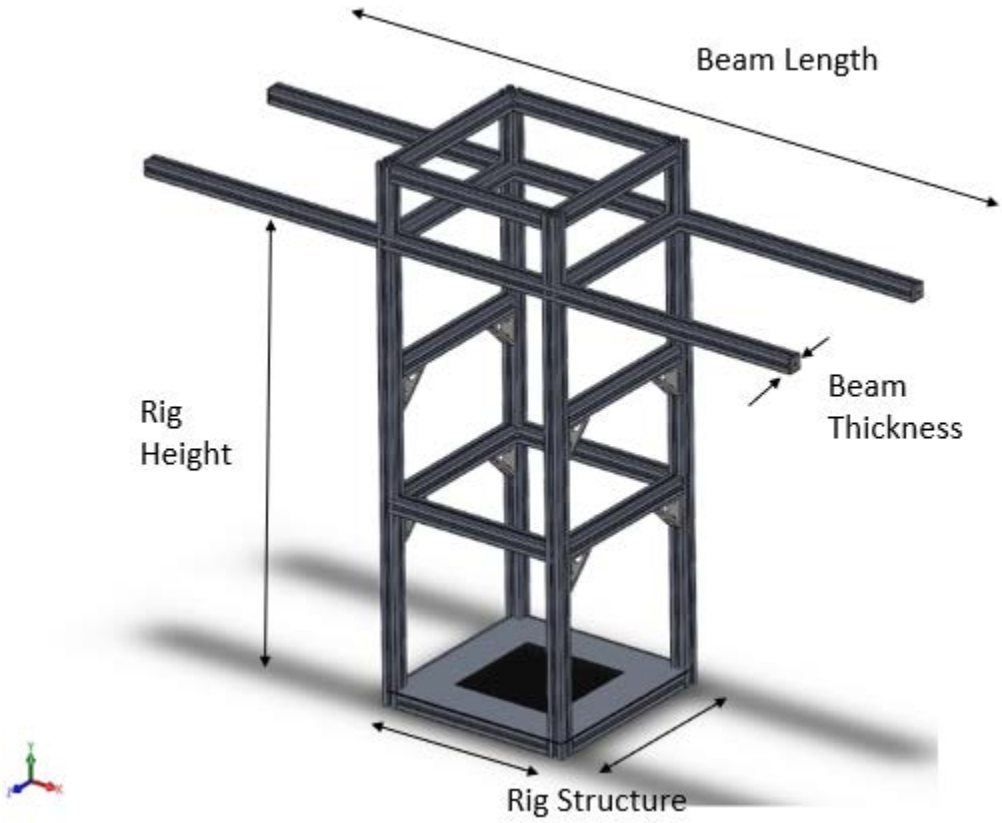

Figure 6. Rig 1 SolidWorks model

Table 1. Rig 1 dimensions

Beam Length	1.6764 meter
Rig Height	0.8763 meter
Rig Structure	0.4572 meter x 0.4752 meter
Beam Thickness	0.381 meter

The lower portion of the rig was designed to hold the 0.3048 meter by 0.3048 meter carbon composite plate flat and securely in place once the rig was submerged into the water chamber, as shown in Figure 7. Aluminum plates measuring 0.4572 meter by 0.4572 meter with a thickness of 0.0048 meter were used on either side of the black carbon composite with 0.0381 meter squares cut out in each corner of the plate to ensure a secure fit within the T-slot structural aluminum beams. These plates have a 0.254 meter by 0.254 meter square cut out in the middle portion of the plate. Two clamps were used on each side of the rig to maintain compression on the black carbon composite plate in order to ensure no movement occurs while underwater. The clamps were tightened to maximum torque with manmade force.

Figure 7. Rig 1 zoomed in

2. Rig 2

Experiment within phase 3 utilized rig 2. As shown in Figure 8, this rig was designed to place the carbon composite plate on its side at a deeper depth than rig 1 achieved. The rig is show upside down in the image used in Figure 8. The materials used in the construction of rig 2 were the same as used for rig 1. Similar to rig 1, rig 2 was also designed using the program SolidWorks. This computer model is shown in Figure 9. The dimensions for this rig are shown in Table 2.

Figure 8. Overview rig 2 (inverted)

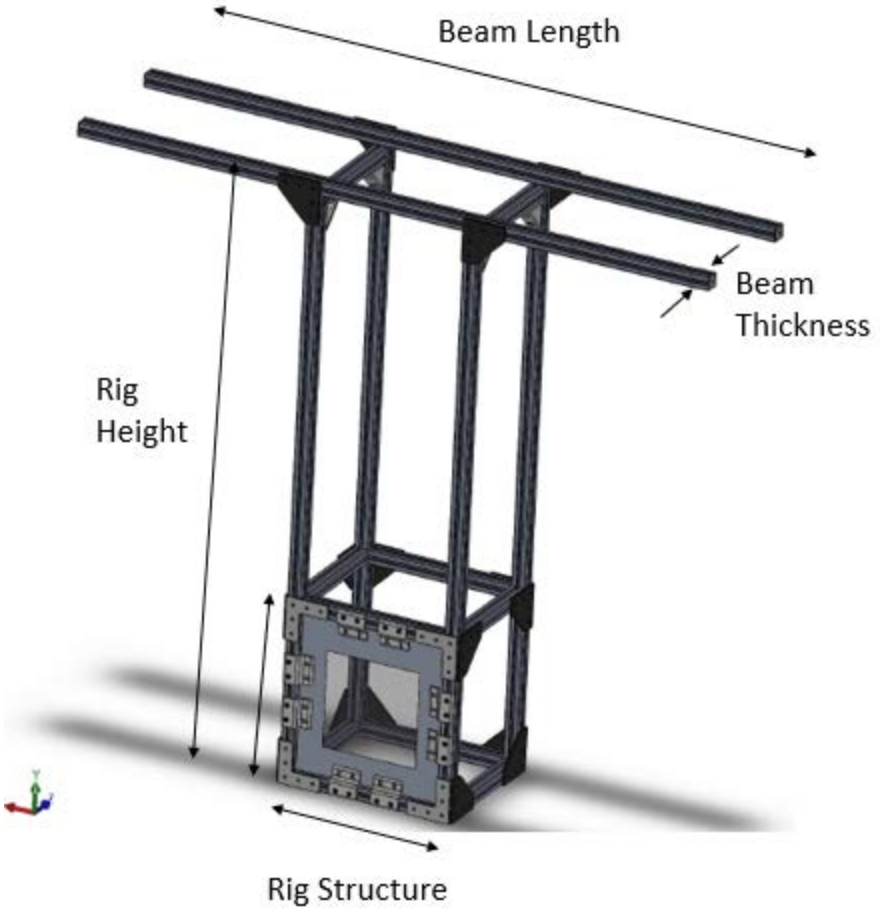

Figure 9. Rig 2 SolidWorks model

Table 2. Rig 2 dimensions

Beam Length	1.6764 meter
Rig Height	0.8763 meter
Rig Structure	0.4572 meter x 0.4752 meter
Beam Thickness	0.381 meter

The lower portion of rig 2 was designed to hold the 0.3048 meter by 0.3048 meter carbon composite plate in place on its side once the rig is submerged into the water chamber. One aluminum plate measuring 0.4572 meter by 0.4572 meter with a thickness

of 0.0048 meter was used on the front side of the black carbon composite. This plate had a 0.254 meter by 0.254 meter cut out in the center of the plate. Instead of using clamps to hold the carbon composite plate in place, fasteners were routed through the T-slots in order to place pressure on the front of the plate, as seen in Figure 10. These holds were flush with the aluminum frame. Figure 11 shows how an alternate type of fastener was used to secure the back of the carbon composite plate. Four individual pieces of aluminum were utilized to compress the composite plate, rather than the one piece of aluminum frame that was used on the front side of the rig. All clamps were tightened to maximum torque with manmade force.

Figure 10. Rig 2 front view

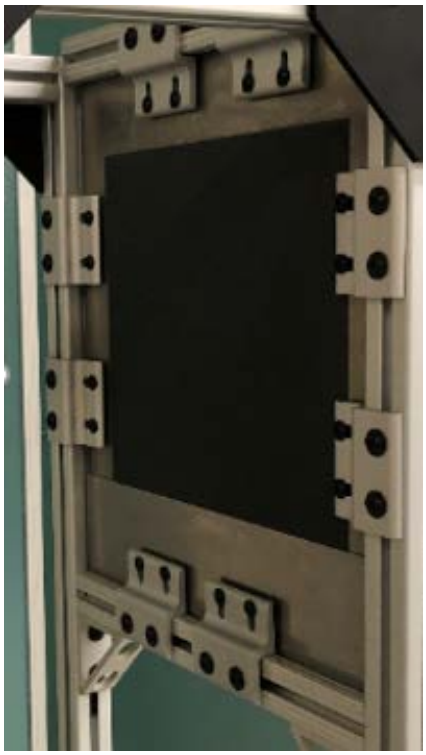

Figure 11. Rig 2 back view

C. SENSORS

1. Pressure

All experiments utilized the PCB Tourmaline underwater blast pressure series 138 pressure sensor set up into different configurations, as pictured in Figure 12. The sensor measured shock wave pressures associated with underwater explosive testing [9] and used a suspended tourmaline crystal that is volumetrically sensitive. The sensor was sealed within a waterproof, oil-filled vinyl tube. This shock wave sensor was specially designed to operate underwater in adverse environments. It had an operating range of 0–6900 kPa. An 3.3528-meter-long sealed waterproof blue cable was used to connect this pressure sensor to the PCB signal conditioner model 482C, displayed in Figure 13. The signal conditioner can process up to four pressure sensors at a time. For all experiments, only two to three sensors were used at a time. The pressure sensor was placed within the anechoic water chamber tank prior to testing in order to allow the sensor to normalize to the underwater pressure of the tank before experimentation commenced.

Figure 12. Pressure sensor

Figure 13. Sensor signal conditioner

Three different methods were used to maintain the pressure sensor in place underwater. In phase 1, monofilament connected a weighted screw anchor to the pressure sensor to maintain the vertical position of the sensor and the desired height underwater. The blue sensor line was led through pre-drilled holes in the aluminum beams to maintain position laterally. In phase 2, the pressure sensors were guided along monofilament running between the protruding clamps on the rig to ensure lateral positioning. Again, the small weighted screw anchors were utilized. Lastly in phase 3, the pressure sensors were attached

to the physical rig with monofilament, allowing them to hang at the same height as the carbon composite plate. Weighted anchors on the bottom of the tank were not utilized in this variation of phase 3 pressure sensor operation.

2. Strain

The strain of the carbon composite plate was determined by attaching three set of strain gages to the plate in a vertical row, as seen in Figure 14. The three gages were centered vertically on the plate with equal space of 0.0635 meters separating each gage. This configuration was utilized for both phase 2 and phase 3 testing.

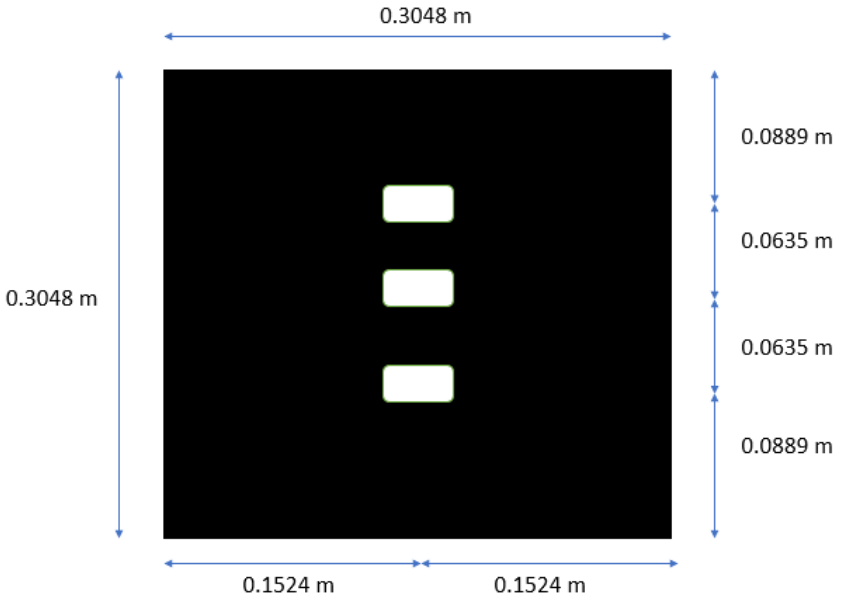

Figure 14. Strain gage set-up

Tee rosette strain gages were used in phase 2 testing to measure the strain in the x and y direction, totaling six channels and shown in Figure 15. Rosette strain gages shown in Figure 16, also measuring the x and y direction in six channels, were used in phase 3 testing. The middle portion of this rosette strain gage was not used in any experiments.

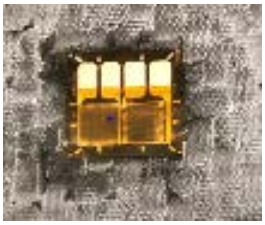

Figure 15. Tee rosette strain gage

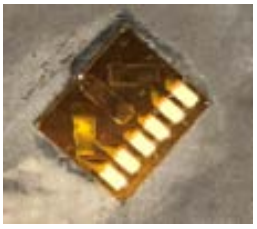

Figure 16. Rosette strain gage

Electrical wires connected to the strain gages on the plate were submerged underwater to the eight channel Wheatstone quarter bridge as shown in Figure 17. The quarter bridge was run through the Hewlett Packard 6214C power supply, shown in Figure 18, with an excitation voltage of 10 volts continuously applied throughout testing that utilized strain measurements.

Figure 17. Quarter-bridge module

Figure 18. Power supply

D. PLATE PREPARATION

Carbon fiber composite layup samples utilized for testing were supplied from the manufacturer Dragon Plate. For phase 2 of testing, an orthotropic laminate twill weave at a 0/90-degree orientation with a textured finish was used, as seen in Figure 19. This plate was fully comprised of a rigid and tough carbon reinforced epoxy matrix [6]. The plate measured 0.3048 meters by 0.3048 meters. Table 3 shows the two different variations of this plate used in phase 2 testing. The average thickness was determined by measuring two different points on each side of the plate utilizing digital calipers and then averaging those values together.

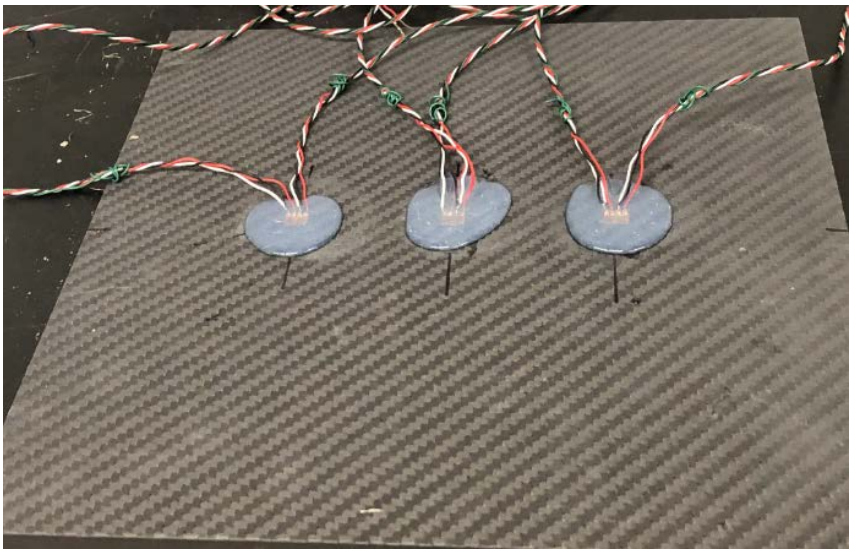

Figure 19. Phase 2 orthotropic plate

Table 3. Phase 2 sample types

Sample Number	**Type**	**Nominal Thickness**	**Average Measured Thickness**
Sample 1	0/90-degree orthotropic weave plate	6.35×10^{-4} m	7.4×10^{-4} m
Sample 2	0/90-degree orthotropic weave plate	1.5875×10^{-4} m	1.34×10^{-4} m

For phase 3 of testing, different variations of various samples were used as seen in Table 4. Sample 1 and 2 were a unidirectional 0-degree plate of 0.25 mm and 0.5 mm nominal thickness, respectively. The average thickness was determined by measuring two different points on each side of the plate and then averaging those values together. These carbon fiber laminates had a textured finish. Sample 3 used a cross-ply plate design that had alternating 0 and 90-degree plies with a thickness of 0.5 mm. Sample 4 also used a cross-ply design but with an additional sheet of 90-degree plie internally. The finish on sample 3 and 4 was also textured. As depicted in Figure 20, all phase 3 samples were much smoother in appearance than the phase 2 orthotropic woven plates.

Table 4. Phase 3 sample types

Sample Number	**Type**	**Nominal Thickness**	**Average Measured Thickness**
Sample 1	0-degree unidirectional plate	$2.5x10^{-4}$ m	$3.3x10^{-4}$ m
Sample 2	0-degree unidirectional plate	$5x10^{-4}$ m	$6.0x10^{-4}$ m
Sample 3	0/90/0-degree cross-ply plate	$5x10^{-4}$ m	$5x10^{-4}$ m
Sample 4	0/90/90/0-degree cross-ply plate	$5x10^{-4}$ m	$5.9x10^{-4}$ m

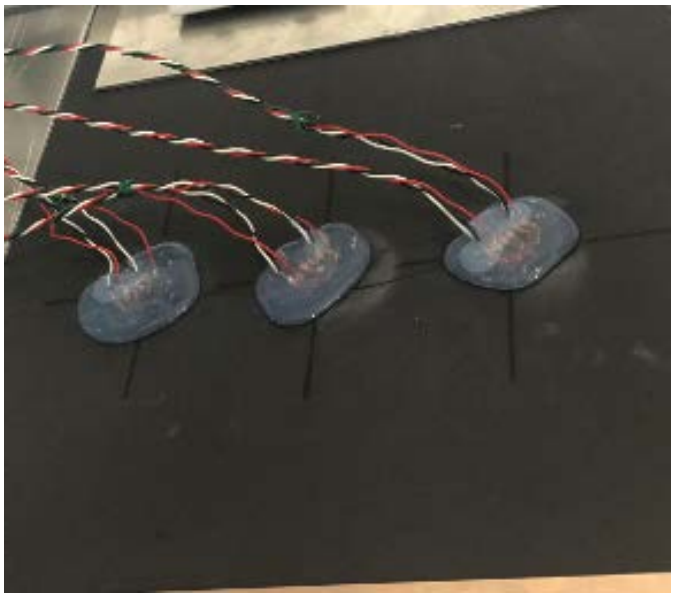

Figure 20. Phase 2 unidirectional plate

Three strain gages were added and centered on the plate. Plate preparation began by sanding down the three locations where the strain gages were attached. Upon sanding, the carbon composite plate samples were first cleaned by using acetone. Once dry, the plate was then cleaned with methanol. Following these steps, tweezers were used to lay the strain gages in the proper location of future attachment. Specialized installation tape was used to hold the strain gages in position and allow glue to be placed under the strain gage. A M-bond curing agent was added to M-bond adhesive resin in order to permanently attach the

strain gage to the carbon plate. Once the glue was placed under the strain gage, the gage and tape were left for 48 hours to complete the hardening and drying phase. After 48 hours, the tape was removed to leave the plate with strain gages secured. The result can be seen in Figure 21.

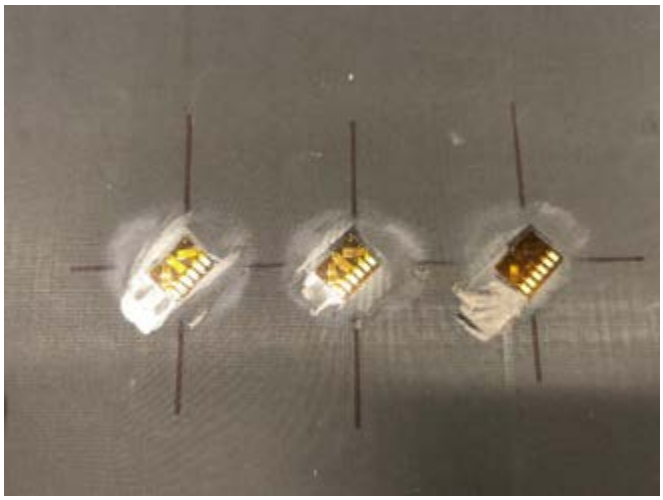

Figure 21. Strain gage attachment

The next step in plate preparation was attaching the proper electrical wires to the strain gage. Prior to attachment, all lead wires were stripped of insulation, twisted tightly together, and dipped in a gel flux. A soldering hot tip and solid wire were used to attach the twisted wire tip to the strain gage channel. Detailed attachment was required to ensure the attached wire did not touch the neighboring channel. All connections were visually inspected followed by a check of resistance to ground readings. The product can be seen in Figure 22.

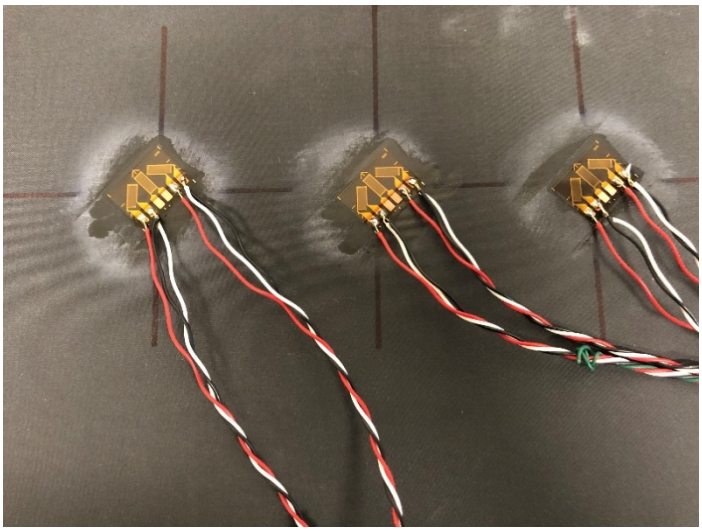

Figure 22. Wire attachment

The last step in plate preparation was waterproofing the insulation free wire and strain gage due to underwater testing. Dow Corning 3140 non-corrosive, flowable, room temperature curing silicon rubber was used as the waterproofing agent. All plates were cured for 48 hours to ensure proper hardening. The final plate with strain gage attachment and waterproofing complete is seen in previous Figures 19 and 20.

E. DATA ACQUISITION SYSTEM

The pressure and strain data were sent to the data acquisition (DAQ) system, which enabled a large amount of data to be processed at a high rate. The DAQ computer processor system utilized was the National Instrument (NI) PXIe-1071. The multifunction DAQ card NI PXIe-6358 was used to connect the pressure and strain signal analyzers. The NI MAX computer program was utilized to zero out the strain gage input channels. The NI Signal Express computer program was used to process and record that data. For the strain measurements, the gage factor and resistance were updated depending on the type of rosette strain gage used. The strain configuration was updated to reflect the quarter bridge set-up. The rate used for all testing was 1 kHz, with a sampling rate of 100 Hz. The rate is the speed of the acquiring signal, while the sampling rate is the number of samples taken. In selecting the appropriate testing rate, the sampling rate should be 1/10 of that value.

F. EXPLOSION SOURCE

The explosion for this experiment was created using liquid nitrogen expanding within a 20-fluid ounce Coca-Cola soda bottle. Due to the cloudy nature of the liquid nitrogen, explosions occurred at different intensities based on how much liquid nitrogen and subsequent air space was left within the bottle once enclosed. The liquid nitrogen reaction allowed for the capped closed bottle to reach its proper position underwater in the tank prior to rupturing. A yellow rope with an anchor chain at the bottom, tied to a hole in the aluminum I-beam, was used to maintain the proper setup for the position of the explosion within the tank, as shown in Figure 23. The rope had various notches that were properly measured to obtain the desired height for the given phase of testing. Monofilament wire was used to secure the soda bottle to the yellow rope utilizing a knot around the rope notch and a second knot around the upper third of the soda bottle, as seen in Figure 24. A piece of plexiglass was placed within the aluminum I-beams to help guide the anchor chain to the bottom of the tank and to ensure the position of the soda bottle did not shift right to left. This set-up can be seen in in Figure 25.

Figure 23. Yellow rope with anchor chain

Figure 24. Coca-Cola bottle attached with monofilament

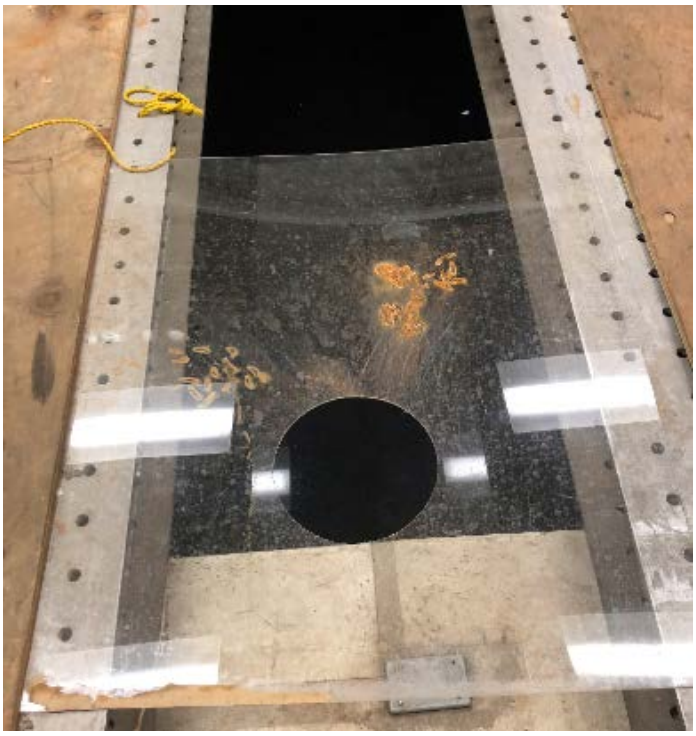

Figure 25. Plexiglass anchor guide

THIS PAGE INTENTIONALLY LEFT BLANK

III. PROCEDURE OVERVIEW

Three phases occurred during testing, each utilizing different procedures, equipment, and tank set-ups. The explosion source and pressure sensor height measurements varied for each phrase as well.

A. PHASE 1

For phase 1 testing, only the explosion source and three pressure sensors were used. This was the most simplistic and minimalist test. The purpose of this test was to create consistent testing conditions while utilizing similar amounts of liquid nitrogen in the Coca-Cola bottle and producing similar sized explosions to measure shock pressure shape and peak at three different locations.

As seen in Figure 26, the explosion and three pressure sensors were all equally spread throughout the tank, with each pressure sensor being placed incrementally further away from the explosion source. The pressure sensors were guided into place by utilizing the already existing holes in the aluminum I-beams in order to allow them to hang with a specific separation distance between each other as well as from the explosion. The explosion source was attached to the yellow rope with an anchor chain at the bottom of the rope and was then lowered through the plexiglass hole to maintain lateral position. This specific setup and execution encouraged uniform testing results.

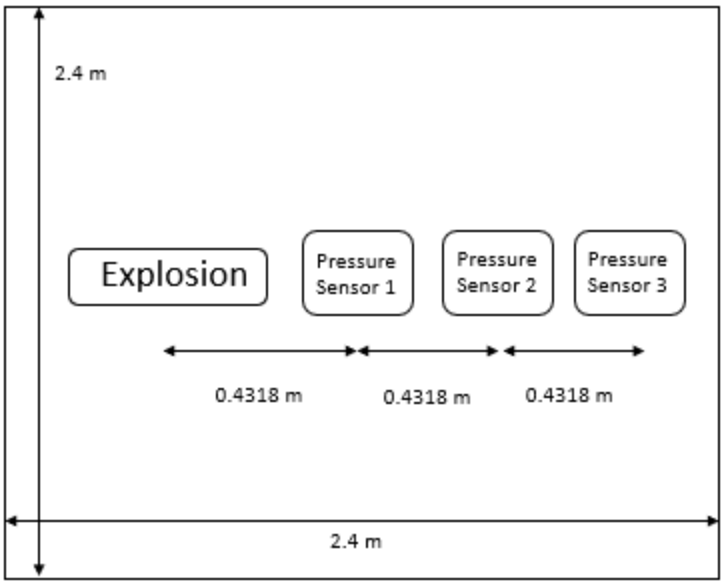

Figure 26. Phase 1 tank top view

As seen in Figure 27, phase 1 testing had all three pressure sensors, as well as the explosion source, suspended 0.6096 meter from the bottom of the tank. The waterline was established at 2.6416 meters for this portion of testing. This pressure sensor height was achieved by using a washer and screw weight attached to monofilament that was then attached to the tip of the pressure sensor. This allowed the pressure sensors to maintain an upright position while in the water, as well as suspending all pressure sensors at a uniform height within the tank. The explosion source height was maintained by attaching the Coca-Cola soda bottle to a pre-measured notch in the yellow rope using monofilament.

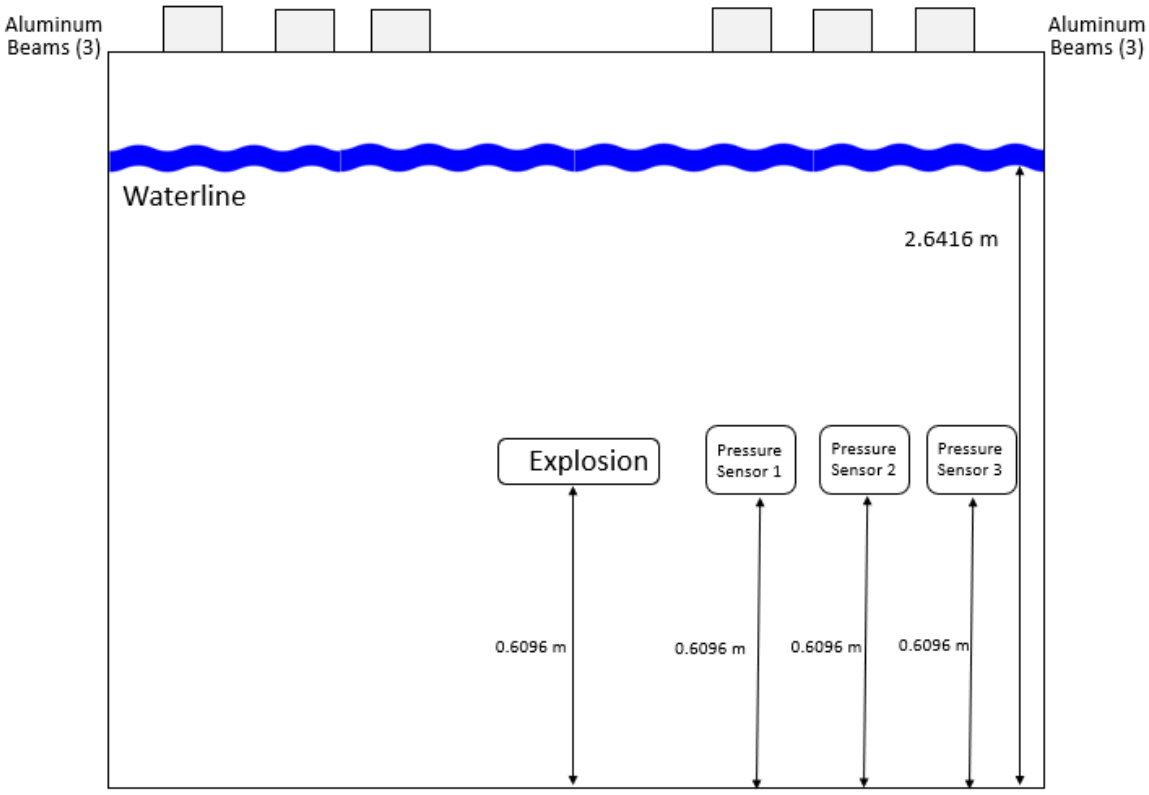

Figure 27. Phase 1 tank side view

Four tests were performed during phase 1 all using the same set-up and materials. The explosion intensity was regulated by attempting to achieve the same level of liquid nitrogen in each soda bottle prior to submerging the explosion source into the water tank. As visualization of this level was difficult to achieve, the valve on the liquid nitrogen tank was held fully open for a set amount of time in order to regulate the amount dispensed into each bottle.

B. PHASE 2

For phase 2 testing, the explosion source, three pressure sensors, and the shallow rig holding a carbon composite plate were used. This was the next step up in complexity from previous phase 1 testing. The purpose of this phase was to measure the impact of an explosion on the orthotropic laminate twill weave texture finished carbon composite plate

that lies on flat above the explosion. This plate had a 0/90-degree weave. The shallow rig previously discussed in Chapter 2, Section B of this paper, was utilized for all this phase.

As seen in Figure 28, the explosion occurred 0.3048 meters in front of the rig. Three pressure sensors were all equally spaced from the rig at 0.0508 meters. These sensors were set up on both sides of the rig, as well as on the far side of the rig, opposite of the explosion. The pressure sensors were guided into place by a channel created between the two clamps used to secure the plate and monofilament attaching to the clamps. Consistent with phase 1, the explosion source was attached to the yellow rope with an anchor chain at the bottom and was lowered through the plexiglass circular insert laid on the aluminum I-beams to maintain lateral position.

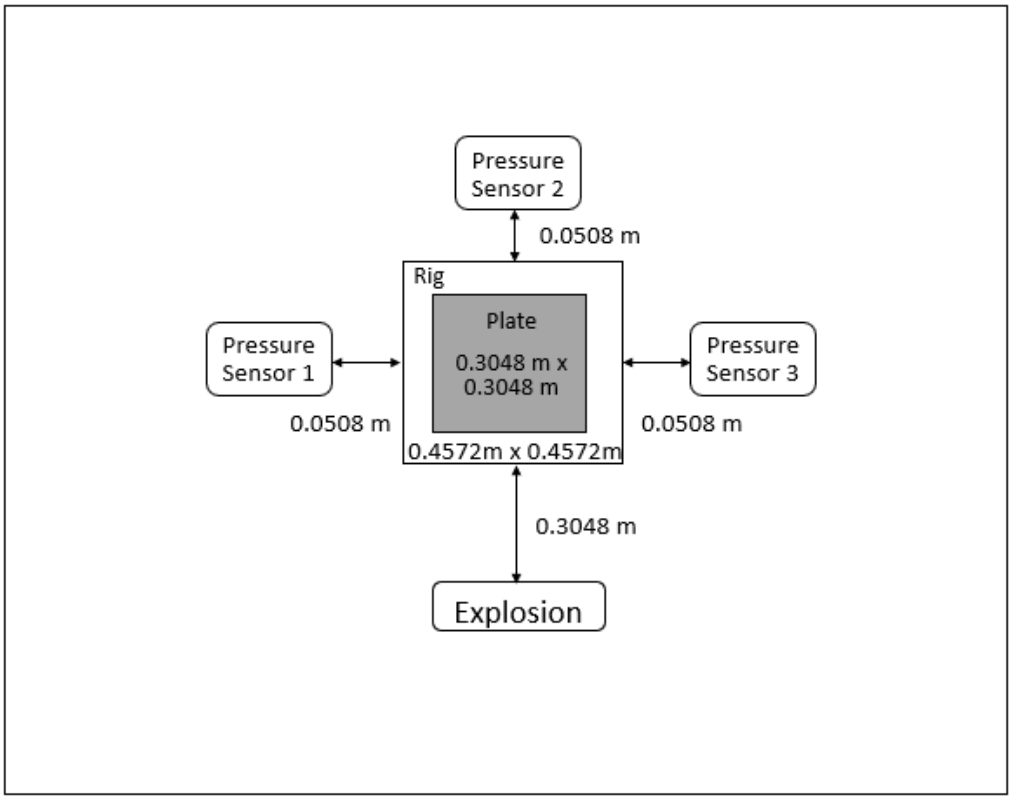

Figure 28. Phase 2 tank top view

As seen in Figure 29, phase 2 testing had all three pressure sensors suspended at the same height of 1.524 meters from the bottom of the tank. The explosion source occurred

at 1.143 meter from the bottom of the water tank. The waterline was established at 2.6416 meters for this entire portion of testing. This pressure sensor and explosion source height was achieved by the same method previously discussed in phase 1 procedure. The major difference in this set-up of phase 2 compared to phase 1 consisted of testing the explosion at a higher height in the tank. Also, rather than having the pressure sensors in a straight line in succession from the explosion, the configuration in phase 2 was changed to model and observe the pressure the plate is feeling upon pressure impact.

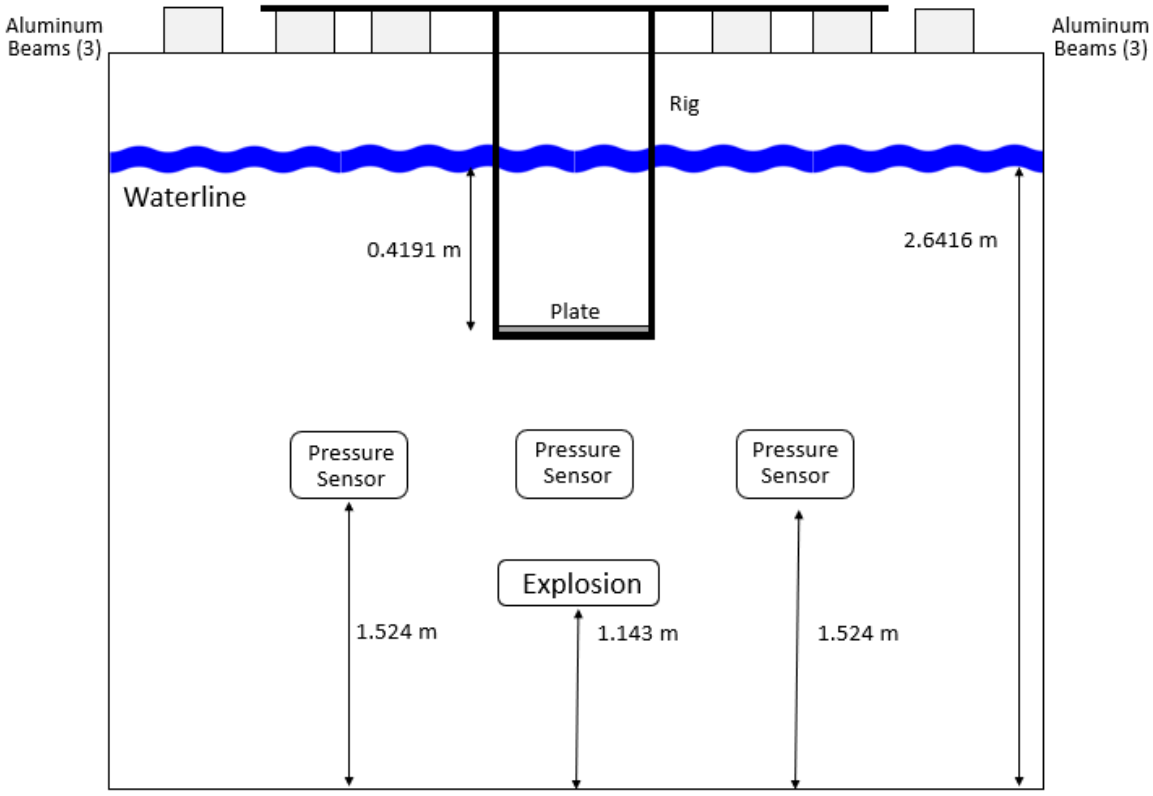

Figure 29. Phase 1 tank side view

Two samples of the orthotropic laminate twill carbon composite plate of different thickness were used for all of phase 2 testing. The thin sample measured at 2.5 x 10–^{3} meter nominal thickness. The thicker sample measured at 5 x 10–^{3} meter nominal thickness. The plate was suspended parallel with the floor surface of the tank. As shown in Figure 30, the three strain gages were arranged in a line from left to right. Because the explosion occurred

0.3048 meter from the rig laterally and under the rig vertically, the strain gages were positioned on the portion of the carbon composite plate where damage would be less likely.

Figure 30. Phase 2 rig underwater

The strain gage electrical wires were attached to the rig to route to the strain sensor equipment outside the tank, shown in Figure 31. The blue pressure sensor insulated wires were also routed vertically up the rig to the pressure sensor equipment located outside the tank. The rig used in this phase of testing was also very shallow so as to still be able to observe the rig and plate visually through the water when submerged.

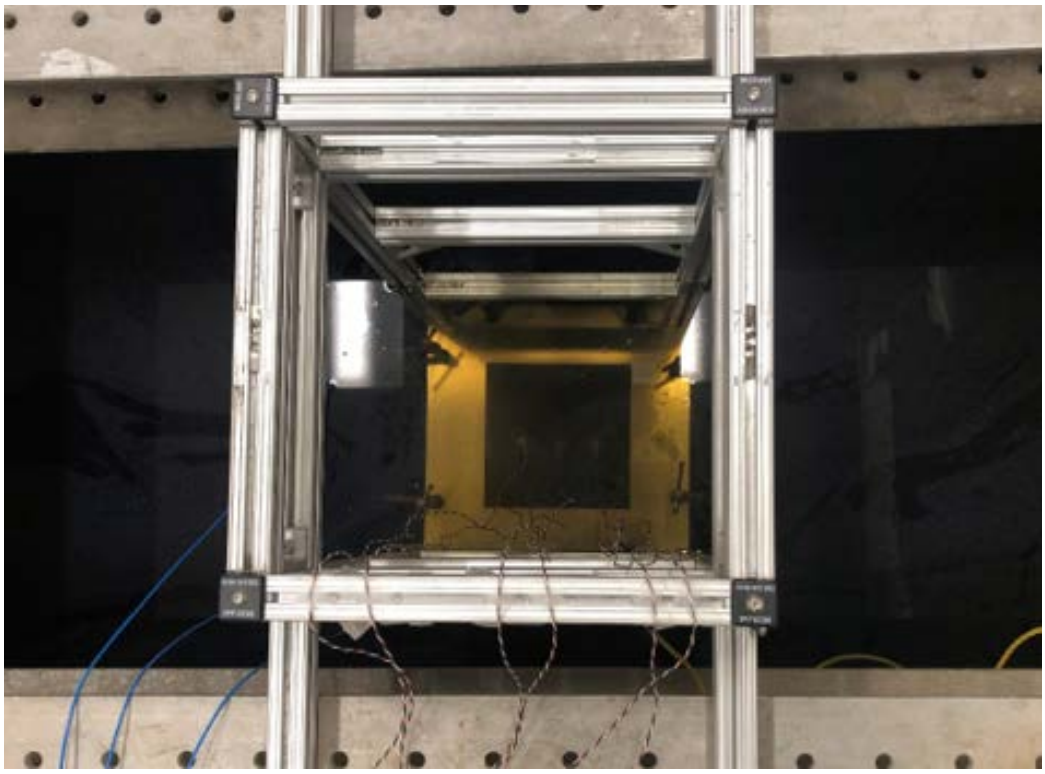

Figure 31. Phase 2 testing set-up

Six tests were performed on each of the two different thickness of plates used during phase 2, all using the same lateral and height measurement set-up. The explosion intensity was regulated using the same method as in phase 1 testing.

C. PHASE 3

For phase 3 testing, the explosion source, two pressure sensors, and the deep rig holding a carbon composite plate were used. The purpose of this phase was to measure the impact of an explosion on the laminate texture finished carbon composite plate while on its side and also while submerged deeper in the tank. This deep rig previously discussed in Chapter 2, Section B of this paper was utilized for all this phase.

For set-up number one of testing within this phase 3, as seen in Figure 32, the explosion occurred 0.3048 meters in front of the rig. Two pressure sensors were equally spaced from the rig at 0.3048 meters distance from the explosion. These sensors were set up on both the left and right sides of the rig. The pressure sensors were maintained in place

by using monofilament to attach the sensor directly to the rig, as shown in Figure 33. Consistent with phase 1, the explosion source was attached to the yellow rope with an anchor chain at the bottom and was lowered through the plexiglass circular insert laid on the aluminum I-beams to maintain lateral position. The two sensors and the plate formed an arc that all had the same radius from the explosion source. This test set-up was designed specifically to ensure the carbon composite plate on its side experienced the same pressure peak as the pressure sensor to the left and right of the rig. This test was performed on all four sample types. Each sample was taken to failure. The number of explosions required for each plate to reach failure varied depending on the type of sample.

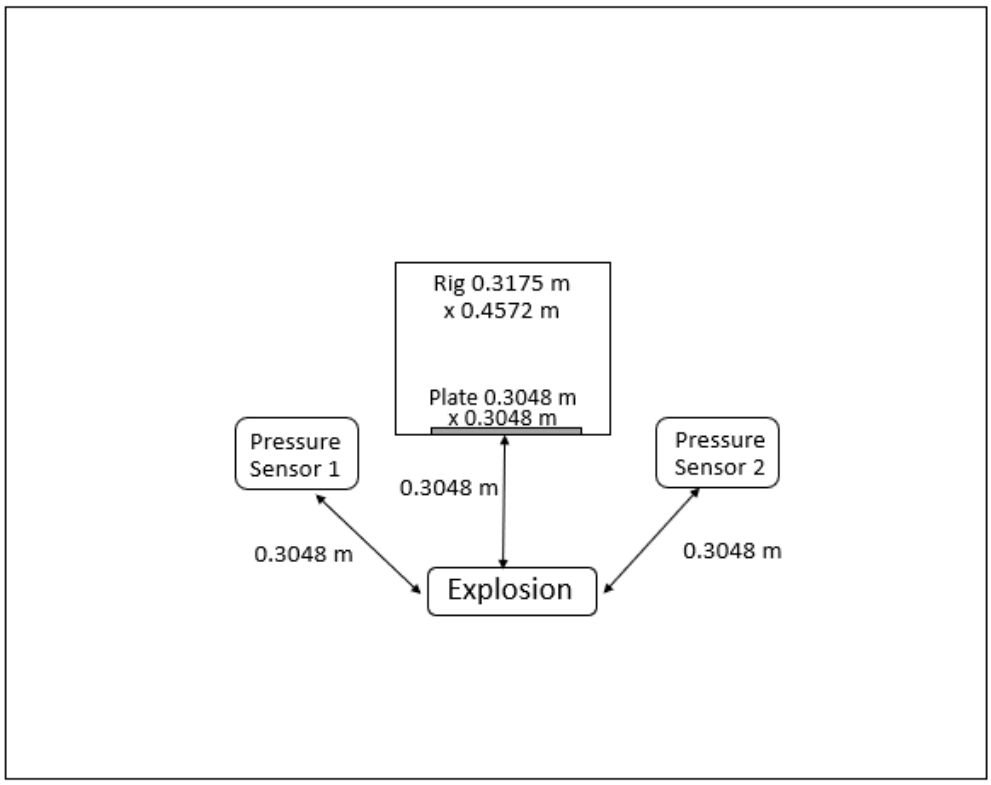

Figure 32. Phase 3 tank top view set-up 1

Figure 33. Pressure sensor placement

For set-up number two of testing within this phase 3, as seen in Figure 34, the explosion occurred 0.4572 meters in front of the rig. Two pressure sensors were equally spaced from the rig at 0.4572 meters distance from the explosion. This test set-up was identical to set-up number one except for shifting the explosion source and pressure sensors to a farther distance away from the plate—from 0.3048 meter to 0.4572 meter. This change was designed specifically to determine if the plates would reach failure at the same time as observed with the previous closer distance. Also, this variation was performed to show whether the failure would appear similar visually to the results achieved in set-up one. As with set-up one, this test was performed on all four sample types, with each sample again taken to failure. As in set-up 1, the four samples required a different number of explosions to fail.

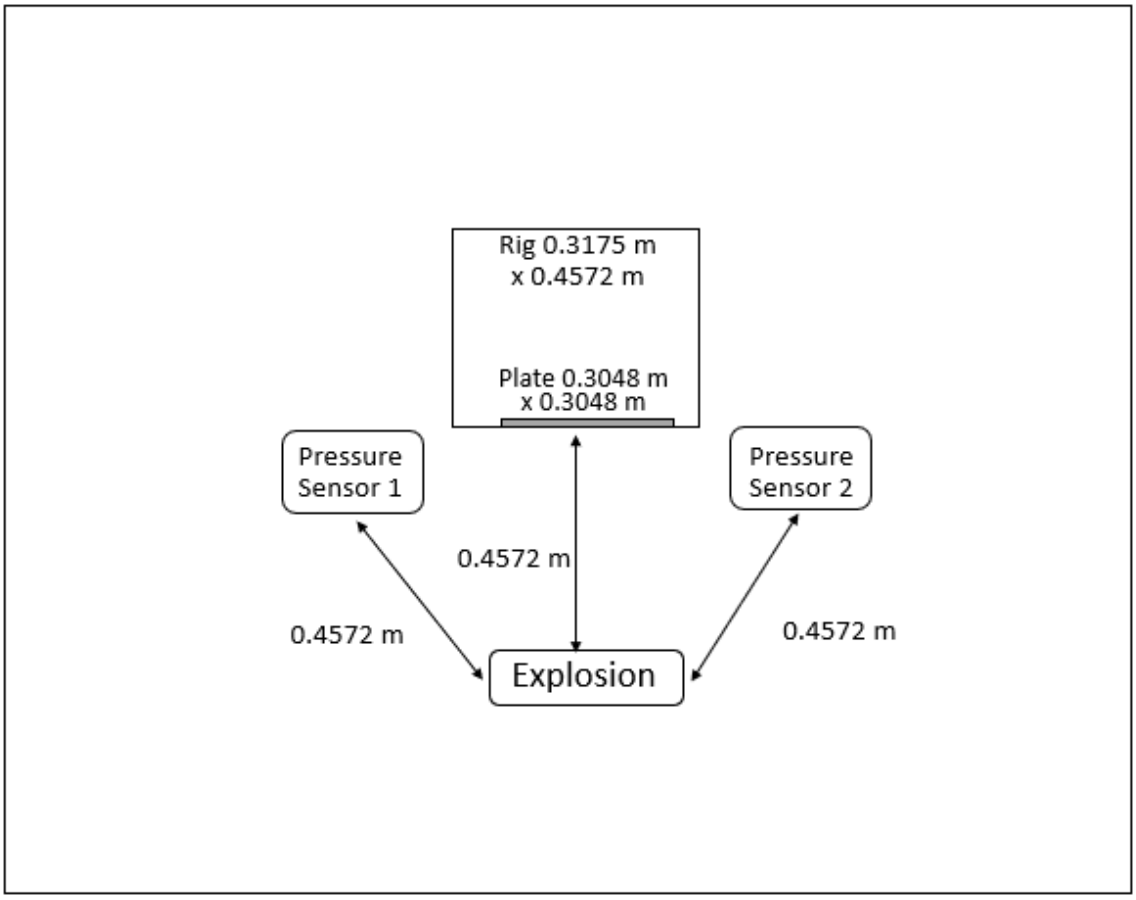

Figure 34. Phase 2 tank top view set-up 2

For samples 3 and 4, a third set-up was used which allowed for variance of the distance of the plate from samples 1 and 2. The third set-up was established having the explosion be 0.381 meters from the plate and from the two pressure sensors. This distance is between the two distances used for set-up 1 and 2 of 0.3048 meters and 0.4572 meters, respectively, and is show in Figure 35.

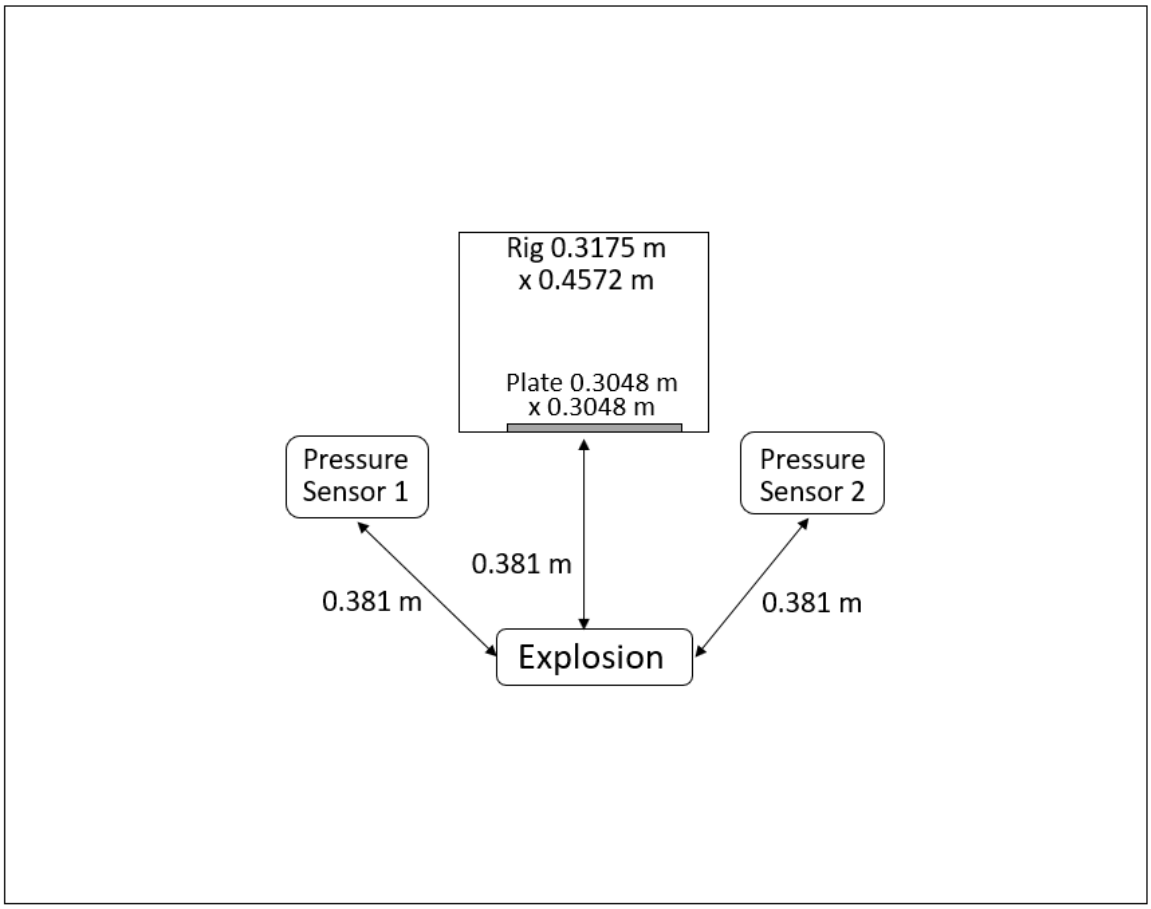

Figure 35. Phase 2 tank top view set-up 3

As seen in Figure 36, phase 3 testing had both pressure sensors, the explosion source, and the center of the carbon composite plate suspended at the same height of 1.778 meters from the bottom of the tank. The side view of the tank was the same for set-up one, two, and three. The waterline was established at 2.6416 meters for this entire portion of testing. The explosion source height was achieved by the same method previously discussed in phase 1 procedure. The major differences in this set-up of phase 3 compared to phase 2 includes the height of the sensors and explosion, the dept of the rig, the orientation of the plate on its side, utilization of four different types of samples, and connecting the pressure sensors directly to the rig.

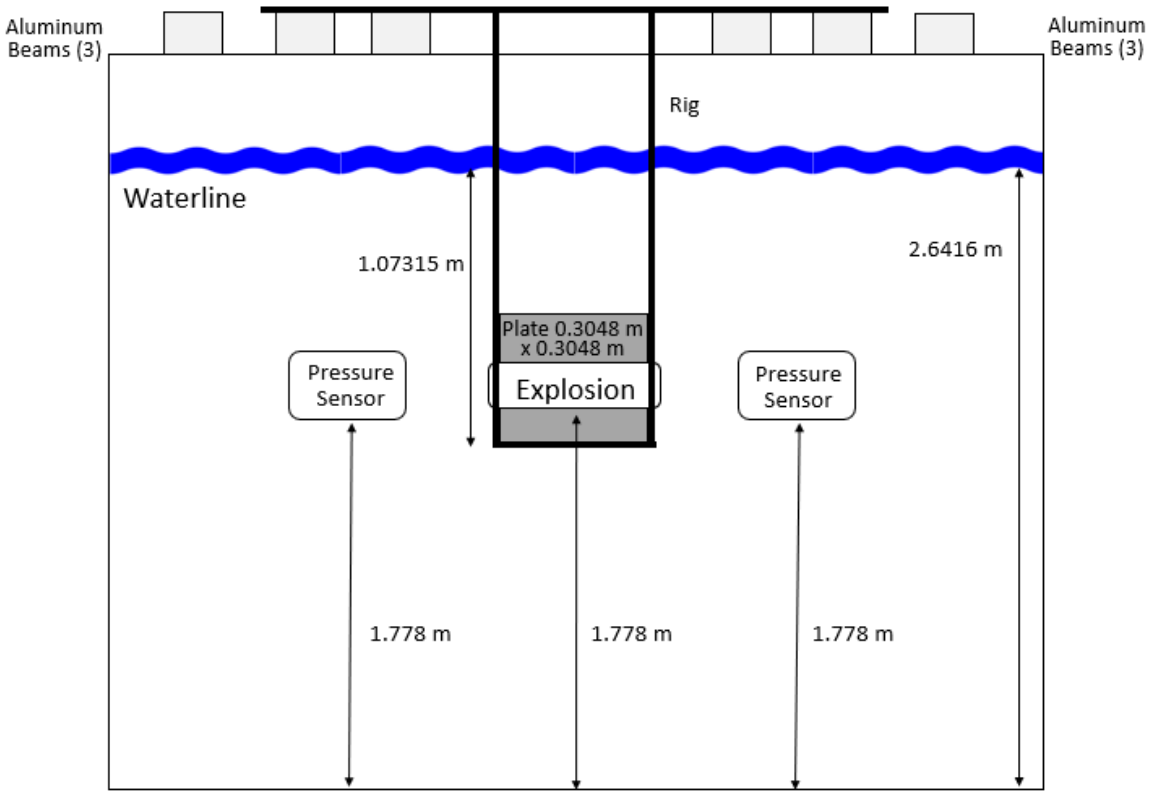

Figure 36. Phase 3 tank side view

The four samples of the laminate carbon composite plate are previously shown in Table 3. The major difference between sample 1 and 2 is the different thickness measuring at 2.5 x 10–^{3} meter nominal thickness and 5 x 10–^{3} meter nominal thickness. For phase 3 testing the plates were always oriented on their side. The three strain gages were arranged in a vertical line from the top of the plate to the bottom. Because the explosion occurred in front of the rig and at the same height, the strain gages were positioned on the back portion of the carbon composite plate where damage would be less likely.

IV. RESULTS AND DISCUSSION

A. PHASE 1 RESULTS

1. Experimental Results

Phase 1 tested the liquid nitrogen explosion by obtaining pressure sensor data from three different, horizontal positions from the same blast. For the purposes of this testing, an "explosion" is defined as a rapid release of energy resulting from a fast chemical reaction [10]. As displayed in Figures 37–40, in all four tests the liquid nitrogen explosions showed similar oscillation shapes. This is consistent with underwater explosion where bubbles of gas and vapor alternate expanding and collapsing [11]. This pattern of expansion and collapsing generates a train of acoustic pulses that propagates through the water, ultimately forming the exponential decay shape as displayed in these results.

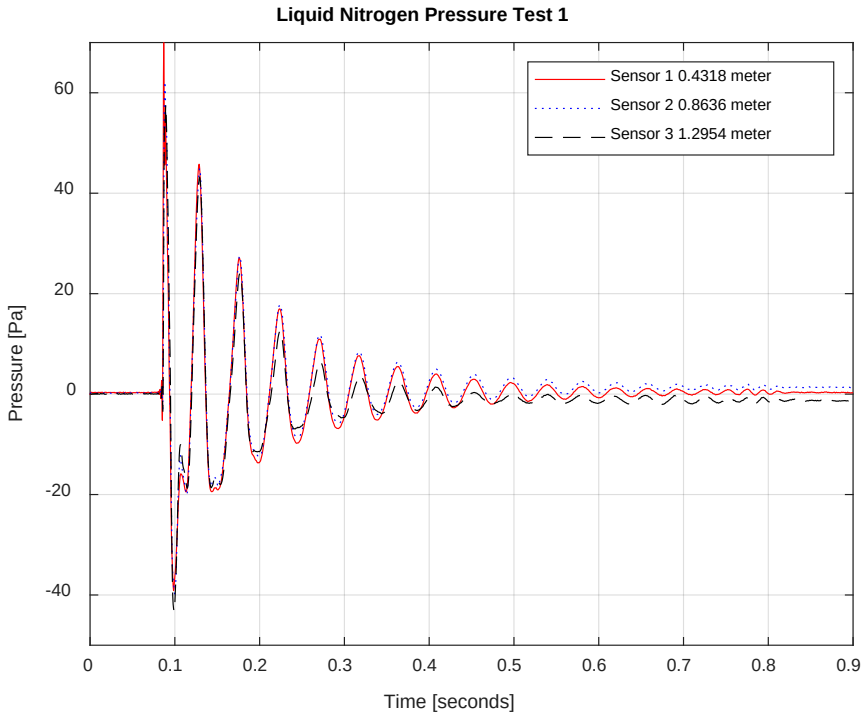

Figure 37. Test 1 liquid nitrogen

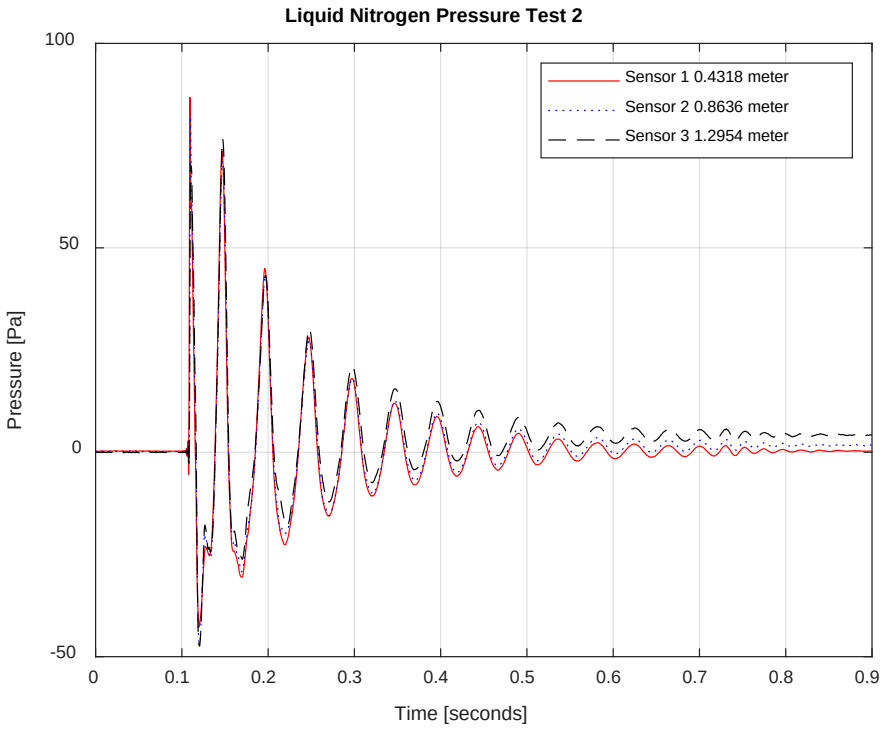

Figure 38. Test 2 liquid nitrogen

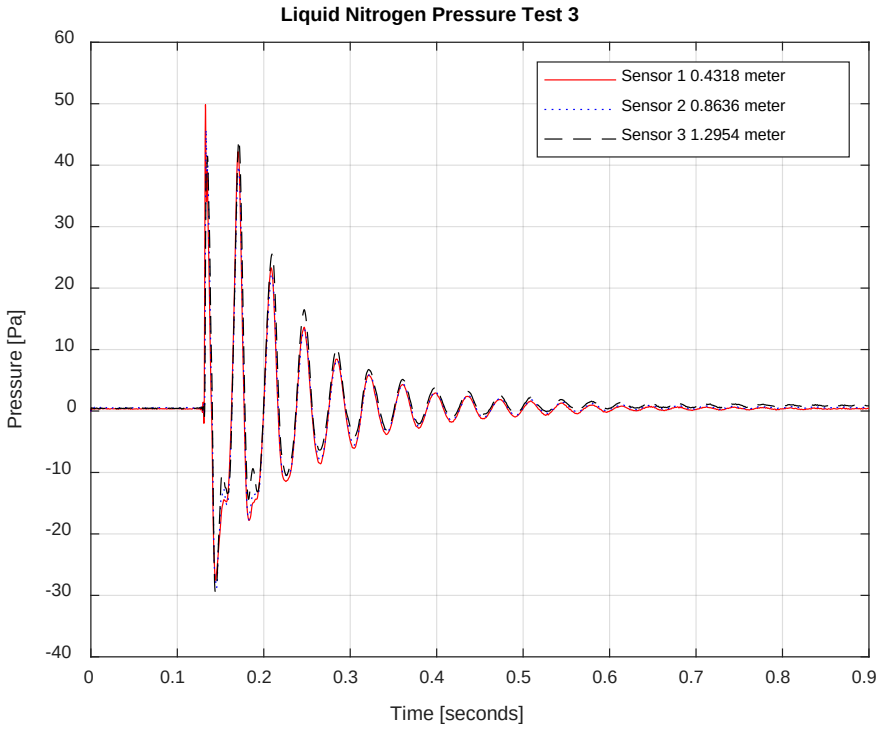

Figure 39. Test 3 liquid nitrogen

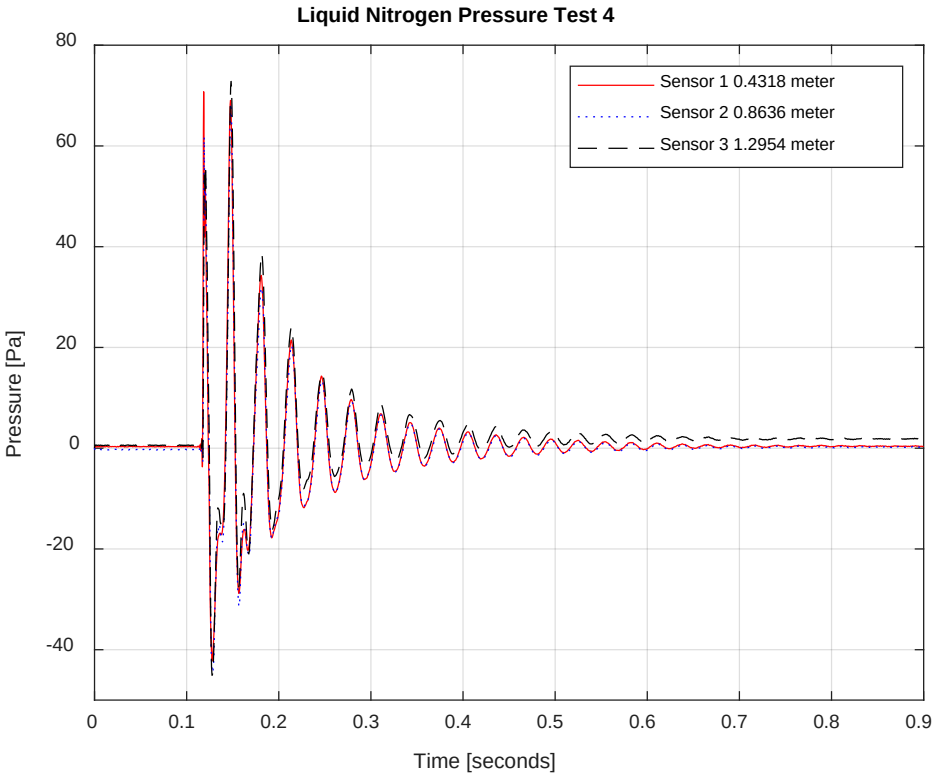

Figure 40. Test 4 liquid nitrogen

Table 5 illustrates the peak pressures as a function of distance. Figure 41 shows a graphical representation of the results. As would be expected, the sensor closest to the blast experienced the highest peak pressure and the pressure sensor farthest from the blast experienced the smallest peak pressure. While Figures 37–40 display what looks to be maximum pressures occurring simultaneously for all three pressure sensors, the peak pressures all occur slightly after each other due to the distance between each sensor. The explosion happens rapidly showing a subsequent exponential decay shape derived from the peak pressures. It is important to note that for this experiment, the explosion source and the three sensors were all in line horizontally as peak pressure is a function of not only radial standoff distance but depth of the explosion within the water column as well.

Table 5. Peak pressure

	Distance 1 0.4318 meters	**Distance 2 0.8636 meters**	**Distance 3 1.2954 meters**
Test 1	69.83 Pa	62.02 Pa	57.09 Pa
Test 2	86.75 Pa	82.10 Pa	70.42 Pa
Test 3	49.82 Pa	45.40 Pa	41.07 Pa
Test 4	70.83 Pa	61.68 Pa	56.17 Pa
Average	69.31 Pa	62.80 Pa	56.19 Pa
Standard Deviation	15.13	15.02	11.99

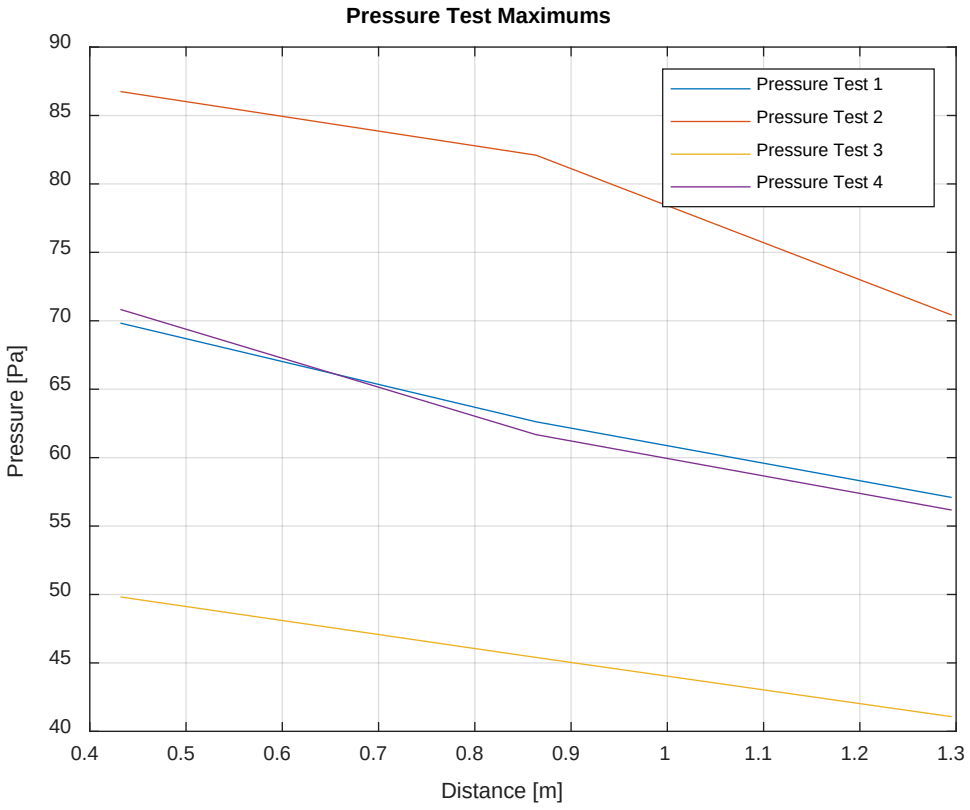

Figure 41. Pressure maximums at three distances

The average peak pressure of all four liquid nitrogen explosion tests was calculated at three distances: 0.4318 meter, 0.8636 meter, and 1.2954 meter. Figure 42 displays the results showing the inverse relationship between the average peak pressure and the distance of the sensor from the explosion source. A linear formulation was used in curve fitting these three points as displayed in Equation 1, where d is defined as the radial distance between the source and the sensor.

$$\text{Pressure} = -15\,d + 76 \tag{1}$$

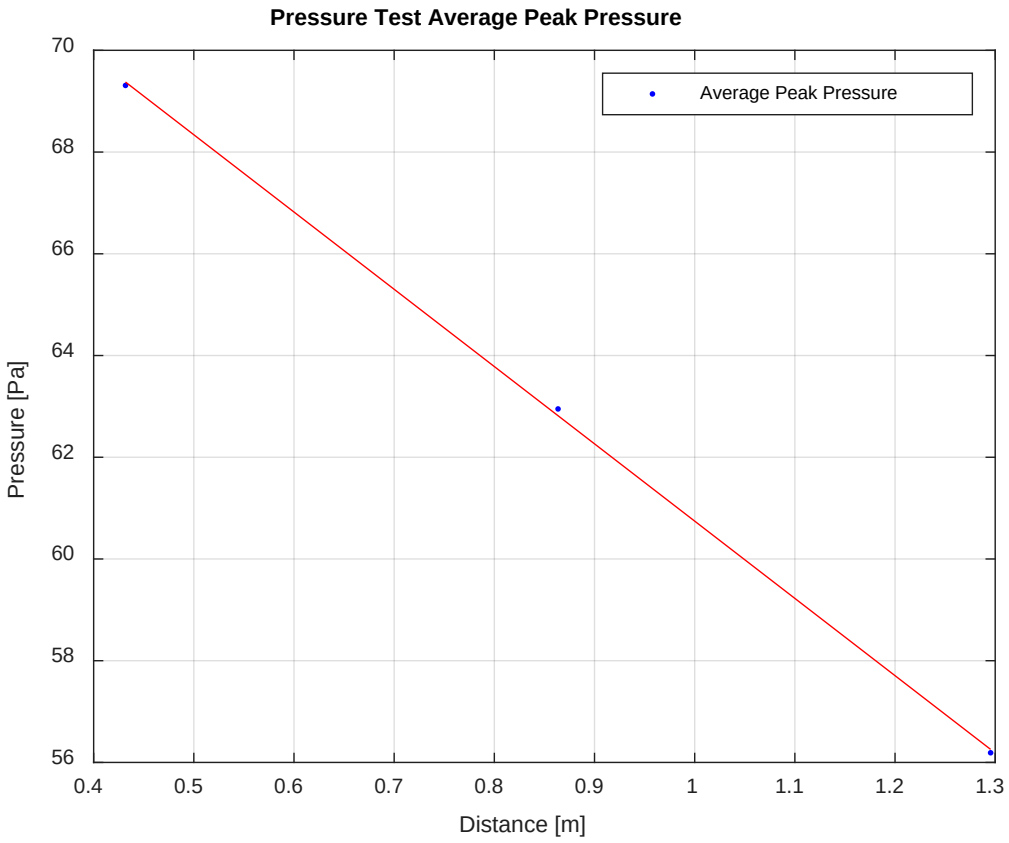

Figure 42. Average Peak Pressure

Utilizing the data from the individual four tests, frequency was determined. As displayed in Figure 43 the period was determined by measuring the space between two successive peaks. In this case the second and the ninth peak were utilized. The 0.4318 meter graph was used for all frequency determinations. The period utilized in this testing is in

units of seconds with frequency being measured in the units of hertz (Hz). The relationship between period and frequency is set forth in Equation 2. Once the period was determined from Figure 37–40 graph data, frequency was calculated. The results are shown in Table 6. The frequency of the liquid nitrogen explosion fell between 20.362 Hz to 30.854 Hz.

$$\text{Frequency (Hz)} = 1 / \text{Period (1/sec)} \quad (2)$$

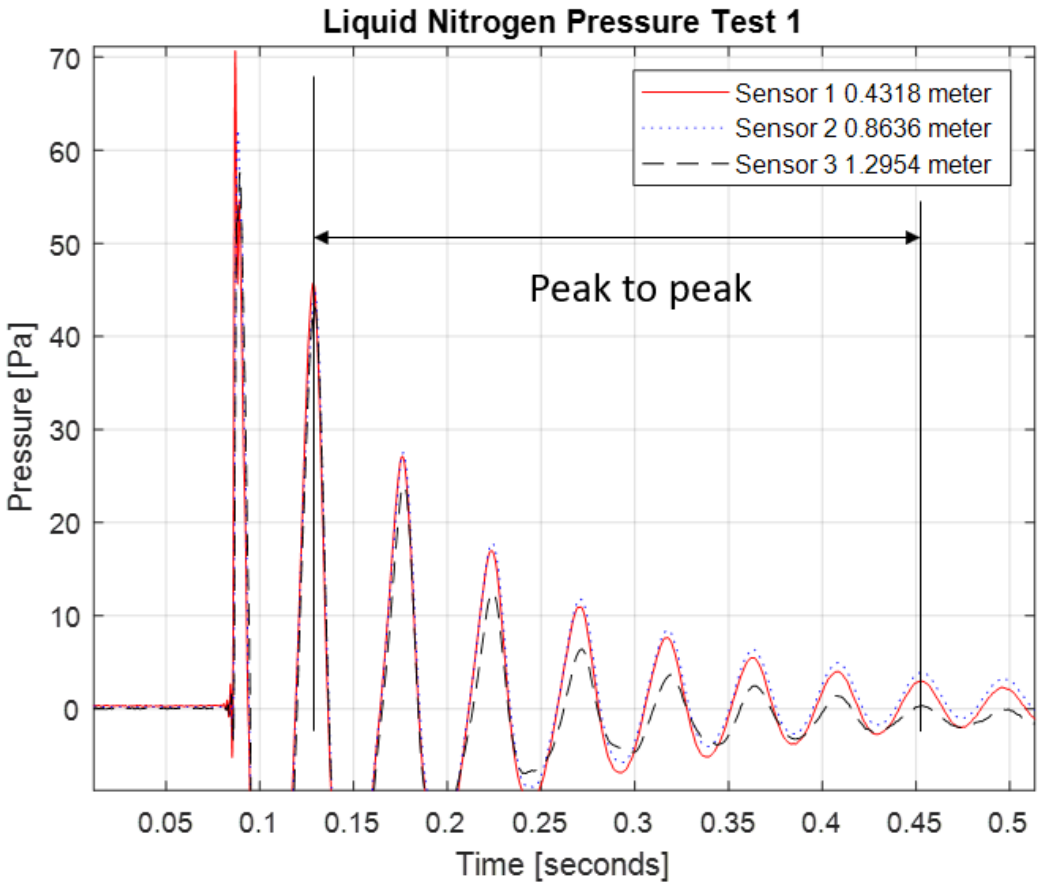

Figure 43. Period, peak-to-peak

Table 6. Pressure test frequency and period

	Period	**Frequency**
Test 1	0.04633 sec	21.584 Hz
Test 2	0.04911 sec	20.362 Hz
Test 3	0.03796 sec	26.344 Hz
Test 4	0.03241 sec	30.854 Hz
Average	0.04145 sec	24.786 Hz
Standard Deviation	0.00767	4.798

2. Simulation Results

Numerical simulations were performed for shock pressure. The one-dimensional spherical wave equation, as displayed in Equation 3, was used employing a numerical analysis technique.

$$\frac{1}{c^2}\frac{\partial^2 p}{\partial t^2} = \frac{\partial^2 p}{\partial r^2} + \frac{2}{r}\frac{\partial p}{\partial r} \tag{3}$$

The shock pressure from the liquid nitrogen was assumed to vary as displayed in Equation 4.

$$p_{LN}(t) = p_o e^{-\alpha t} \tag{4}$$

The pressure time histories, at a value of α=0.4 meters, were plotted as displayed in Figures 44 and 45.

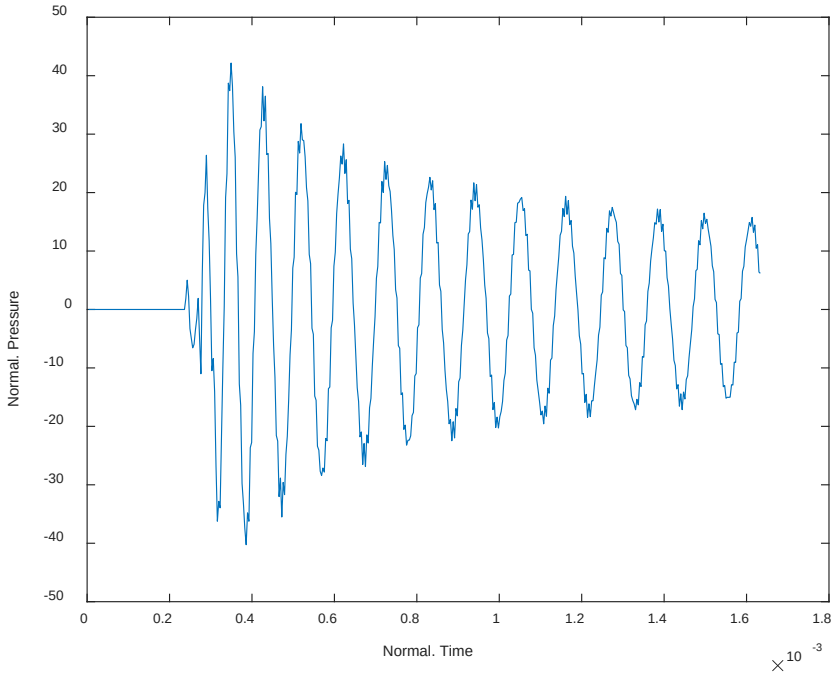

Figure 44. Simulation 1

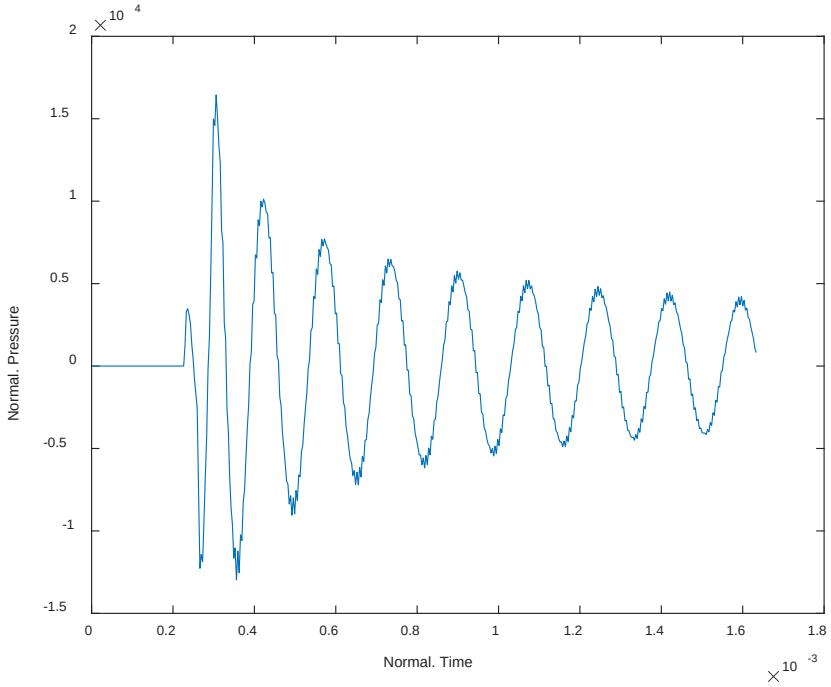

Figure 45. Simulation 2

These results revealed two findings qualitatively. First, that the pressure is oscillating positive and negative, as shown in the pressure reading within the experiment, while the peak pressure decays. Secondly, that depending on the conversion rate from the liquid to gas state of the liquid nitrogen, the maximum positive pressure may occur during the first or second peak, as observed in the experiment and simulation. This provides some qualitative explanation of the pressure behavior however, the oscillation frequency is much higher for the numerical results than the experimental data. One possible reason for this is that it may be related to the number of sampling points in the data acquisition system [12].

B. PHASE 2 RESULTS

Phase 2 testing was designed to determine the impact of an explosion on a plate submerged underwater using rig 1. Six tests were performed on one thin plate nominally 6.35×10^{-4} meter thick and six tests were also performed on one thick plate nominally 1.5875×10^{-4} meter thick. Both plates, despite their thickness, utilized the same orthotropic laminate twill weave texture finish.

The peak pressures experienced throughout all testing for both the thin and thick plate is listed in Table 7. The pressure graphs for this data can be seen in Appendix B and C. For these resulting peak pressures, pressure sensor one was utilized for all data listed. Both plates had similar averages with the thin plate at 48.54 Pa and the thick plate at 52.35 Pa. In phase 1, a derivation of an equation for distance versus pressure was determined, as displayed in Equation 1. The distance used for this calculation applying it to phase 2 data was 0.602 meter with a resulting peak pressure of 66.97 Pa. The reason for this disparity between calculated equation value versus the experimental value could be the distance from the explosion to the center of the plate. The circle within the plexiglass piece through which the explosion source was submerged had a diameter of 0.3048 meter, contributing to the possible error by potentially increasing the actual distance the explosion occurs from the plate.

Table 7. Peak pressure phase 2

	Thin Plate	**Thick Plate**
Test 1	60.95 Pa	58.82 Pa
Test 2	44.16 Pa	59.09 Pa
Test 3	44.28 Pa	51.11 Pa
Test 4	41.14 Pa	47.56 Pa
Test 5	57.55 Pa	45.29 Pa
Test 6	43.17 Pa	52.22 Pa
Average	48.54 Pa	52.35 Pa
Standard Deviation	8.44	5.69

1. Sample 1 Thin Plate

The strain gages measured both the x-direction and the y-direction. This horizontal configuration set-up of the strain gages positioned left, center, and right shown in Figure 46 were utilized for all phase 2 testing. Figures 47–51 show the strain experienced by the carbon composite plate throughout the six explosions. Between each of the six tests, the plate and rig were removed from the water to observe if any visual failure was present. Six blasts were performed to attempt to apply enough load to produce a visible failure on the plate. Figure 49 depicts the plate at the end of testing. Due to the woven nature of this plate, and despite its thin nature, it was not seen to split or noticeably fail in any region.

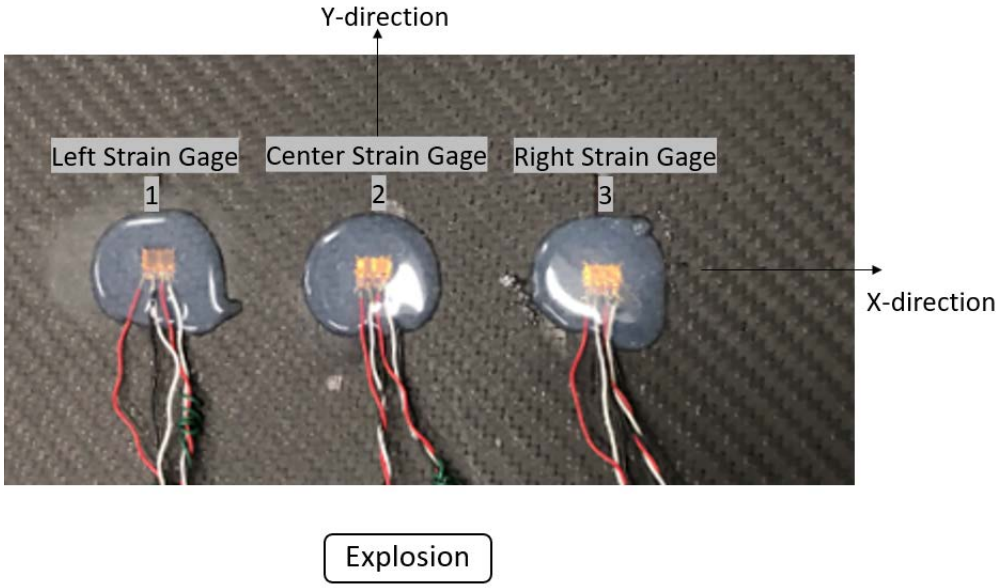

Figure 46. Top surface strain gage set-up

From the results shown in Figures 47, 50, 51, and 52, the x-direction showed that the lowest strain was observed from the middle strain gage (strain gage two) with the largest horizontal strains observed by both the outermost strain gages (strain gages one and three). Figure 48 and 49 show that an error occurred with strain gage two and three, which is the center and right strain gage, in the x-direction for test two and three. This error resulted from a malfunction with the strain gage from the explosion, which eventually resolved itself for the follow-on explosions. This resulting error makes it difficult to interpret the unexpected result of a lower maximum strain in the center gage in comparison to the outermost strain gages.

The first test produced the highest strain in the x-direction with a value of 0.003579. This correlates with the pressure data from test 1, in which the maximum peak pressure out of all six tests was produced at 60.95 Pa. In all six tests, the x-direction showed higher strain rates than the y-direction by at least double the value, with Figure 46 showing the corresponding x and y direction. Unlike the x-direction, the y-direction saw a more uniform effect from the explosion on all three strain gages.

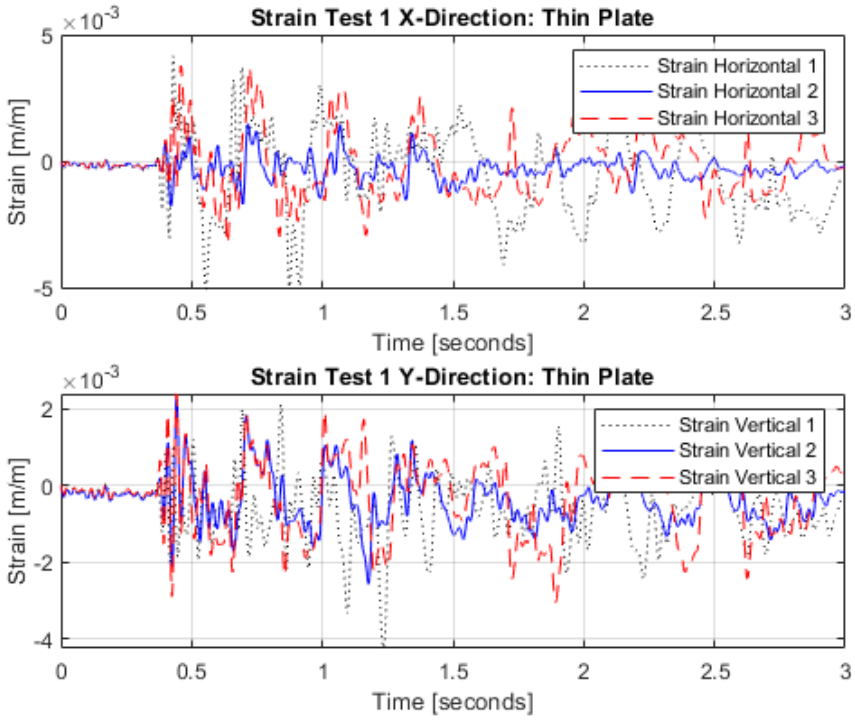

Figure 47. Strain thin plate 1st blast

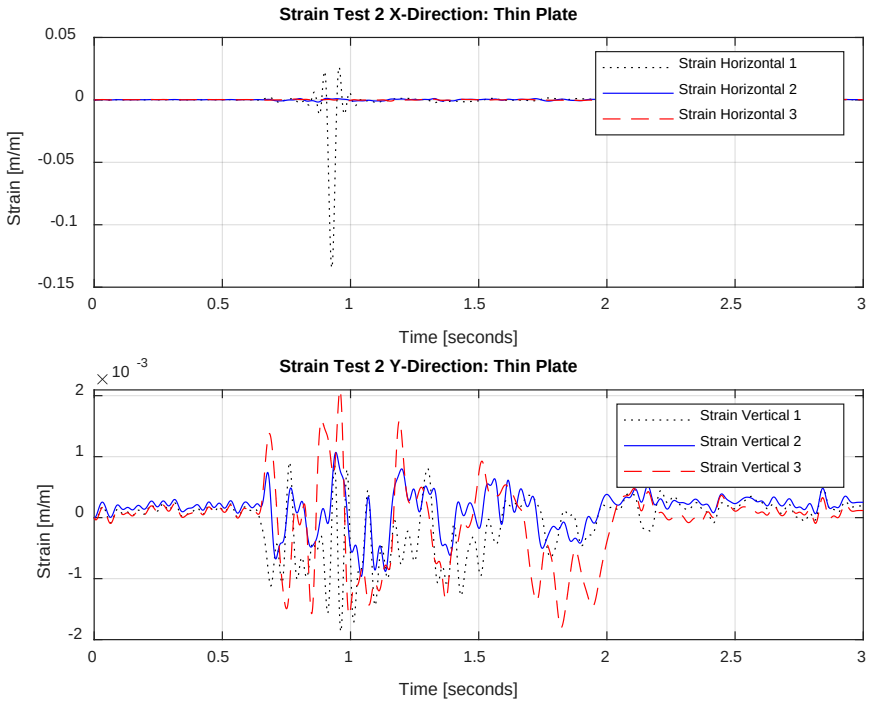

Figure 48. Strain thin plate 2nd blast

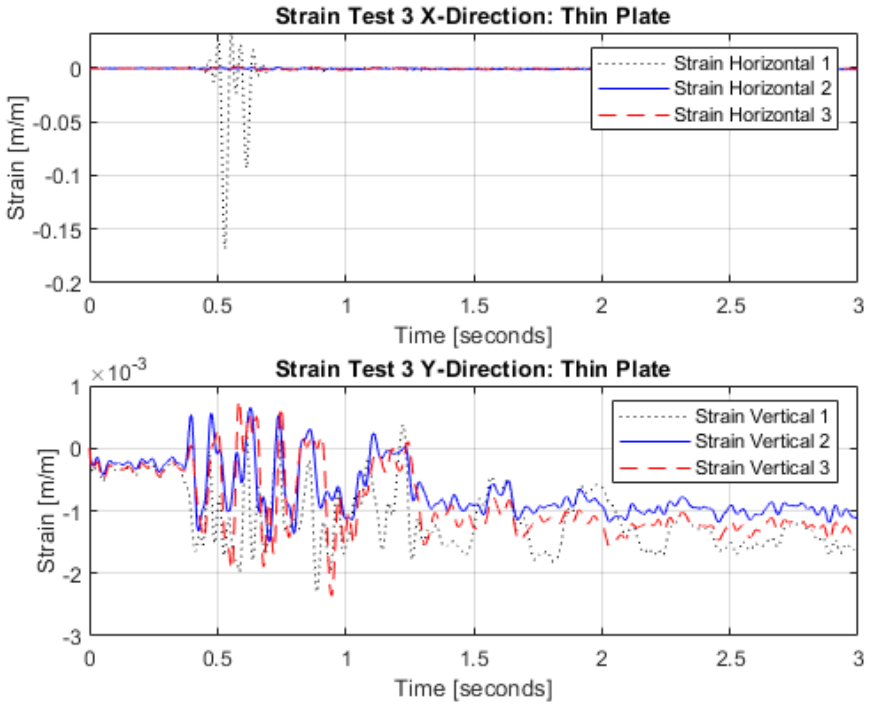

Figure 49. Strain thin plate 3rd blast

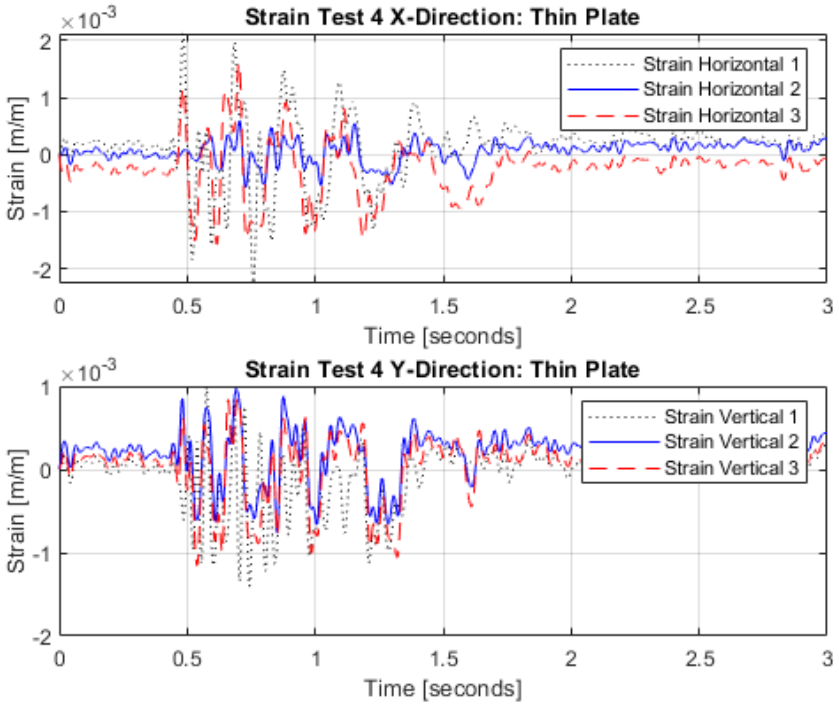

Figure 50. Strain thin plate 4th blast

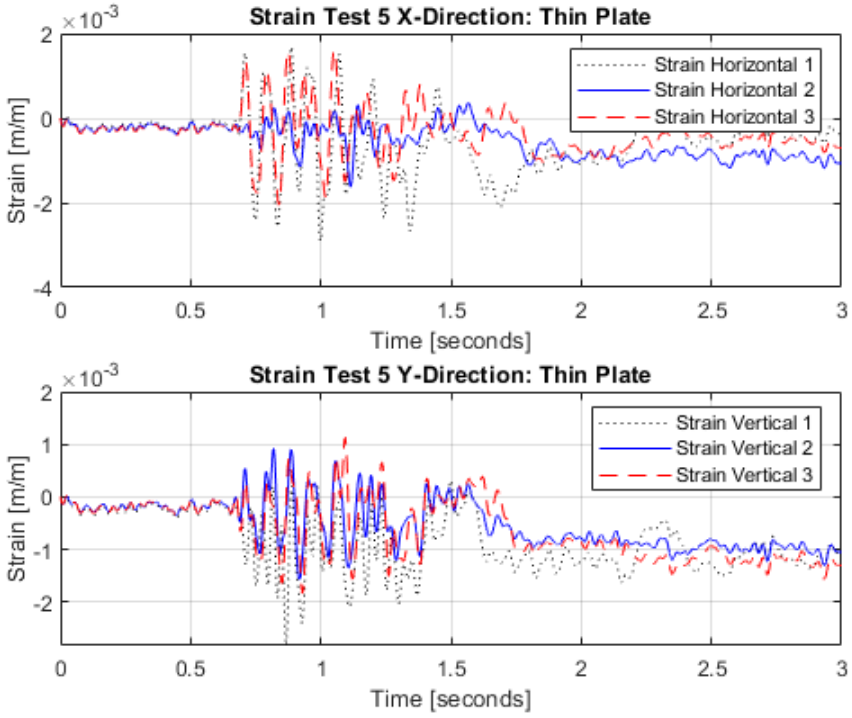

Figure 51. Strain thin plate 5th blast

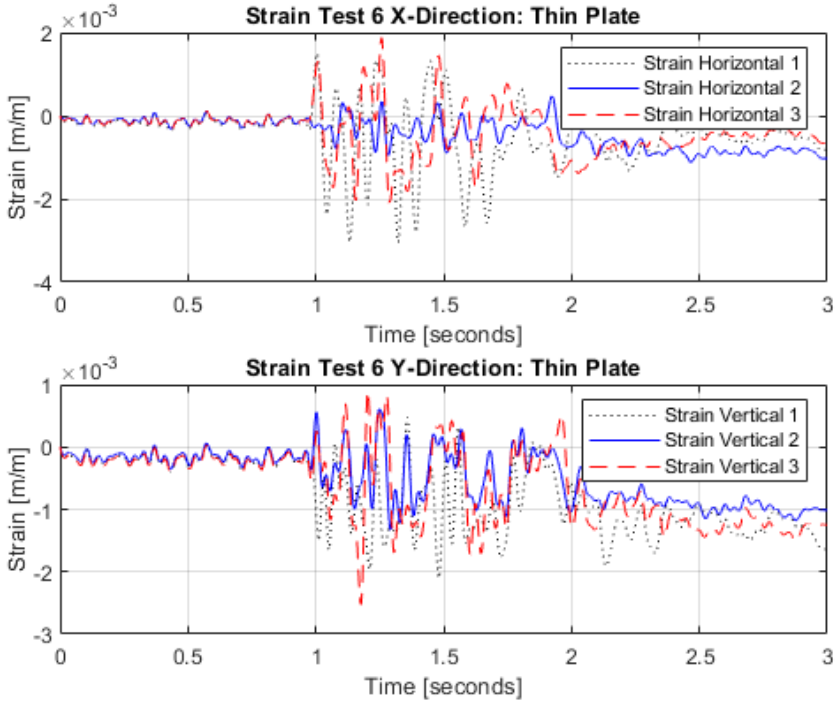

Figure 52. Strain thin plate 6th blast

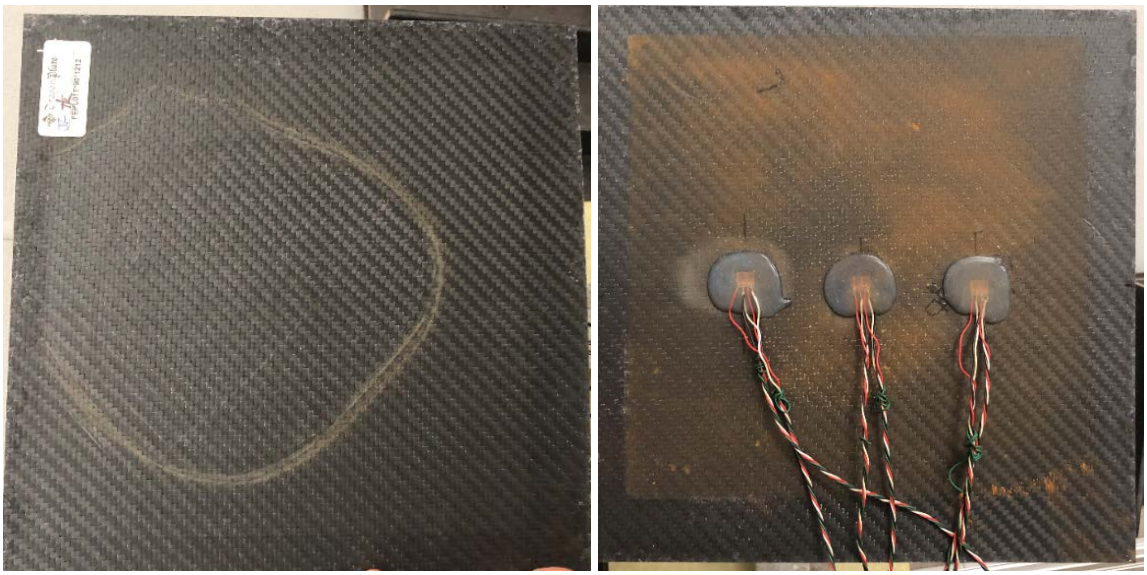

Figure 53. Final thin plate response bottom (left) and top (right)

Figure 53 shows the orthotropic carbon composite laminate twill weave plates after the six explosive tests. The brown layer of dust present on the top of the plate is due to rust from the clamps that formed on the plate after each subsequent explosion. The circle on the bottom plate is a water mark from removing the plate and rig with sitting water remaining on the plate. Of note, neither the top nor the bottom of the thin plate showed any visible signs of failure or indentation.

2. Sample 2 Thick Plate

Figures 54–59 show the strain experienced by the carbon composite plate throughout six explosions. The same horizontal strain gage orientation seen in Figure 46 from Sample 1 configuration was used on Sample 2 as well. As with the thin plate testing, between each of the six tests the plate and rig were removed from the water in order to observe if any visual failure was present. Six blasts were also performed on this sample. Due to the performance of the thin plate and its lack of visibly observable failure, it was anticipated the thick plate would similarly not show any signs of significant failure. Figure 60 shows the plate at the end of testing and, as predicted, no visual signs of failure were present in any region.

From the results figures, the x-direction shows that the right-most strain gage, horizontal strain gage 3 which is referenced in Figure 46, showed the highest strain for all six tests. This did not hold true in the y-direction where the middle strain gage saw the highest values. All thick plate testing showed similar strain values when comparing the x-direction and y-direction for each test individually. Within test 2, the vertical 1 strain gage, which was the left strain gage referenced in Figure 46, experienced a malfunction in reading at the time of the blast. It is not consistent with the resulting information collected by the remaining two vertical strain gages within that same test, as well as the subsequent vertical readings for follow on tests 3–6.

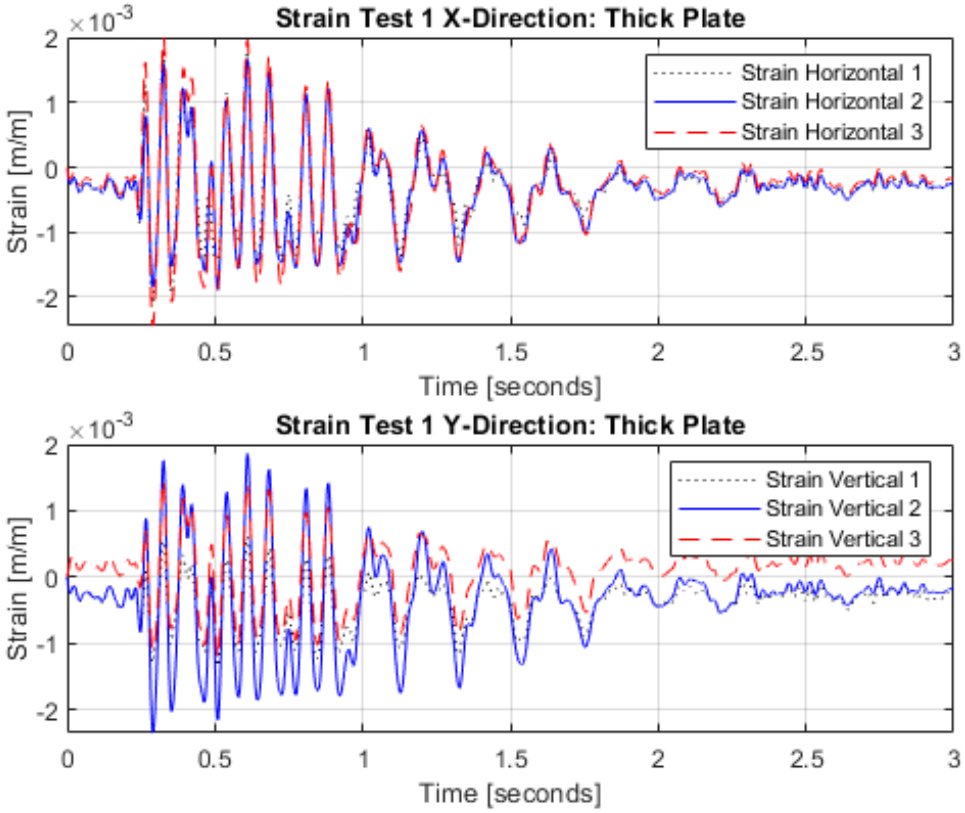

Figure 54. Strain thick plate 1st blast

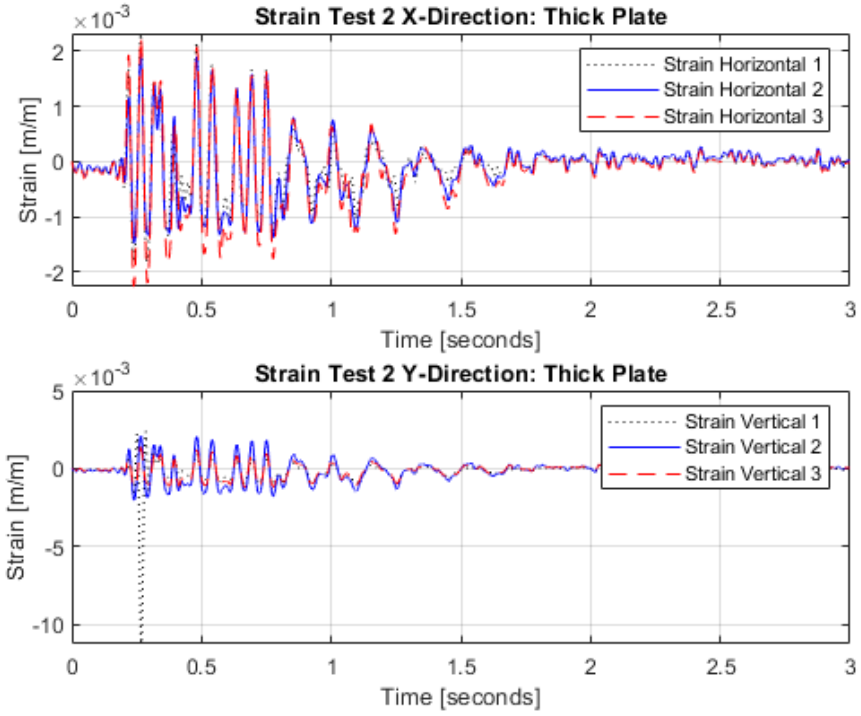

Figure 55. Strain thick plate 2nd blast

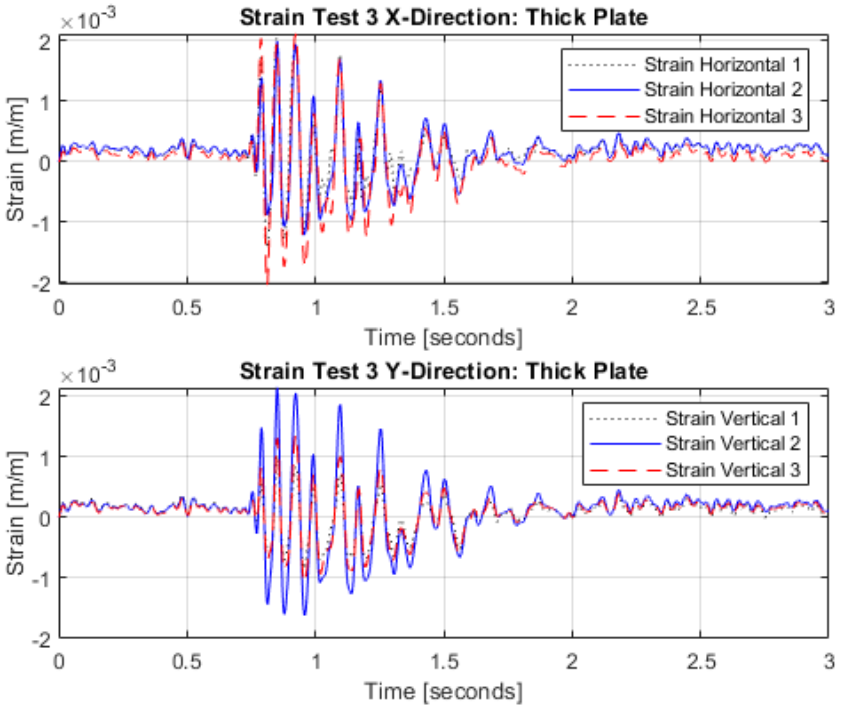

Figure 56. Strain thick plate 3rd blast

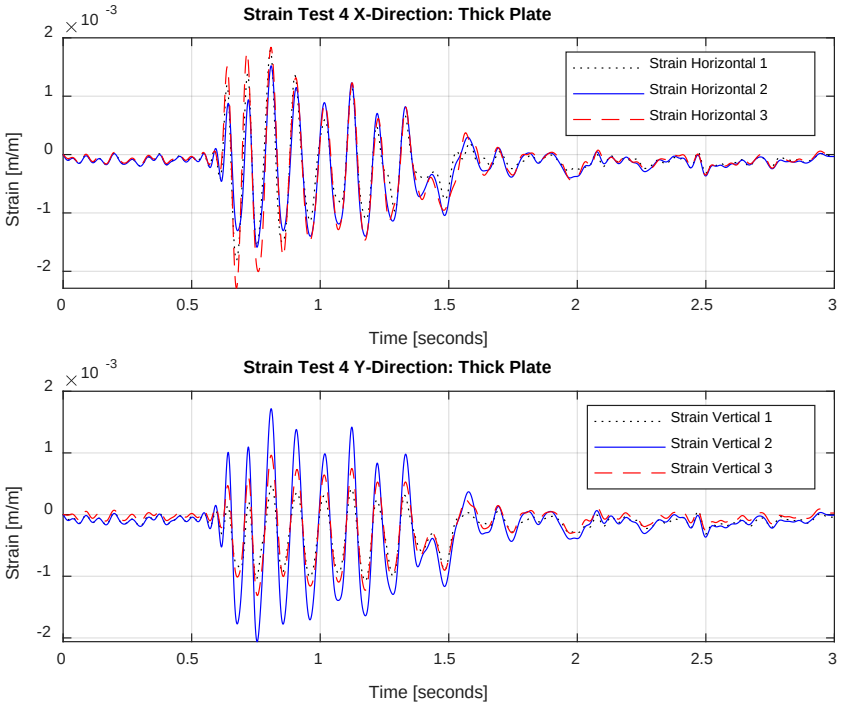

Figure 57. Strain thick plate 4th blast

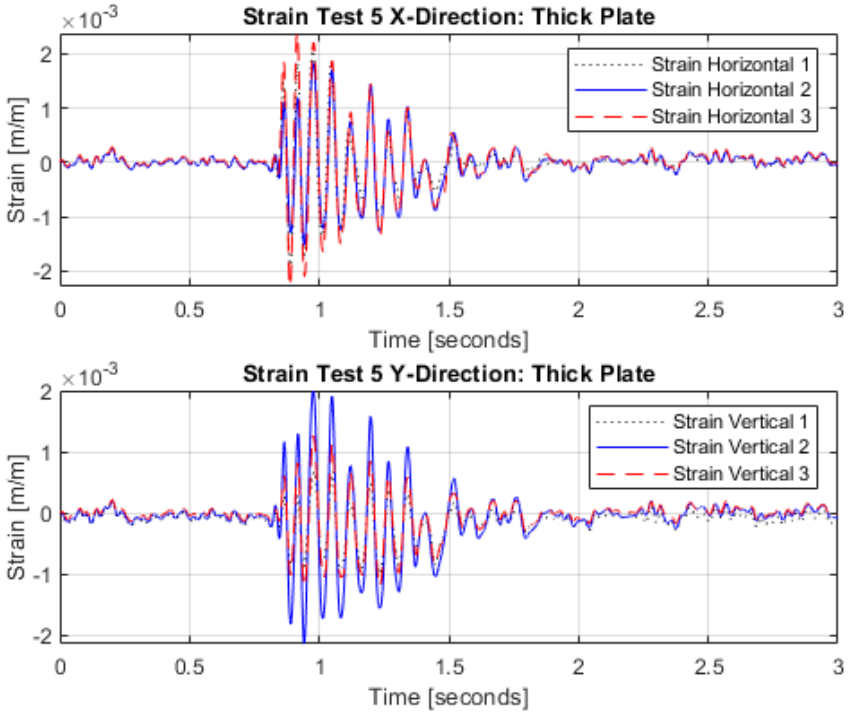

Figure 58. Strain thick plate 5th blast

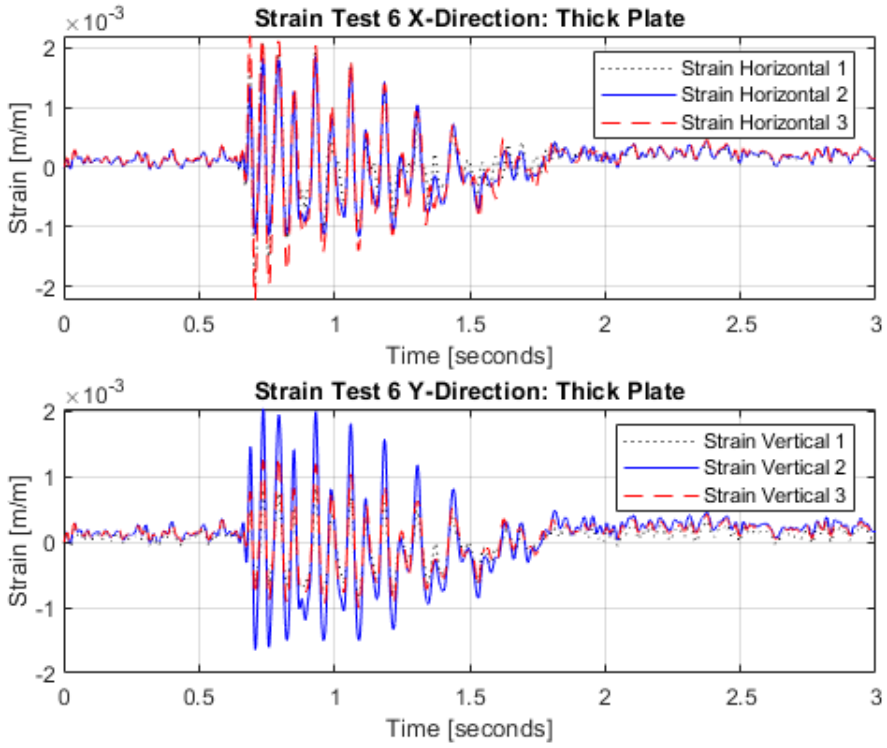

Figure 59. Strain thick plate 6th blast

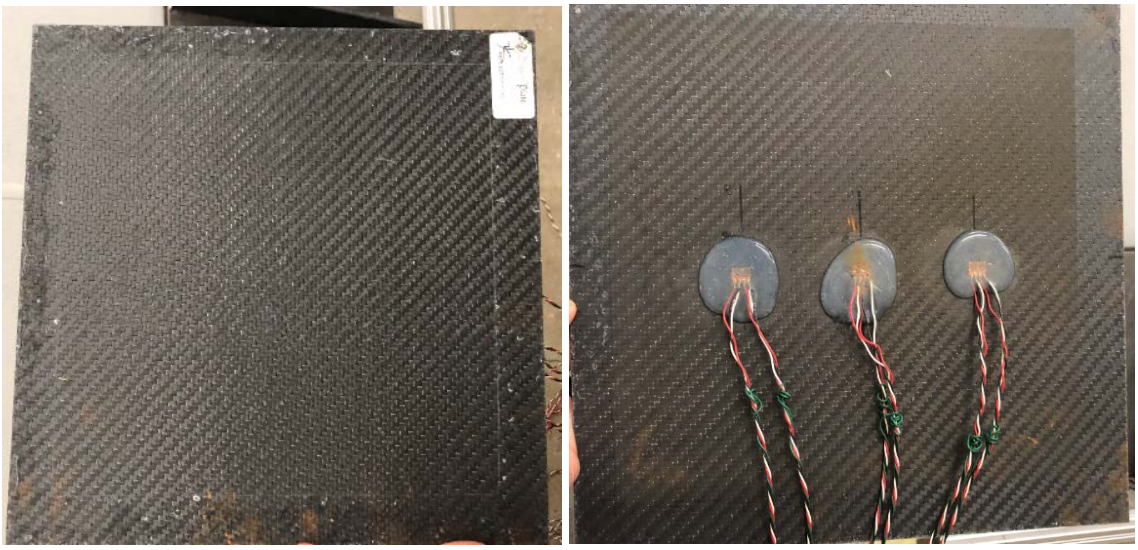

Figure 60. Final thick plate response bottom (left) and top (right)

As displayed in Figure 60, neither the top nor bottom of the thick orthotropic laminate twill weave carbon composite experienced any visible failure or indentation.

3. Thin versus Thick Plate

Due to the results observed in the thin plate, it was not anticipated that the thick plate would show any visible signs of failure after six explosion events. This theory held true for phase 2 testing. Thin and thick plate average peak pressures remained relatively consistent, allowing for a comparison between maximum strain values of each. Having similar pressures applied to each plate, the thick plate showed greater strain values consistently for each test in the y-direction, as shown in Table 9. This was not an anticipated distinction. Table 8 shows this was not true in the x-direction. No data was available for the x-direction for test 2 and 3. Test 1 and 6 showed a greater strain value in the thick plate, while test 4 and 5 showed a greater strain value in the thin plate. When subjected to similar pressures, it would be anticipated that the thin plate would have experienced more strain than the plate twice as thick.

The ratio between the peak pressure and the peak strain were determined as shown in Table 8 and Table 9. Table 8 shows the values for the x-direction, while Table 9 shows the values for the y-direction. During all tests, the thick plate ratio values stayed relatively consistent in the x and y direction. The thin plate, however, showed more variance in ratio values in the x and y direction. The x direction can be disregarded since two data points are missing from the results.

Table 8. Peak pressure and peak strain x-direction

	Thin Plate			**Thick Plate**		
	Peak Pressure	Peak Strain	Ratio of Peak Strain to Peak Pressure	Peak Pressure	Peak Strain	Ratio of Peak Strain to Peak Pressure
Test 1	60.95 Pa	0.004137	6.788×10^{-5}	58.82 Pa	0.001992	3.387×10^{-5}
Test 2	44.16 Pa	-	-	59.09 Pa	0.002416	4.089×10^{-5}
Test 3	44.28 Pa	-	-	51.11 Pa	0.00212	4.148×10^{-5}
Test 4	41.14 Pa	0.002113	5.136×10^{-5}	47.56 Pa	0.002005	4.216×10^{-5}
Test 5	57.55 Pa	0.001676	2.912×10^{-5}	45.29 Pa	0.002901	6.405×10^{-5}
Test 6	43.17 Pa	0.002290	5.304×10^{-5}	52.22 Pa	0.001995	3.820×10^{-5}
Average	48.54 Pa	0.002554	5.035×10^{-5}	52.35 Pa	0.002238	4.344×10^{-5}
Standard Deviation	8.44	1.09×10^{-3}	1.598×10^{-5}	5.69	3.63×10^{-4}	1.054×10^{-5}

Table 9. Peak pressure and peak strain y-direction

	Thin Plate			**Thick Plate**		
	Peak Pressure	Peak Strain	Ratio of Peak Strain to Peak Pressure	Peak Pressure	Peak Strain	Ratio of Peak Strain to Peak Pressure
Test 1	60.95 Pa	0.002389	3.919×10^{-5}	58.82 Pa	0.001829	3.110×10^{-5}
Test 2	44.16 Pa	0.002092	4.737×10^{-5}	59.09 Pa	0.002187	3.701×10^{-5}
Test 3	44.28 Pa	0.001028	2.322×10^{-5}	51.11 Pa	0.002034	3.980×10^{-5}
Test 4	41.14 Pa	0.000963	2.340×10^{-5}	47.56 Pa	0.001859	3.909×10^{-5}
Test 5	57.55 Pa	0.001084	1.884×10^{-5}	45.29 Pa	0.002595	5.730×10^{-5}
Test 6	43.17 Pa	0.001367	3.167×10^{-5}	52.22 Pa	0.001892	3.623×10^{-5}
Average	48.54 Pa	0.001487	2.238×10^{-5}	52.35 Pa	0.002066	4.009×10^{-5}
Standard Deviation	8.44	6.07×10^{-4}	3.062×10^{-6}	5.69	2.915×10^{-4}	8.972×10^{-6}

C. PHASE 3 RESULTS

Phase 3 testing was designed to test and observe the impact of an explosion occurring directly in front of a vertical plate submerged underwater. Testing was performed on four different samples using rig 2. Sample 1 and 2 were each unidirectional, laminate textured finish, 0-degree plates of 0.25 mm and 0.5 mm nominal thickness respectively. Sample 3 was a cross-ply plate design that had alternating 0 and 90-degree plies with a thickness of 0.5 mm. Sample 4 also used a cross-ply design but with an additional sheet of 90-degree plie internally. All phase 3 testing used the configuration seen in Figure 61 with the strain gage orientation vertically orientated.

1. Sample 1

Sample 1 was the thinnest plate subjected to explosion testing. Two different set-up configurations were conducted for this sample. The only difference between the two set-ups was the distance between the explosion and the sample. In the first set-up, the explosion occurred at 0.3048 meter distance from the vertical plate, whereas the second set-up utilized an extended distance of 0.4572 meter. For both set-ups, successive explosions were performed until the plate exhibited visual signs of failure. Figure 61 shows the fiber orientation for sample 1 unidirectional 0-degree plate.

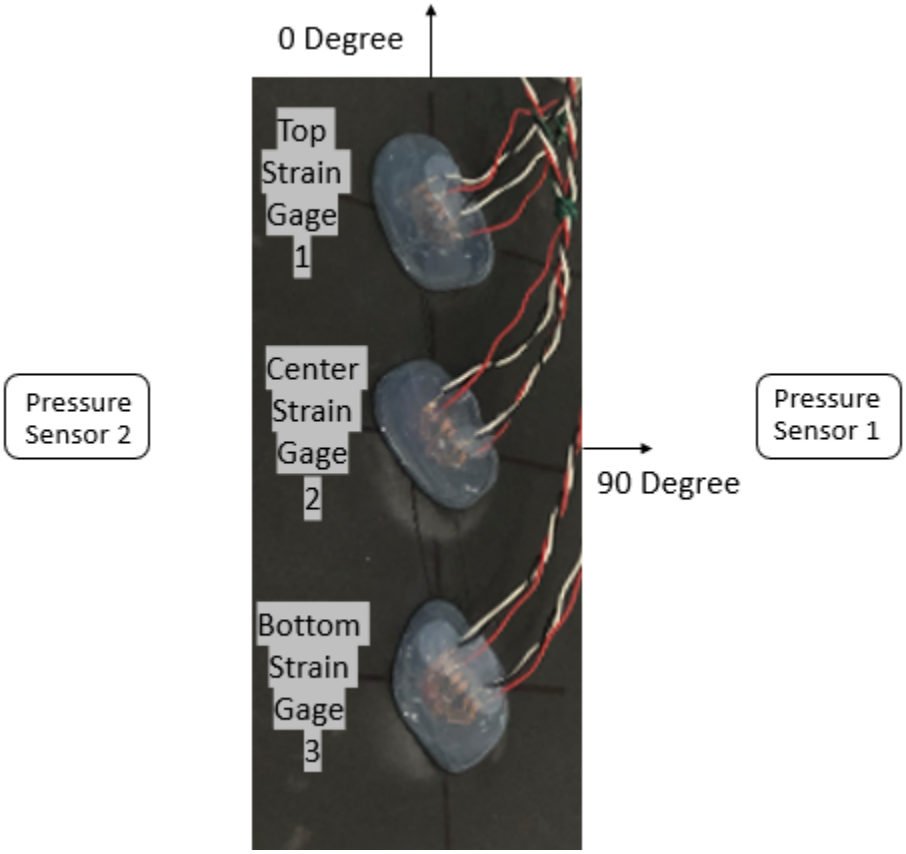

Figure 61. Fiber orientation

a. Set-up 1

The carbon composite sample 1 plate failed after one blast. The peak pressure it experienced was 46.41 Pa, as shown in Figure 62. Figure 63 shows that an error occurred

in the x-direction with both strain gage two and three (center and bottom strain gages respectively). This figure does show that the x-direction strain gage one (top strain gage) experienced a maximum tensile strain of 0.06091 and a maximum compressive stress of 0.4546. Figure 63 also shows the maximum tensile strain experienced in the y-direction at a value of 0.02943 also occurred in the strain gage one (top strain gage). The maximum compressive strain in the y-direction was 0.02137 in the center strain gage two. This resulting effect correlates with the maximum pressure measured during this blast as seen on pressure sensor 2, which is the sensor closest to strain gage one. This failure can be seen in Figure 64 where the right side of the plate split in three locations, severing the plate into pieces.

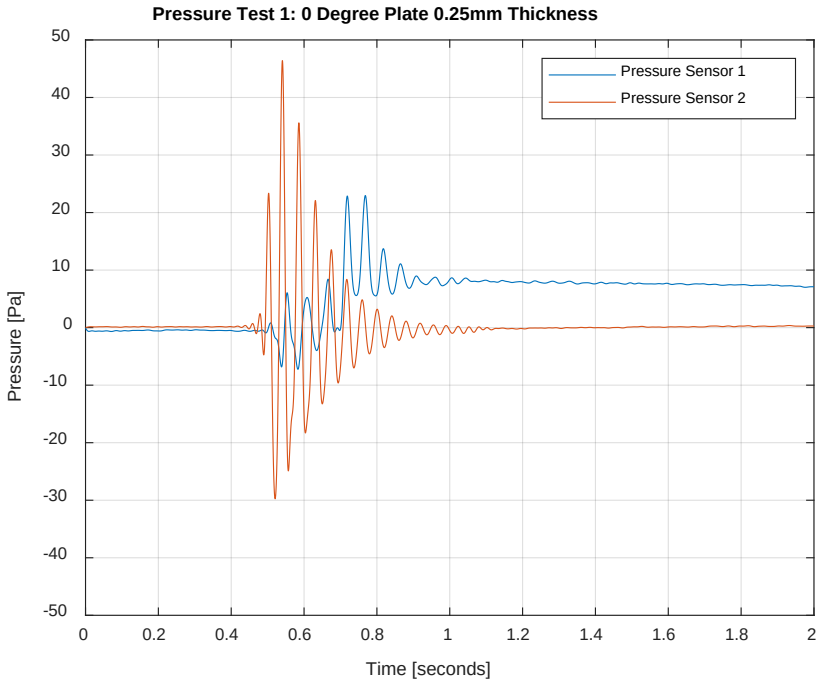

Figure 62. Set-up 1 Sample 1 pressure 1st blast

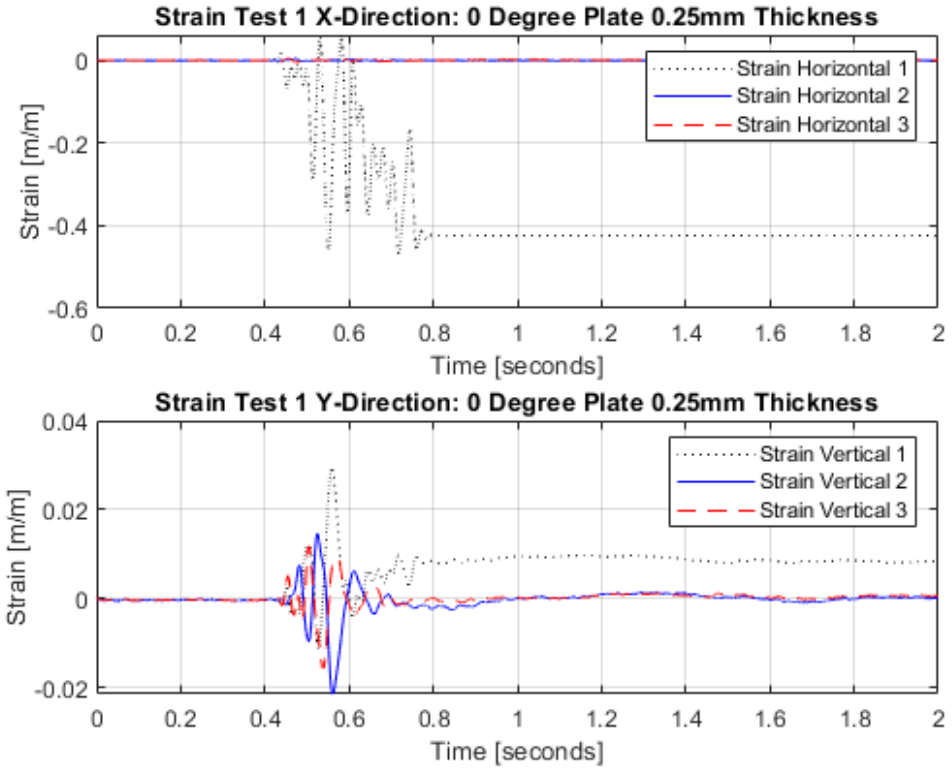

Figure 63. Set-up 1 sample 1 strain 1st blast

Figure 64. Set-up 1 sample 1 failure

b. Set-up 2

Due to set-up 1 failing after one blast, set-up 2 was pursued to see if moving the explosion an additional one-half of the initial distance away from the plate would still lead to the same failure after a single blast. The result observed for the carbon composite sample 1 plate held true in set-up 2. The peak pressure it experienced was 43.81 Pa, as shown in Figure 65. As anticipated, based on the increased distance between the explosion and the plate, the peak pressure value observed in set-up 2 is less than the peak pressure experienced in set-up 1.

The pressure graph, Figure 65, showed pressure sensor 2 capturing a steep negative value and then returning to reach a steady state back at zero pascals. This was the first time in testing that a sensor reading of this kind had been observed. However, after conducting all phase 3 testing, this result was seen in numerous other tests displayed in Appendix D, E, F, G and H. The only notable difference between the pressure sensors within phase 3 versus phase 1 and 2 is their placement. In phase 3 the sensors were attached directly to the rig using filament and the explosion occurred directly in front of the sensor. Based on the unusual pressure curve and particular pattern observed in phase 2, more testing should be performed in order to determine specifically where the bubble from the explosion is collapsing and/or if the peak pressure and force of the explosion had a subsequent impact on the sensor.

Figure 66 shows that the x-direction strain gage two (center strain gage), experienced a maximum tensile strain of 0.004125 and strain gage three (bottom strain gage) showed a maximum compressive stress of 0.005846. It also shows that the maximum tensile strain experienced in the y-direction at a value of 0.004502 occurred in the strain gage one (top strain gage) and a maximum compressive strain of 0.006249 in strain gage three (bottom strain gage). The visible failure can be seen in Figure 67 where the right side of the plate split in one location and completely severed the plate into two pieces.

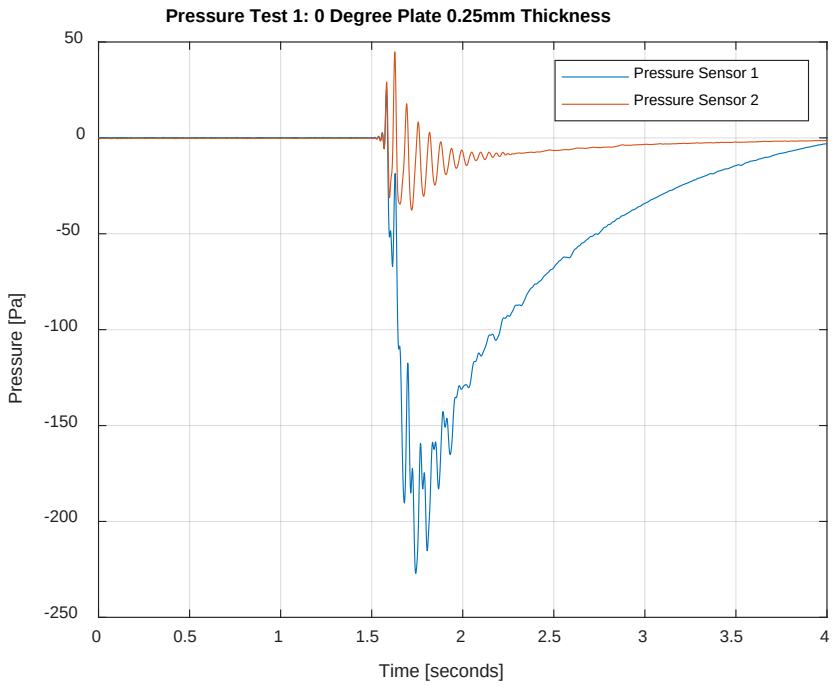

Figure 65. Set-up 2 sample 1 pressure 1st blast

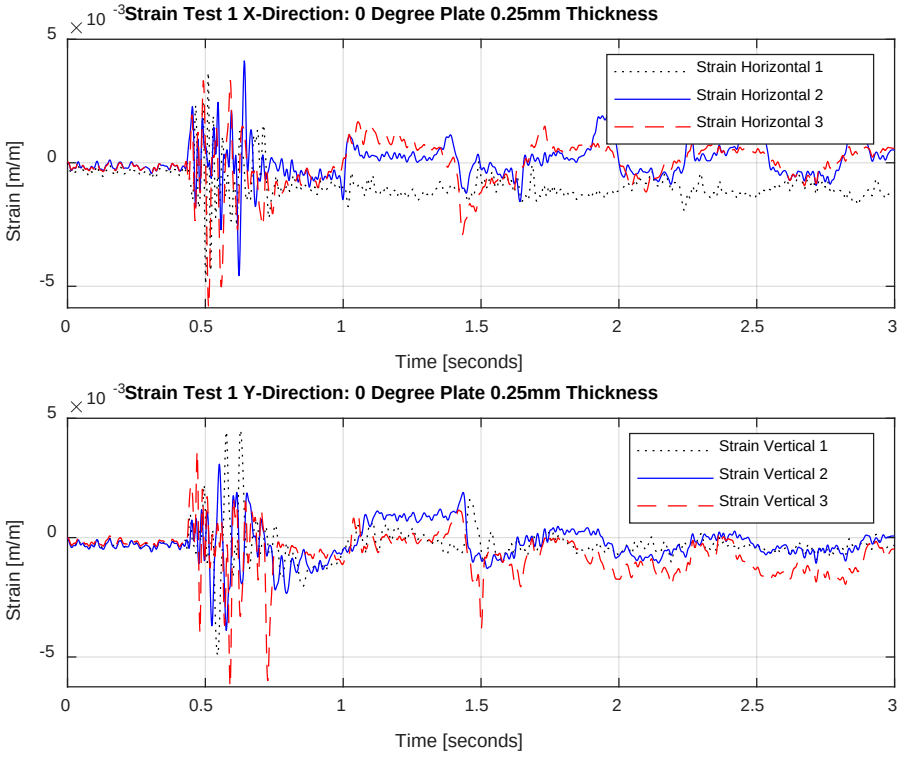

Figure 66. Set-up 2 sample 1 strain 1st blast

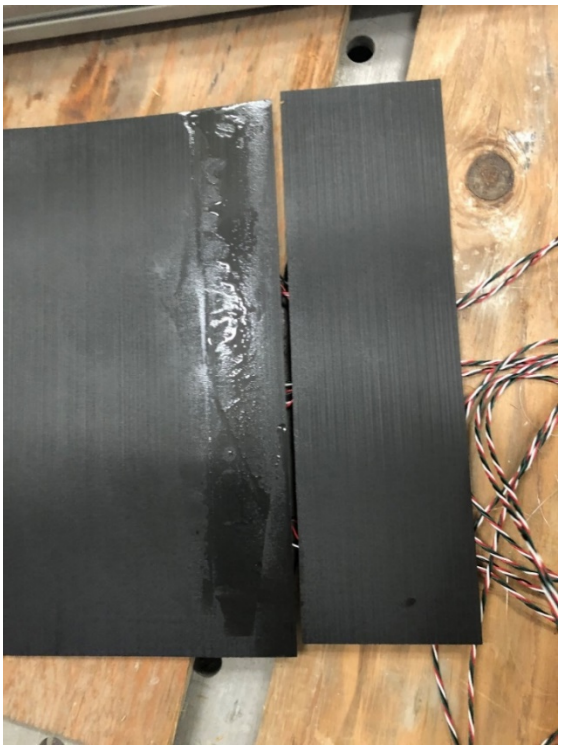

Figure 67. Set-up 2 sample 1 after 1st blast

c. Set-up 1 and 2 Comparison

Table 10 compares the peak pressure and peak compressive and tensile strain values of the two different set-ups that utilized the sample 1 plate type. Set-up 1 showed higher strain values in both the x-direction and y-direction due to the explosion occurring in closer proximity to the plate. Sample 1 was a 0-degree unidirectional plate. The failure for both set-ups occurred in this weakest direction that had no reinforcement, which was the 90-degree plane. Under set-up 1, the plate was completely severed in three locations with visual evidence of failure in another two locations after one blast. Set-up 2's only visible failure was one complete separation, severing the entire plate also occurring after only one explosion. The conclusions for sample 1 supported the expected results for this section. Upon visual inspection, the failure appears to be more severe with decreasing distance of the explosion source to the plate shown in set-up 1, while also having a higher maximum peak pressure, maximum tensile and compressive strain.

Table 10. Sample 1 peak values

	Set-up 1: 0.3048 m	**Set-up 2: 0.4572 m**
Peak Pressure	46.41 Pa	43.81 Pa
Peak Tensile Strain x-direction	0.06091	0.004125
Peak Compressive Strain x-direction	0.4645	0.005846
Peak Tensile Strain y-direction	0.02943	0.004502
Peak Compressive Strain y-direction	0.02141	0.006249

2. Sample 2

Sample 2 utilized the same layout as sample 1 but was twice as thick. This plate was the second weakest plate subject to explosion testing within phase 3. The same two set-up configurations were used for this sample as were performed on sample 1. In the first set-up, the explosion occurred at 0.3048 meter distance from the vertical plate, whereas the second set-up utilized an extended distance of 0.4572 meter. For both set-ups, successive explosions were performed until the plate exhibited visual signs of failure.

a. Set-up 1

The carbon composite sample 2 plate failed after two blasts within set-up 1. The peak pressure it experienced was 48.99 Pa, as shown in Figure 68. Figure 69 shows that the x-direction strain gage two (center strain gage) experienced a maximum tensile strain of 0.001923 and a maximum compressive strain of 0.001556. Figure 68 also shows the maximum tensile strain experienced in the y-direction at a value of 0.006092 also occurred in the strain gage two (center strain gage). The maximum compressive strain occurred in strain gage three (bottom strain gage) at a value of 0.001005. This first explosion caused a small sliver of visible failure, as seen in Figure 70, in the bottom left corner of the plate. The severed piece of the plate measures at 0.0762 meter, about ¼ the entire width measurement of the plate.

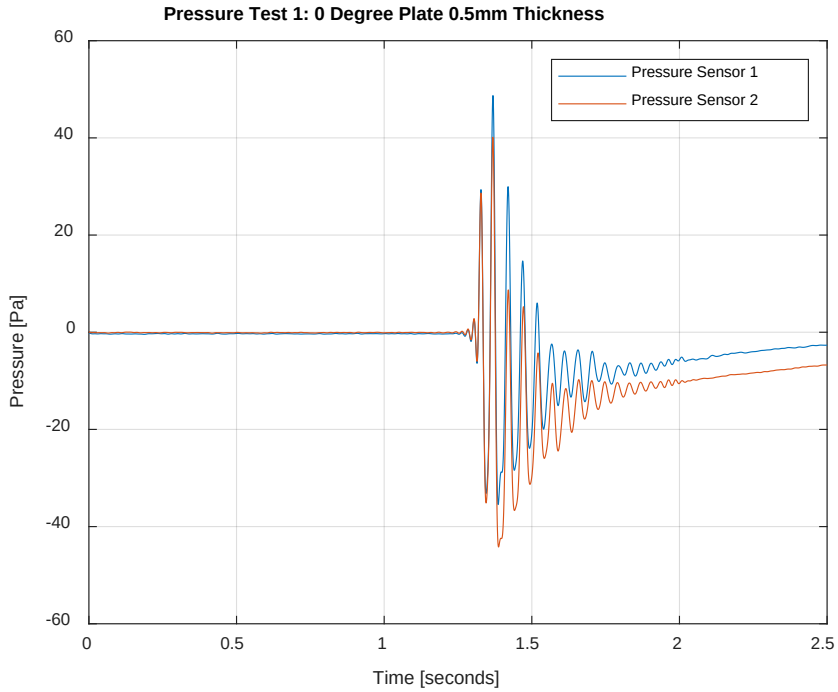

Figure 68. Sample 1 pressure 1st blast

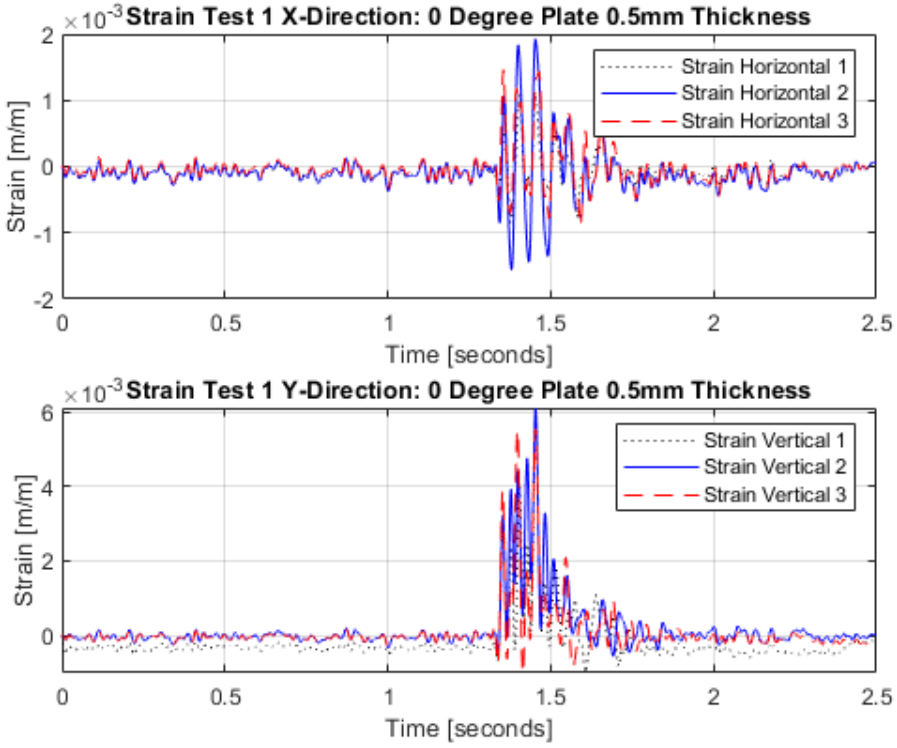

Figure 69. Sample 2 strain 1st blast

Figure 70. Sample 2 after 1st blast

The second blast further impacted the initial failure already established from the first blast, causing full failure. The peak pressure it experienced was 50.32 Pa, as shown in Figure 71. This was a similar pressure experienced in the first blast within 2 Pa. Strain gage 2 fully failed in the x-direction, not showing a measurable peak value. Figure 72 also shows the maximum tensile strain experienced in the y-direction at a value of 0.005772 in the strain gage three (bottom strain gage) and a maximum compressive strain of 0.01613 in strain gage two (center strain gage). Also similar to the first blast, the center strain gage 2 showed the failure, as displayed in Figure 73. This second explosion caused the sample 2 plate to sever in two places. The slice closest to the center shows why the center strain gage no longer was reading in the x-direction. In comparison to sample 1, this exact set-up took only one blast to break sample 1 but took two blasts to break sample 2 as it utilized the same layup but was twice as thick.

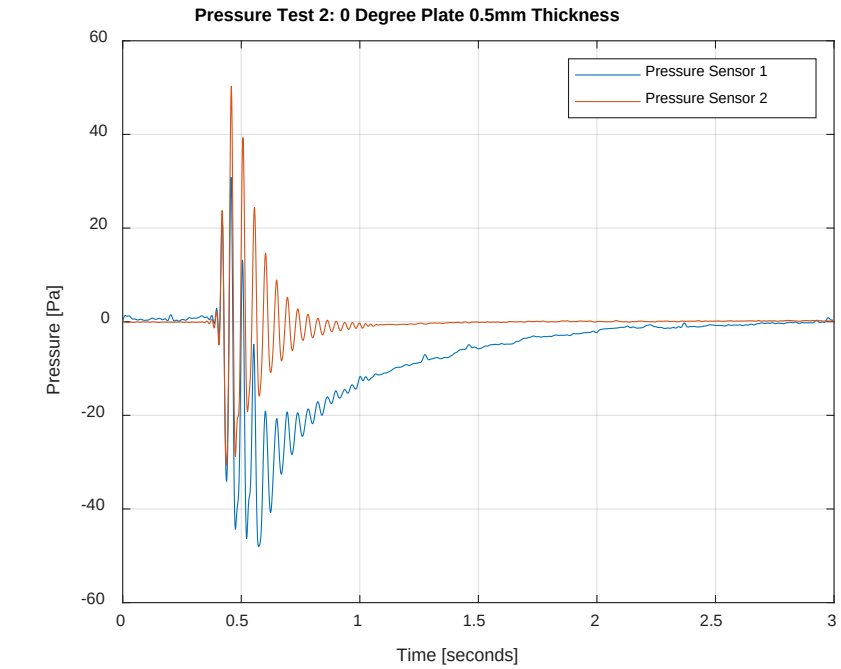

Figure 71. Sample 2 pressure 2nd blast

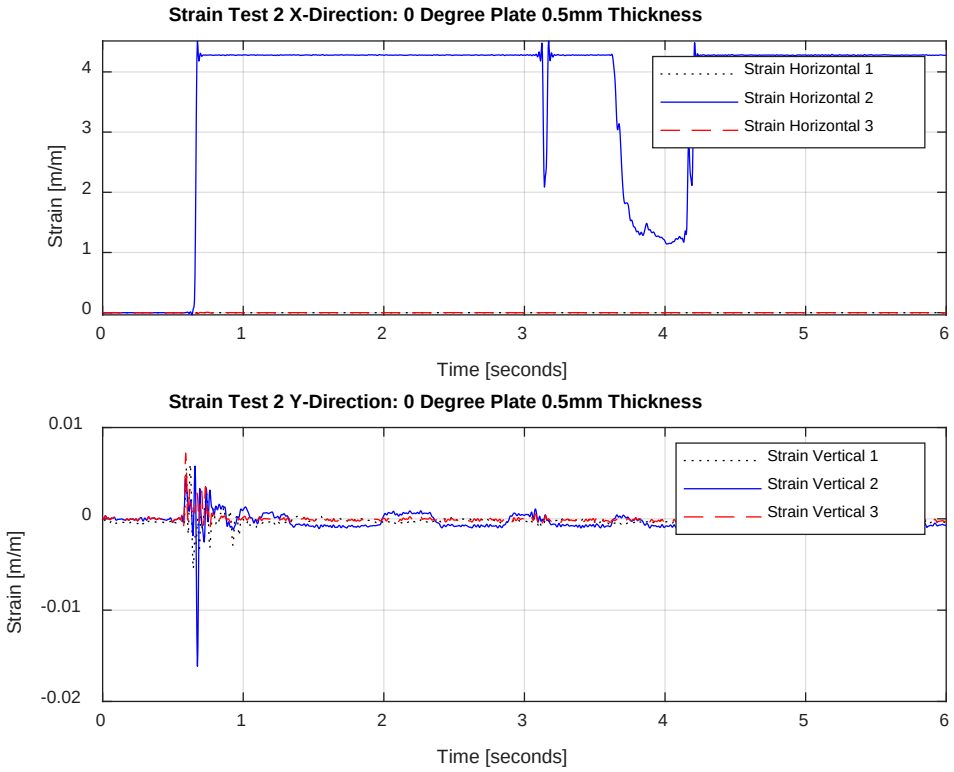

Figure 72. Sample 2 strain 2nd blast

Figure 73. Sample 2 failure after 2nd blast

b. Set-up 2

Due to set-up 1 failing after two blasts, set-up 2 was pursued to see if moving the explosion an additional one-half of the initial distance away from the plate would still lead to the same failure after a two blasts of similar maximum peak pressure. The result observed for the carbon composite sample 2 set-up 1 plate held true in set-up 2. The peak pressure it experienced was 30.82 Pa, as shown in Figure 74. As anticipated based on the increased distance between the explosion and the plate, the peak pressure value observed in set-up 2 is less than the peak pressure experienced in set-up 1. This difference could also be attributed to less liquid nitrogen in the coke bottle to produce the explosion.

Figure 75 shows that the x-direction strain gage three (bottom strain gage) experienced a maximum tensile strain of 0.003139 and maximum compressive strain of 0.001702, respectively. Figure 75 also shows the maximum tensile strain experienced in the y-direction at a value of 0.001511 also occurred in the strain gage two (center strain gage). The maximum compressive strain in the y-direction occurred in strain gage three (bottom strain gage) at 0.0009277. This first explosion caused no visible failure in the plate.

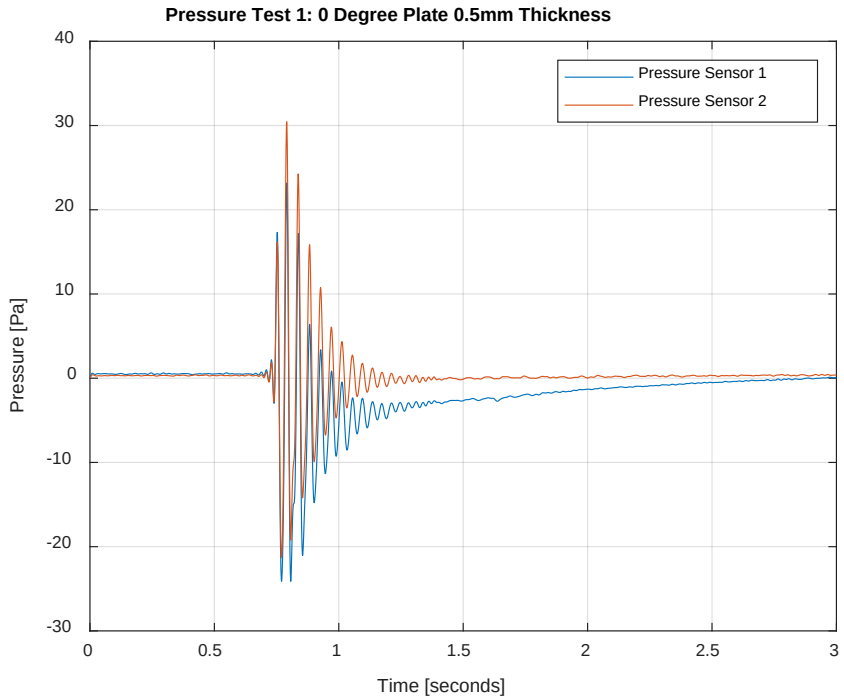

Figure 74. Sample 2 pressure 1st blast

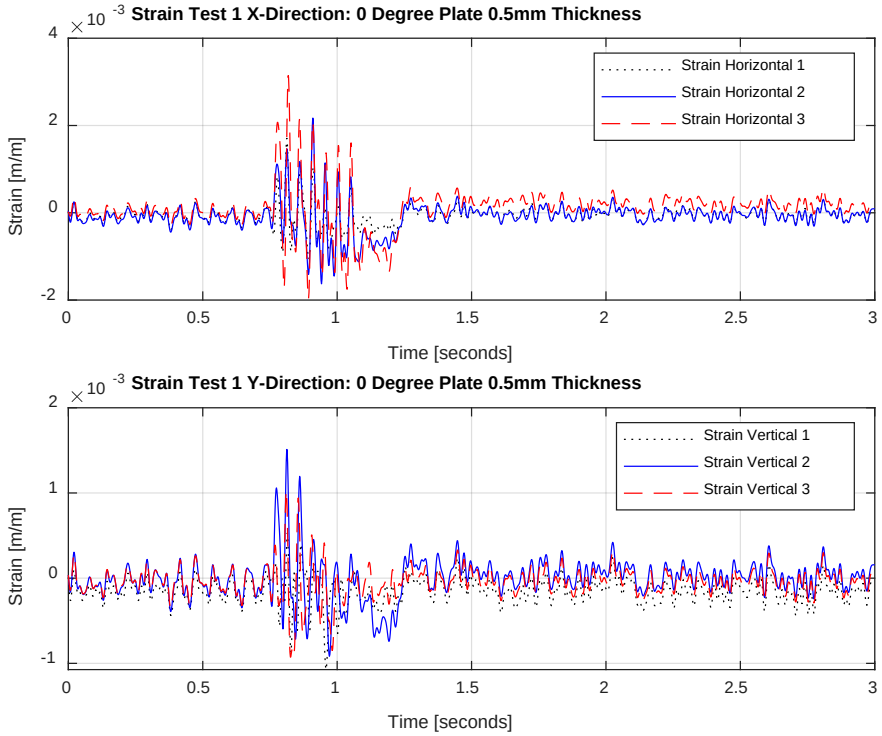

Figure 75. Sample 2 strain 1st blast

A second explosion was performed on Sample 2. The peak pressure it experienced was 35.17 Pa, as shown in Figure 76. This was a similar pressure experienced in the first blast within 5 Pa. Again, as anticipated based on the increased distance between the explosion and the plate, the peak pressure value observed in set-up 2 is substantially less than the peak pressure experienced in set-up 1 for sample 2. The bottom strain gage 3 showed a peak maximum tensile strain value of 0.004223 and a maximum compressive strain value of 0.003061, as displayed in Figure 77. This figure also shows the maximum tensile strain experienced in the y-direction at a value of 0.01104 and maximum compressive strain of 0.009985 also occurring in the strain gage three (bottom strain gage). The initial blast for set-up 2 of sample 2 may have established internal failure not visible externally. Blast 2 showed visible failure severing the plate in three locations, as displayed in Figure 78.

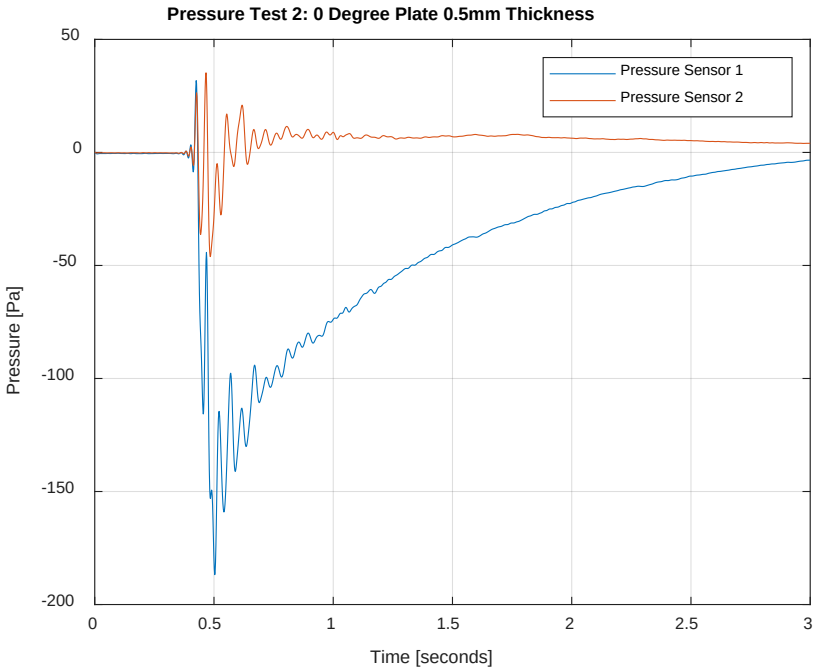

Figure 76. Sample 2 pressure 2nd blast

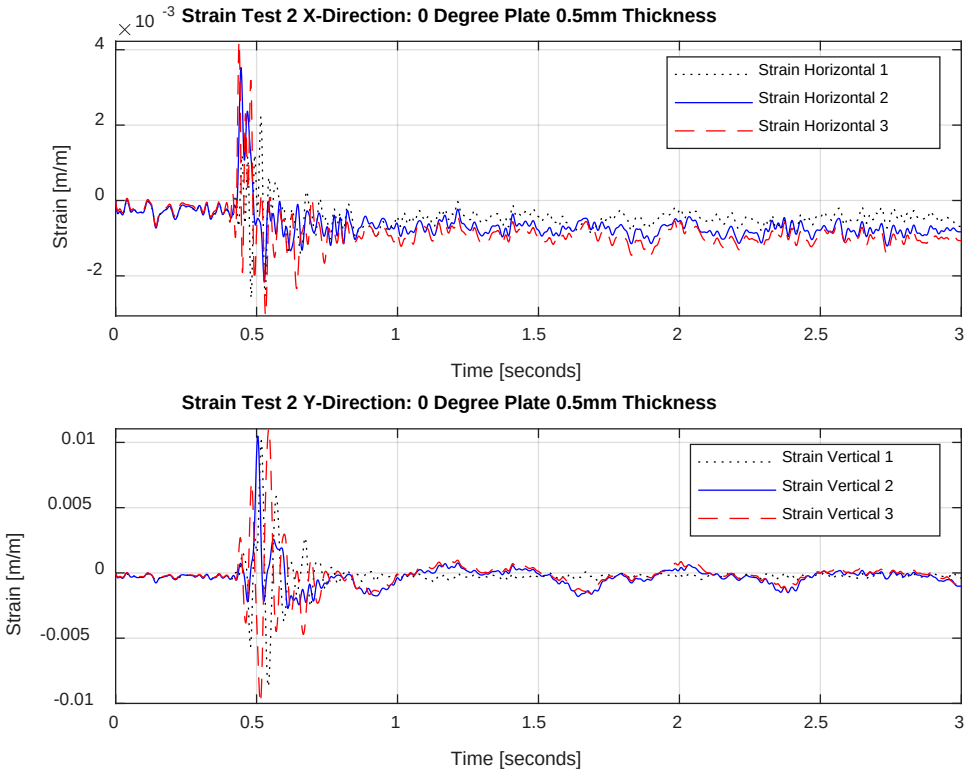

Figure 77. Sample 2 strain 2nd blast

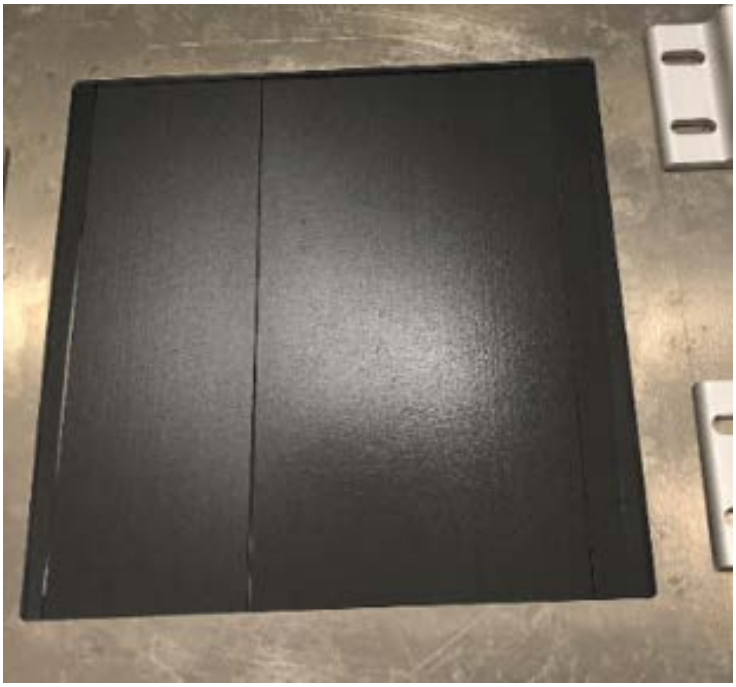

Figure 78. Sample 2 failure after 2nd blast

c. Set-up 1 and 2 Comparison

Table 11 compares the peak pressure and peak tensile and compressive strain values for the first and second explosion that occurred with the two different set-ups utilizing sample 2 plates. Set-up 1 showed no strain value in the x-direction for blast 2 due to the explosion failing the strain gage in this direction. Sample 2 was a 0-degree unidirectional plate that was twice as thick as sample 1. The failure for both set-ups occurred in this weakest direction that had no reinforcement, which was the 90-degree plane, on the second blast. Each measured peak pressure was consistent for the set-up. Set-up 1 showed peak pressure within 2 Pa between blasts, while set-up 2 showed peak pressure within 5 Pa between explosion one and two.

Under set-up 1 blast 1, the plate experienced an initial, small, partially severed failure and subsequently experienced complete severance at the same failure site after being subjected to a subsequent explosion. Set-up 2 had no visible failure in the first blast however it exhibited complete failure after the second blast, showing a peak tensile strain in the y-direction.

Table 11. Sample 2 peak values

	Set-up 1 Blast 1 0.3048 m	**Set-up 1 Blast 2 0.3048 m**	**Set-up 2 Blast 1 0.4572 m**	**Set-up 2 Blast 2 0.4572 m**
Peak Pressure	48.99 Pa	50.32 Pa	30.82 Pa	35.17 Pa
Peak Tensile Strain x-direction	0.001923	-	0.003139	0.004223
Peak Compressive Strain x-direction	0.001556	-	0.001702	0.003061
Peak Tensile Strain y-direction	0.006092	0.007244	0.001511	0.011030
Peak Compressive Strain y-direction	0.001005	0.01613	0.000927	0.009885

3. Sample 3

Sample 3 utilized a cross-ply plate design that had alternating 0 and 90-degree plies with a thickness of 0.5 mm. The outside plies were oriented to 0-degree while the interior plie was oriented to 90-degree, forming a 0–90-0 plate. This plate was strongest plate in the 0-degree direction subject to explosion testing within phase 3. Due to the additional plies and non-unidirectional set-up of this plate, it was not expected to fail in the same manner observed in sample 1 and 2, with failing occurring straight down the 90-degree direction. The same two set-up configurations were used for this sample as were performed on sample 1 and 2, with the addition of set-up 3 which utilized the median distance between set-up 1 and 2 in attempt to better understand the failure of this sample and at what distance it first occurs. In the first set-up, the explosion occurred at 0.3048 meter distance from the vertical plate, the second set-up utilized an extended distance of 0.4572 meter, and the third set-up took place at 0.381 meter. For all set-ups, successive explosions were performed until the plate exhibited visual signs of failure.

a. Set-up 1

The carbon composite sample 3 plate failed after two blasts within set-up 1. The peak pressure it experienced was 50.06 Pa, as shown in Figure 79. Figure 80 shows that the x-direction strain gage three (bottom strain gage) experienced a maximum tensile strain of 0.01465 and a maximum compressive strain of 0.01225. Figure 80 also shows the maximum tensile and compressive experienced in the y-direction also occurred in the strain gage three (bottom strain gage) at a value of 0.01032 and 0.006701, respectively. This first explosion caused no visible failure after removing the plate and rig from the water chamber tank.

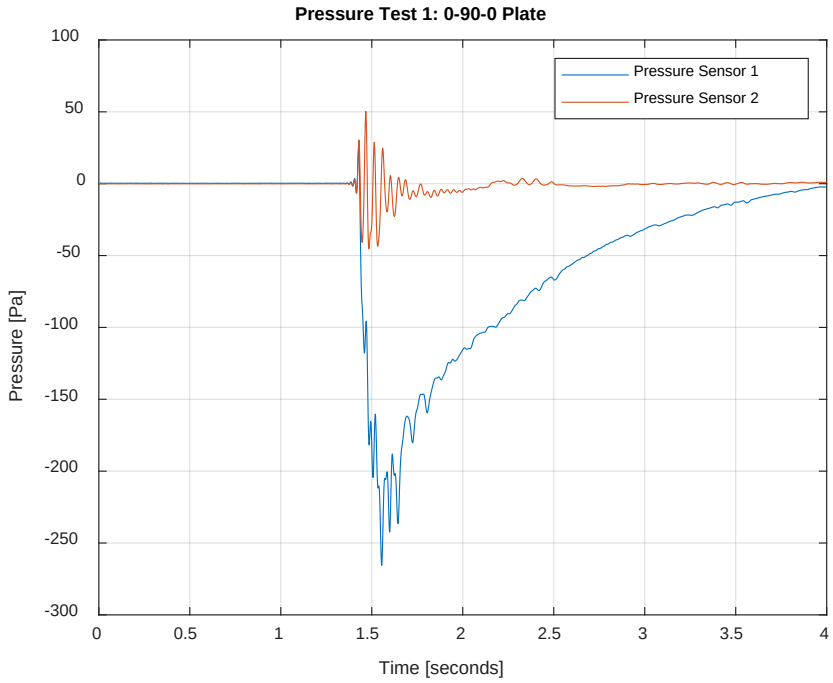

Figure 79. Sample 3 pressure 1st blast

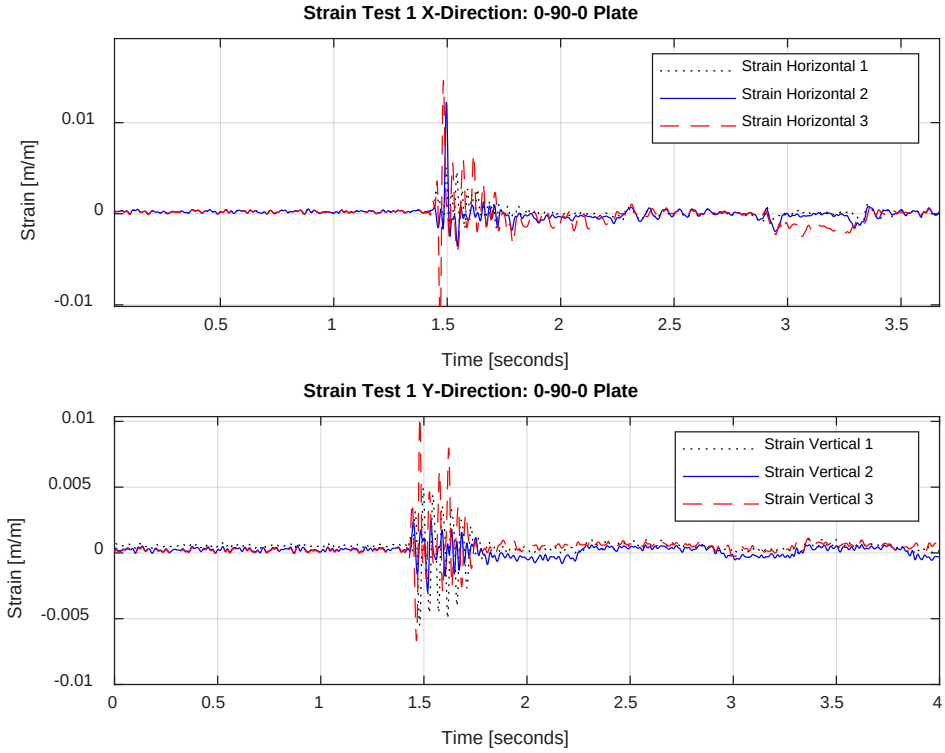

Figure 80. Sample 3 strain 1st blast

A second explosion was performed on Sample 3. The peak pressure it experienced was 93.06 Pa, as shown in Figure 81 and was roughly double the pressure experienced in the first blast. This substantial difference occurred due to placing more liquid nitrogen in the bottle than the previous blast. The bottom strain gage 3 showed a peak maximum tensile strain value of 0.008246 and a maximum compressive strain value of 0.02653 in the x-direction, as displayed in Figure 82. This figure also shows absolute failure in strain gage 1 in the x-direction due to failure of the plate. The maximum tensile strain experienced in the y-direction at a value of 0.02073 and maximum compressive strain of 0.01315 occurring in the strain gage three (bottom strain gage). The initial blast for set-up 2 of sample 3 may have established internal failure but was not visible externally. Blast 2 showed visible failure impacting the plate in two different locations, as displayed in Figure 83. This failure looked visibly different than the previous severing of sample 1 and 2. Both failures have a splinter appearance with the left failure also severing higher into the plate. The plate did not fully split in any location. The right most failure impacted the plate by creating a splinter failure measuring 0.0508 m.

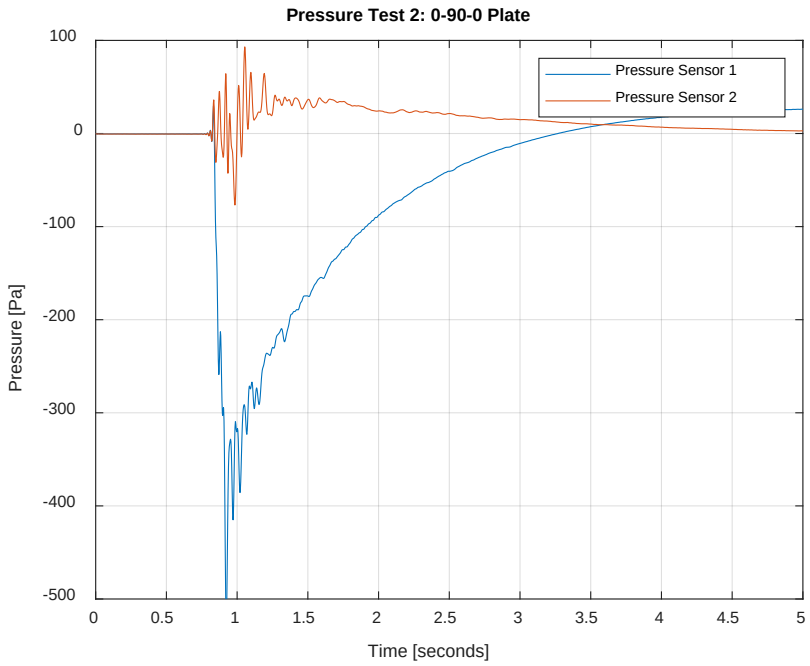

Figure 81. Sample 3 pressure 2nd blast

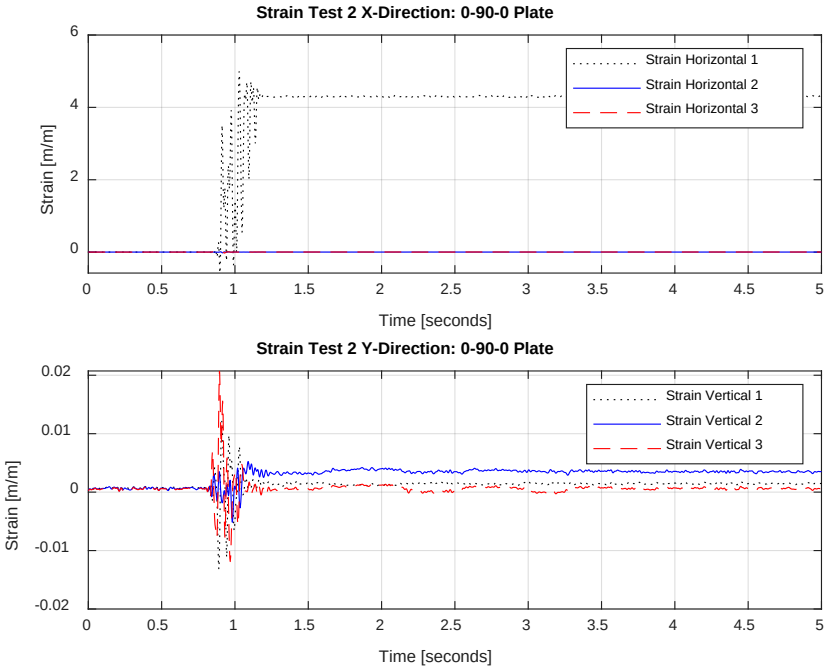

Figure 82. Sample 3 strain 2nd blast

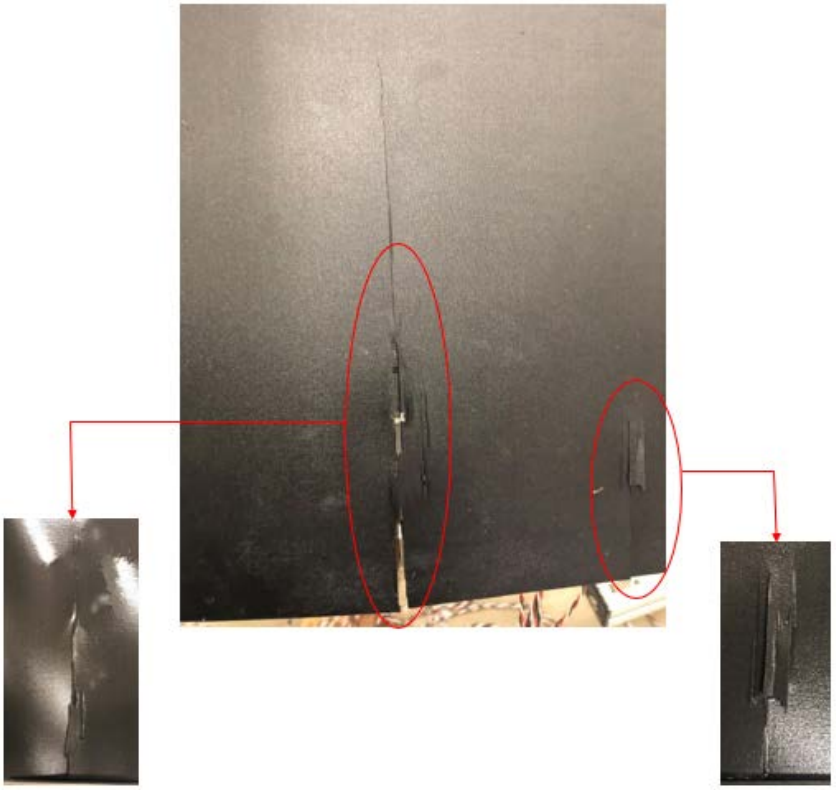

Figure 83. Sample 3 failure after 2nd blast

b. Set-up 2

The carbon composite sample 3 plate was subjected to six blasts within phase 3, set-up 2. The plate did not experience any visual failure within this set-up. The peak pressures for each of the six blasts experienced throughout set-up 2 are shown in Table 12, with the graphical representations displayed in Appendix D. The average peak pressure was 42.55 Pa, with a standard deviation of 7.91. The major outliers were blast 1, which was low due to less liquid nitrogen and being the first test of the sequence, and blast 4, which had a peak higher than all other blasts. Table 13 shows that the x-direction and Table 14 displays the y-direction strain gage maximum tensile strain and maximum compressive strain. These tables also list the ratio of peak compressive or tensile strain to peak pressure. The values in parentheses following the peak strain values indicate which strain gage experienced the maximum value. Strain gage 3 (bottom strain gage) consistently showed the peak tensile and compressive values for all six blasts as displayed in Appendix D. In blast six, the strain gage 3 failed shown in Figure 84. This result could be predicted from the peak tensile strain in stain gage 3 from the previous blast, blast 5. Table 13 shows this value of 0.02004, which is on the same figure of values in set-up 1 that failed the plate. This plate only showed one indentation mark after the six iterations of blasts as seen in Figure 85. Based on the strain values measured, this plate is expected to have internal failure. Potential further blasts would most likely have led to external failure. Shifting from set-up 1 to set-up 2, consisting of moving the blast distance farther away for similar peak pressure values, was shown to have a large effect and subsequently end in the plate not visibly failing.

Table 12. Peak pressure sample 3 set-up 2

Blast Number	Peak Pressure
Blast 1	30.77 Pa
Blast 2	42.14 Pa
Blast 3	47.43 Pa
Blast 4	53.44 Pa
Blast 5	37.24 Pa
Blast 6	44.30 Pa
Average	42.55 Pa
Standard Deviation	7.91

Table 13. Peak strain sample 3 set-up 2 x-direction

Blast Number	Peak Compressive Strain x	Ratio of Peak Compressive Strain to Peak Pressure	Peak Tensile Strain x	Ratio of Peak Tensile Strain to Peak Pressure
Blast 1	0.000778 (2)	2.528×10^{-5}	0.001974 (2)	6.415×10^{-5}
Blast 2	0.005152 (3)	1.223×10^{-4}	0.005205 (3)	1.235×10^{-4}
Blast 3	0.007318 (3)	1.543×10^{-4}	0.01069 (3)	2.254×10^{-4}
Blast 4	0.006696 (3)	1.253×10^{-4}	0.01006 (3)	1.882×10^{-4}
Blast 5	0.004071 (3)	1.093×10^{-4}	0.02004 (3)	5.381×10^{-4}
Blast 6	0.000376 (2)	8.488×10^{-6}	0.003182 (3)	7.183×10^{-5}

Table 14. Peak strain sample 3 set-up 2 y-direction

Blast Number	Peak Compressive Strain y	Ratio of Peak Compressive Strain to Peak Pressure	Peak Tensile Strain y	Ratio of Peak Tensile Strain to Peak Pressure
Blast 1	0.002148 (3)	$6.981x10^{-5}$	0.002172 (3)	$7.059x10^{-5}$
Blast 2	0.002826 (3)	$6.706x10^{-5}$	0.006466 (3)	$1.534x10^{-5}$
Blast 3	0.003929 (3)	$8.284x10^{-5}$	0.005576 (3)	$1.176x10^{-4}$
Blast 4	0.003829 (3)	$7.165x10^{-5}$	0.004004 (3)	$7.493x10^{-5}$
Blast 5	0.00552 (3)	$1.482x10^{-4}$	0.006609 (3)	$1.778x10^{-4}$
Blast 6	0.002487 (3)	$5.614x10^{-5}$	0.002589 (3)	$5.844x10^{-5}$

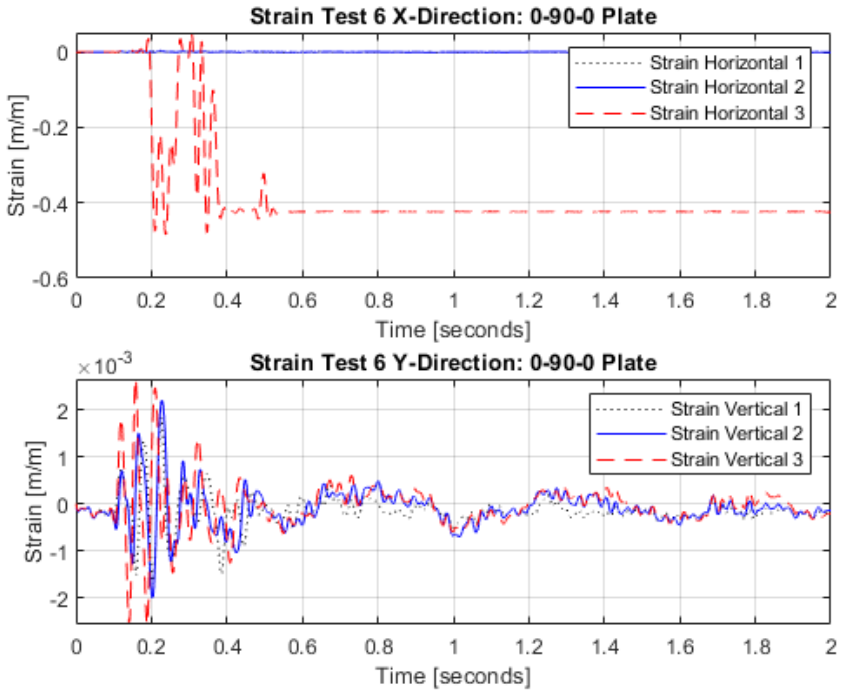

Figure 84. Sample 3 strain 6th blast

Figure 85. Sample 3 failure after 6th blast

c. Set-up 3

The carbon composite sample 3 plate experienced six blasts within phase 3, set-up 3. The plate failed within this set-up after being subjected to the sixth blast. The peak pressures experienced throughout set-up 3 are shown in Table 15, with the graphical representations of this data being displayed in Appendix E. The average peak pressure was 41.03 Pa, with a standard deviation of 4.40. The only major outlier was blast 4, which was noticeably high due to more liquid nitrogen used in the explosion source. Table 16 shows that the x-direction and Table 17 displays the y-direction strain gage maximum tensile strain and maximum compressive strain. These values occurred most prominently in strain gage three. This could be due to a weakness in the plate in this location, or the explosion could have been occurring slightly below center leading to an explosion directly in front of strain gage 3. As shown in Figure 86, strain gage 3 (bottom strain gage) failed in the y-direction on blast six. Strain gage 3 also showed the highest compressive and tensile strain in the x-direction during this sixth blast as well. This plate indicated no visual sign of failure until the sixth iteration of the blasts. After the sixth blast, the plate failed in the center as

displayed in Figure 87. Shifting from set-up 2 to set-up 3 by moving the distance closer for similar peak pressure values was shown to have a large effect on the visible failure.

Table 15. Peak pressure sample 3 set-up 3

Blast Number	Peak Pressure
Blast 1	37.57 Pa
Blast 2	39.85 Pa
Blast 3	37.73 Pa
Blast 4	48.97 Pa
Blast 5	43.18 Pa
Blast 6	38.86 Pa
Average	41.03 Pa
Standard Deviation	4.40

Table 16. Peak strain set-up 3 x-direction

Blast Number	Peak Compressive Strain x	Ratio of Peak Compressive Strain to Peak Pressure	Peak Tensile Strain x	Ratio of Peak Tensile Strain to Peak Pressure
Blast 1	0.01937 (2)	5.156×10^{-4}	0.04251 (3)	1.10×10^{-3}
Blast 2	0.005336 (3)	1.339×10^{-4}	0.003791 (3)	9.513×10^{-5}
Blast 3	0.001043 (3)	2.764×10^{-5}	0.004482 (3)	1.188×10^{-4}
Blast 4	0.002698 (3)	5.510×10^{-5}	0.01775 (3)	3.625×10^{-4}
Blast 5	0.001689 (3)	3.912×10^{-5}	0.003796 (3)	8.791×10^{-5}
Blast 6	0.01975 (2)	5.082×10^{-4}	0.06477 (2)	1.700×10^{-3}

Table 17. Peak strain set-up 3 y-direction

Blast Number	Peak Compressive Strain y	Ratio of Peak Compressive Strain to Peak Pressure	Peak tensile Strain y	Ratio of Peak Tensile Strain to Peak Pressure
Blast 1	0.002912 (3)	$7.751x10^{-5}$	0.00557 (3)	$1.483x10^{-4}$
Blast 2	0.003329 (3)	$8.354x10^{-5}$	0.005909 (3)	$1.483x10^{-4}$
Blast 3	0.003427 (3)	$9.083x10^{-5}$	0.006394 (3)	$1.695x10^{-4}$
Blast 4	0.004429 (3)	$9.044x10^{-5}$	0.007377 (3)	$1.506x10^{-4}$
Blast 5	0.003032 (3)	$7.022x10^{-5}$	0.005431 (2)	$1.258x10^{-4}$
Blast 6	-	-	-	-

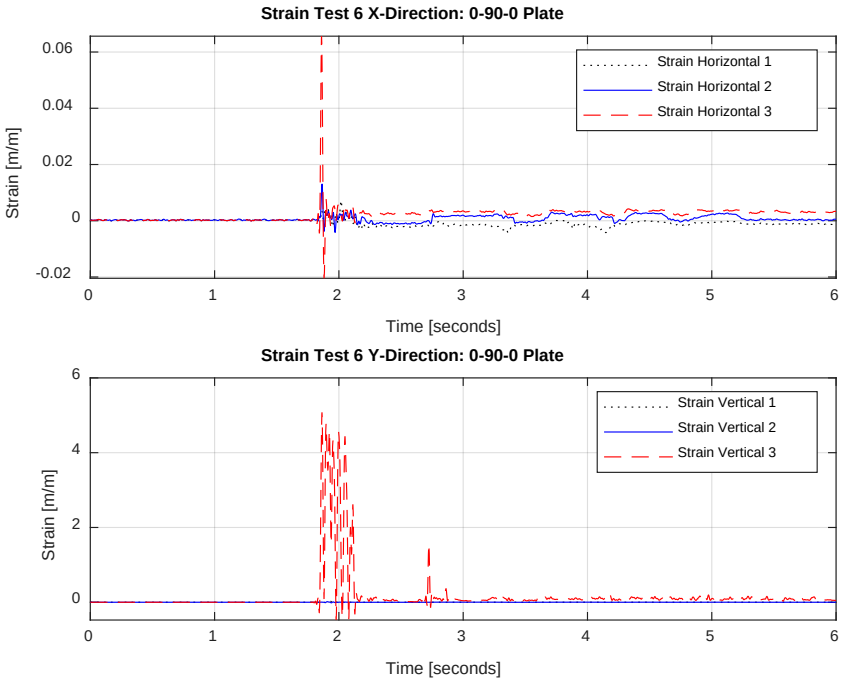

Figure 86. Sample 3 strain 6th blast

Figure 87. Sample 3 set-up 3 after 6th blast

d. Set-up 1, 2, and 3 Comparison

In the first set-up, two explosions occurred at 0.3048 meter distance from the vertical plate. In the second set-up, the extended distance of 0.4572 meter was utilized with six explosions performed. In the third set-up, the distance between the explosion and the plate was changed to 0.381 meter. This distance was selected as it was halfway between set-up 1 and 2 and again six explosions performed. Within set-up 1, the plate experienced failure at two sites after the second blast. One failure resulted in almost complete severance of the plate as show in Figure 88. After the six blasts in set-up 2, the plate had no visible failure but did show an indentation. Set-up 3's final evaluation showed a complete severance through the plate in the same 90-degree direction as set-up 1. Within both set-up 1 and 3 the failure was not a clean split, but in both cases showed a splintered effect.

Figure 88. Phase 3 sample 3 failure comparison

Set-up 2 and 3 were comparable and consistent tests due to performing the same six blasts in both cases, as well as having similar average pressures throughout all six blasts as shown in Table 16. Set-up 1 failed after two blasts, most likely due to having such a higher average pressure than set-up 2 or 3. For better comparable results between all three set-ups, set-up 1 should be performed with average pressure occurring in the lower 40 Pa in order to be more consistent with the pressures show in set-up 2 and 3. The peak compressive and tensile strains between the two plates that exhibited failure in set-up 1 and 3 were similar in the final blast performed on the plate, shown in Table 18. Based on the peak strain value, a failure result more than just an indentation on set-up 2 was expected. This result in set-up 2 occurred primarily due being the farthest distance from the plate to the explosion. Investigating various additional distances within these three set-ups would results in further failure analysis with respect to distance for sample 3 plate.

Table 18. Average pressure sample 3

Set-up Number	**Average Pressure**	**Peak Strain**
Set-up 1	71.56 Pa	0.02653
Set-up 2	42.55 Pa	0.02004
Set-up 3	41.03 Pa	0.01975

4. Sample 4

Sample 4 utilized a cross-ply plate design that had alternating 0-degree and 90-degree plies with a thickness of 0.5 mm. The outside plies were oriented to 0-degree while the interior plies were oriented to 90-degree, forming a 0–90-90-0 plate. This plate was the strongest plate in the 90-degree direction subjected to explosion testing within phase 3 testing. Due to the additional plies and non-unidirectional set-up of this plate, it was expected to fail in the same manner observed in sample 3 but after being subjected to additional blasts. This later anticipated failure is due to the addition 90-degree layer internally and the associated increase in support. The same two set-up configurations were used for this sample as were performed on sample 1, 2, and 3, with the addition of set-up 3, which utilized the median distance between set-up 1 and 2 in attempt to better understand the failure of this sample and at what distance it first occurs. In the first set-up, the explosion occurred at 0.3048 meter distance from the vertical plate, the second set-up utilized an extended distance of 0.4572 meter, and the third set-up took place at 0.381 meter. For all set-ups, successive explosions were performed until the plate exhibited visual signs of failure.

a. Set-up 1

The carbon composite sample 4 plate failed after three blasts within set-up 1. The peak pressure it experienced within the three blasts is shown in Table 19, with figures in Appendix F. All of the peak pressure values were substantially higher than all other maximum pressures experienced in phase 3 testing. Table 20 and 21 show the x-direction and y-direction maximum tensile and compressive strain. The ratio between peak strain to peak pressure is also shown for the tensile and compressive strains. This value is significant in order to determine the characteristics of the elastic region based on when the various set-ups visibly fail. Figure 89 and 90 shows the tensile and compressive strain experienced in the x-direction and y-direction. After removing the plate and the rig from the water chamber tank it was determined that this first explosion caused no visible failure. The second blast, however, did cause an indentation in the center of the plate, as well as failure in the lower left corner of the plate measuring 0.0653 meter, as displayed in Figure 91. This

initial visibly failure in this region of the plate is to be expected since both the first two blasts strain gage 3 (bottom strain gage) experienced the maximum tensile and compressive stress in the x and y direction.

Table 19. Peak pressure sample 4 set-up 1

Blast Number	Peak Pressure
Blast 1	165.7 Pa
Blast 2	364.6 Pa
Blast 3	347.7 Pa

Table 20. Peak strain sample 4 set-up 1 x-direction

Blast Number	Peak Compressive Strain x	Ratio of Peak Compressive Strain to Peak Pressure	Peak tensile Strain x	Ratio of Peak Tensile Strain to Peak Pressure
Blast 1	0.002127 (3)	1.284×10^{-5}	0.003983 (2)	2.404×10^{-5}
Blast 2	0.009517 (3)	2.610×10^{-5}	0.005917 (3)	1.623×10^{-5}
Blast 3	0.009905 (3)	2.849×10^{-5}	0.01128 (3)	3.244×10^{-5}

Table 21. Peak strain sample 4 set-up 1 y-direction

Blast Number	Peak Compressive Strain y	Ratio of Peak Compressive Strain to Peak Pressure	Peak tensile Strain y	Ratio of Peak Tensile Strain to Peak Pressure
Blast 1	0.002451 (3)	1.479×10^{-5}	0.007103 (3)	4.287×10^{-5}
Blast 2	0.01014 (3)	2.781×10^{-5}	0.0147 (2)	4.032×10^{-5}
Blast 3	0.008447 (3)	2.429×10^{-5}	0.01168 (3)	3.359×10^{-5}

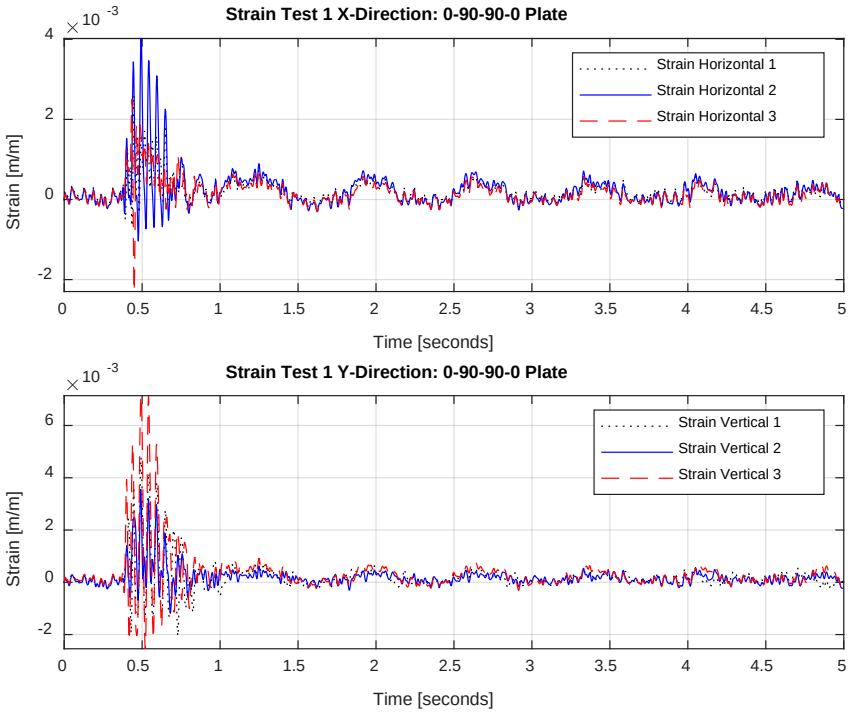

Figure 89. Sample 4 strain 1st blast

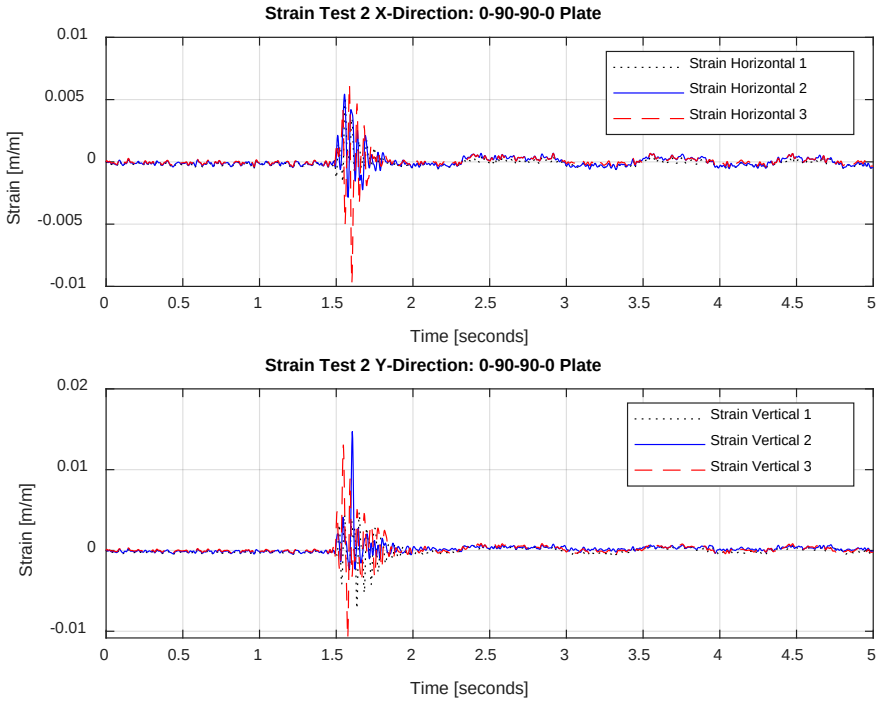

Figure 90. Sample 4 strain 2nd blast

Figure 91. Sample 4 failure after 2nd blast

After the initial lower splinter failure on sample 4, the third and final blast utilized this pre-existing flaw and further splintered the left-hand corner. In Figure 92, the tensile and compressive strain experienced in both the x-direction and y-direction show peak pressures detected by strain gage 3 (bottom strain gage). The last blast exacerbated the initial splinter to a longer length of 0.1016 meter while also connecting the lower splinter with the center indentation as displayed in Figure 93. The location of the initial visibly failure was anticipated in the lower portion of the plate since both in the first two blasts strain gage 3 (bottom strain gage) experienced the maximum tensile and compressive stress in the x and y-direction.

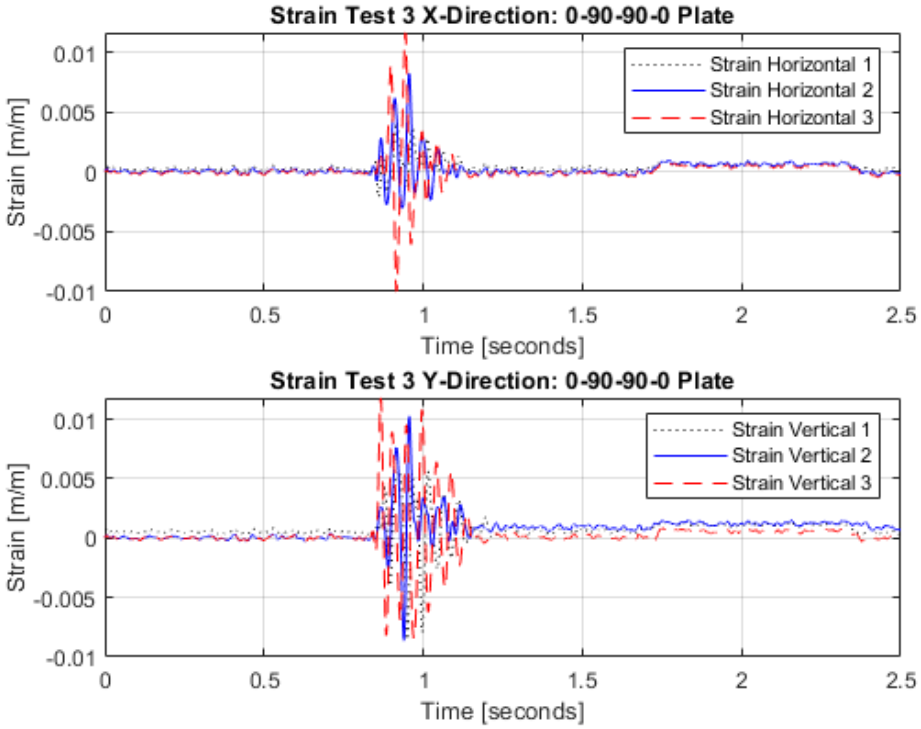

Figure 92. Sample 4 strain 3rd blast

Figure 93. Sample 4 failure after 3rd blast

b. Set-up 2

The carbon composite sample 4 plate was subjected to six blasts within phase 3, set-up 2. The plate did not experience any visual failure within this set-up. The peak pressures for each of the six blasts experienced throughout set-up 2 are shown in Table 22, with the graphical representations displayed in Appendix G. The average peak pressure was 43.56 Pa, with a standard deviation of 4.36. The major outliers were blast 3, which was low due to less liquid nitrogen and being the first test of the sequence, and blast 4, which had a peak higher than all other blasts. Table 23 (depicting the x-direction) and Table 24 (depicting the y-direction) show strain gage maximum tensile strain and maximum compressive strain. Unlike previous sample 3 results, one specific strain gage did not consistently show the peak tensile and compressive values for all six blasts. As shown in Table 22 and Table 23 through the values in parentheses, different strain gages showed peak values for the six different blasts. This result could have contributed to the plate not visibly failing. More consistency in the blast location and the amount of liquid nitrogen could better improve the results. The impact of shifting from set-up 1 to set-up 2, consisting of moving the blast distance farther away for similar peak pressure values, was shown to have a large effect on the plate not visibly failing.

Table 22. Peak pressure sample 4 set-up 2

Blast Number	Peak Pressure
Blast 1	41.89 Pa
Blast 2	42.48 Pa
Blast 3	37.48 Pa
Blast 4	50.07 Pa
Blast 5	42.60 Pa
Blast 6	46.86 Pa
Average	43.56 Pa
Standard Deviation	4.36

Table 23. Peak strain sample 4 set-up 2 x-direction

Blast Number	Peak Compressive Strain x	Ratio of Peak Compressive Strain to Peak Pressure	Peak Tensile Strain x	Ratio of Peak Tensile Strain to Peak Pressure
Blast 1	0.001371 (2)	3.265×10^{-5}	0.002766 (3)	6.589×10^{-5}
Blast 2	0.03789 (1)	8.920×10^{-4}	0.008899 (1)	2.095×10^{-4}
Blast 3	0.0009182 (2)	2.450×10^{-5}	0.001565 (3)	4.176×10^{-5}
Blast 4	0.001289 (2)	2.574×10^{-5}	0.002443 (3)	4.879×10^{-5}
Blast 5	0.001345 (3)	3.157×10^{-5}	0.002735 (1)	6.420×10^{-5}
Blast 6	0.001444 (3)	3.082×10^{-5}	0.002692 (2)	5.745×10^{-5}

Table 24. Peak strain sample 4 set-up 2 y-direction

Blast Number	Peak Compressive Strain y	Ratio of Peak Compressive Strain to Peak Pressure	Peak Tensile Strain y	Ratio of Peak Tensile Strain to Peak Pressure
Blast 1	0.0014 (1)	3.335×10^{-5}	0.003141 (1)	7.482×10^{-5}
Blast 2	0.002836 (3)	6.676×10^{-5}	0.003489 (1)	8.213×10^{-5}
Blast 3	0.002164 (3)	5.774×10^{-5}	0.001656 (1)	4.418×10^{-5}
Blast 4	0.002885 (3)	5.762×10^{-5}	0.003900 (2)	7.789×10^{-5}
Blast 5	0.003097 (3)	7.270×10^{-5}	0.003768 (3)	8.845×10^{-5}
Blast 6	0.002914 (3)	6.219×10^{-5}	0.003889 (1)	8.299×10^{-5}

c. Set-up 3

The carbon composite sample 3 plate experienced six blasts within phase 3, set-up 3. The plate failed within this set-up after being subjected to the third blast. The peak pressures experienced throughout set-up 3 are shown in Table 25, with the graphical representations of this data being displayed in Appendix H. The average peak pressure was 48.75 Pa, with a standard deviation of 13.32. The only major outliers were blast 5 and 6, which were noticeably high due to more liquid nitrogen used in the explosion source. Table 26 shows that the x-direction and Table 27 displays the y-direction strain gage maximum tensile strain and maximum compressive strain for the first four blasts. All strain gages failed on blast 5 and 6. The maximum x-direction and y-direction strain values occurred in the tensile positive direction. As shown in Figure 94, the failure occurred in the center upper portion of the plate measuring 0.1524 meter after the third blast. The blasts were continued up to the sixth blast. The initial visual failure did not progress nor completely severe the plate. As shown in Table 25, the sixth blast was increased in an attempt to take the plate to failure.

Table 25. Peak pressure sample 4 set-up 3

Blast Number	Peak Pressure
Blast 1	31.96 Pa
Blast 2	49.03 Pa
Blast 3	46.32 Pa
Blast 4	42.53 Pa
Blast 5	50.31 Pa
Blast 6	72.37 Pa
Average	48.75 Pa
Standard Deviation	13.32

Table 26. Peak strain sample 4 set-up 2 x-direction

Blast Number	Peak Compressive Strain x	Ratio of Peak Compressive Strain to Peak Pressure	Peak Tensile Strain x	Ratio of Peak Tensile Strain to Peak Pressure
Blast 1	0.00114 (3)	3.567×10^{-5}	0.001281 (3)	4.081×10^{-5}
Blast 2	0.3881 (3)	7.900×10^{-3}	2.258 (3)	4.610×10^{-2}
Blast 3	0.004857 (1)	1.049×10^{-4}	0.006359 (2)	1.373×10^{-4}
Blast 4	0.2882 (3)	6.800×10^{-3}	2.252 (3)	5.300×10^{-2}

Table 27. Peak strain sample 4 set-up 2 y-direction

Blast Number	Peak Compressive Strain y	Ratio of Peak Compressive Strain to Peak Pressure	Peak Tensile Strain y	Ratio of Peak Tensile Strain to Peak Pressure
Blast 1	0.3316 (3)	1.040×10^{-2}	0.002674 (3)	8.367×10^{-5}
Blast 2	0.3384 (3)	6.900×10^{-3}	4.81 (1)	9.810×10^{-2}
Blast 3	2.013 (2)	4.350×10^{-2}	1.358 (3)	2.930×10^{-2}
Blast 4	4.817 (2)	1.133×10^{-1}	4.646 (3)	1.092×10^{-1}

Figure 94. Sample 4 set-up 3 after 3rd blast

d. Set-up 1, 2, and 3 Comparison

In the first set-up, three explosions occurred at 0.3048 meter distance from the vertical plate. In the second set-up, the extended distance of 0.4572 meter was utilized with six explosions performed. In the third set-up, the distance between the explosion and the plate was changed to 0.381 meter. This distance was selected as it was halfway between set-up 1 and 2; again, six explosions were performed. Within set-up 1, the plate experienced failure after the second blast, further failing following the third and final blast. After the six blasts in set-up 2, the plate had no visible failure. Set-up 3's final evaluation showed a partial split through the plate in the same 90-degree direction as sample 3. Within both set-up 1 and 3, the failure was not a clean split, but rather a splintered effect similar to sample 3, as shown in Figure 95.

Figure 95. Phase 3 sample 4 failure comparison

If performed again, set-up 1 should utilize less liquid nitrogen since all of the peak pressure values were drastically higher by 250 Pa then the averages experienced in set-up 2 and 3.

V. CONCLUSION AND FUTURE WORK

A. CONCLUSION

Within this study the three phases of testing yielded different results, some of which lead to further questions and studies. In phase 1 of testing, pressure oscillated positive and negative, as shown by pressure readings within all phases of the study, while the peak pressure consistently decayed. Secondly, depending on the conversion rate from the liquid to gas state of the nitrogen, the maximum positive pressure produced from each explosion may occur during the first or second peak, as observed in the experiment and simulation. More investigation must be pursued within the pressure results seen in phase 1.

Phase 2 showed both the strength and future application of the orthotropic laminate twill weave at a 0/90-degree orientation with a textured finish. In the phase 2 orientation, none of these plates showed any indications of failure. Further studies must be performed to test the limitations of this strong performing plate in the phase 3 orientation. From phase 2 testing, it appears that this plate type is able to perform even stronger than the best performing sample 4 plate did in phase 3 testing.

Despite consistent conditions, Phase 3 samples exhibited various types of failure. Sample 1 and 2 were each unidirectional, laminate plates of 0.25 mm and 0.5 mm nominal thickness respectively. These two plates failed in a severed manner with clean breaks. Sample 3 was a cross-ply plate design that had two outer 0-degree plie with a 90-degree plie in the center forming a 0–90-0 plate of thickness 0.5 mm. Sample 4 also used a cross-ply design but with an additional sheet of 90-degree plie internally forming a 0–90-90-0 plate. Both sample 3 and sample 4 failed in a splintered manner. Not all of the plates that exhibited visual signs of failure severed all the way through – in some instances, visual failure was only observed on the small corners of the plate or otherwise presented as an indentation. Additionally, sample 3 and 4 pursued the added variable of distance to the experiment. Further experiments should pursue optimal failure distance for the given liquid nitrogen blast.

B. FUTURE WORK

The primary focus of this study was to investigate the failure point of carbon composite plates when submerged in water and held in place by a rig. Future work should investigate the failure of these same carbon composite plates within a closed pressure vessel air-backed system. The plate should have water on one side and air on the other side. This air backed set-up would contribute to modeling the failure of carbon composites in a more similar setting to the shipboard use of future applications of this material.

Another avenue of investigation should be through simulation and computer modeling utilizing finite element method (FEM). This could be used to validate the results of the various experiments already conducted within the water chamber as well as any new air backed testing using the same carbon composite plates.

Furthermore, examination should be conducted on the cause behind the pressure sensor activity observed in phase 3 of testing. On numerous occasions the sensor went drastically negative, hit a peak minimum pressure, and then returned to a steady state value. High speed video as well as underwater video would allow for more data on this particular point.

APPENDIX A. CALIBRATION DATA

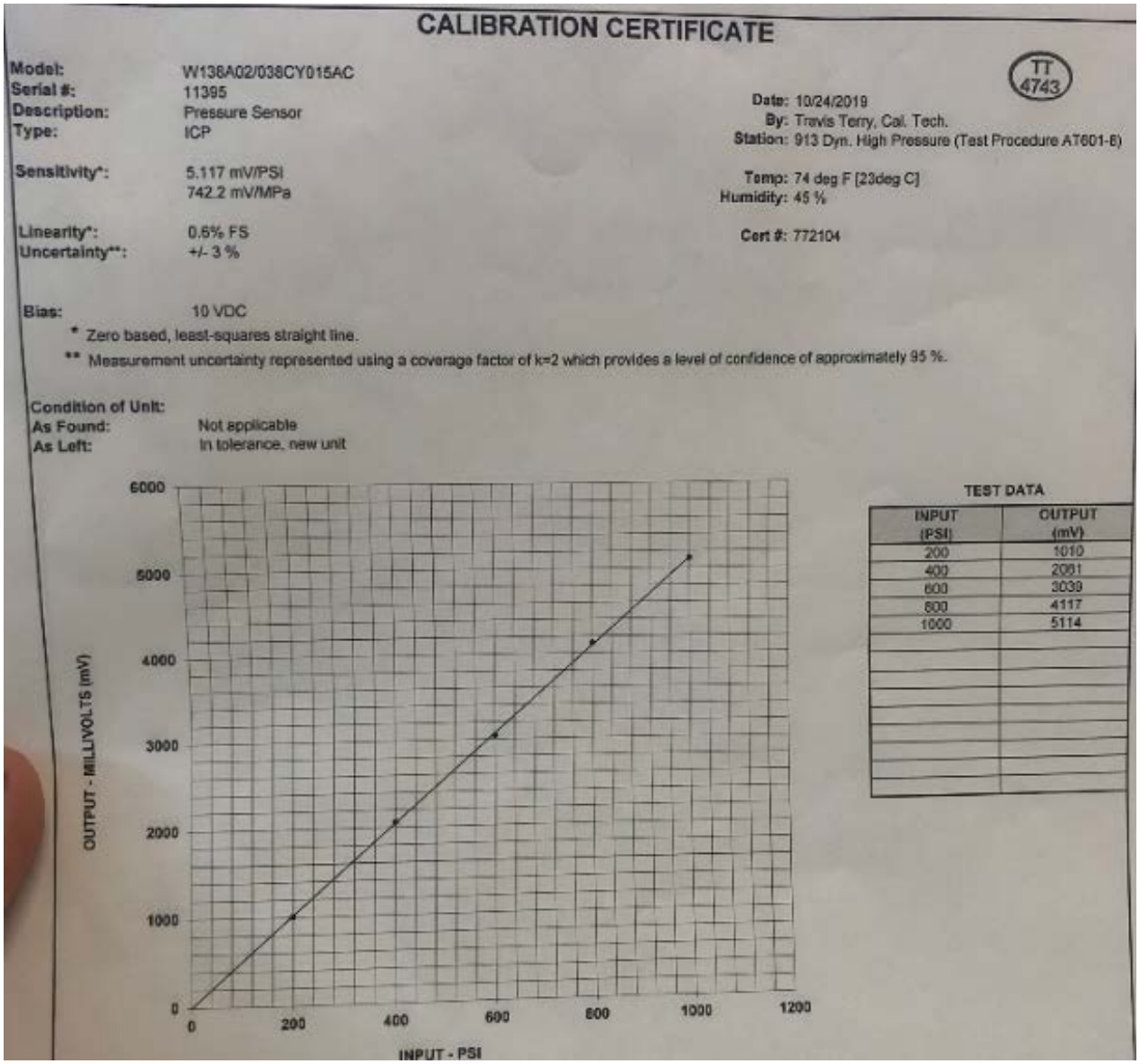

CALIBRATION CERTIFICATE

TT 4743

Model: W136A02/038CY015AC
Serial #: 11395
Description: Pressure Sensor
Type: ICP

Date: 10/24/2019
By: Travis Terry, Cal. Tech.
Station: 913 Dyn. High Pressure (Test Procedure AT601-8)

Sensitivity*: 5.117 mV/PSI
742.2 mV/MPa

Temp: 74 deg F [23deg C]
Humidity: 45 %

Linearity*: 0.6% FS
Uncertainty**: +/- 3 %

Cert #: 772104

Bias: 10 VDC

* Zero based, least-squares straight line.

** Measurement uncertainty represented using a coverage factor of k=2 which provides a level of confidence of approximately 95 %.

Condition of Unit:
As Found: Not applicable
As Left: In tolerance, new unit

TEST DATA

INPUT (PSI)	OUTPUT (mV)
200	1010
400	2061
600	3039
800	4117
1000	5114

OUTPUT - MILLIVOLTS (mV)

6000
5000
4000
3000
2000
1000
0

0 200 400 600 800 1000 1200

INPUT - PSI

Figure 96. Calibration certificate pressure sensor 1

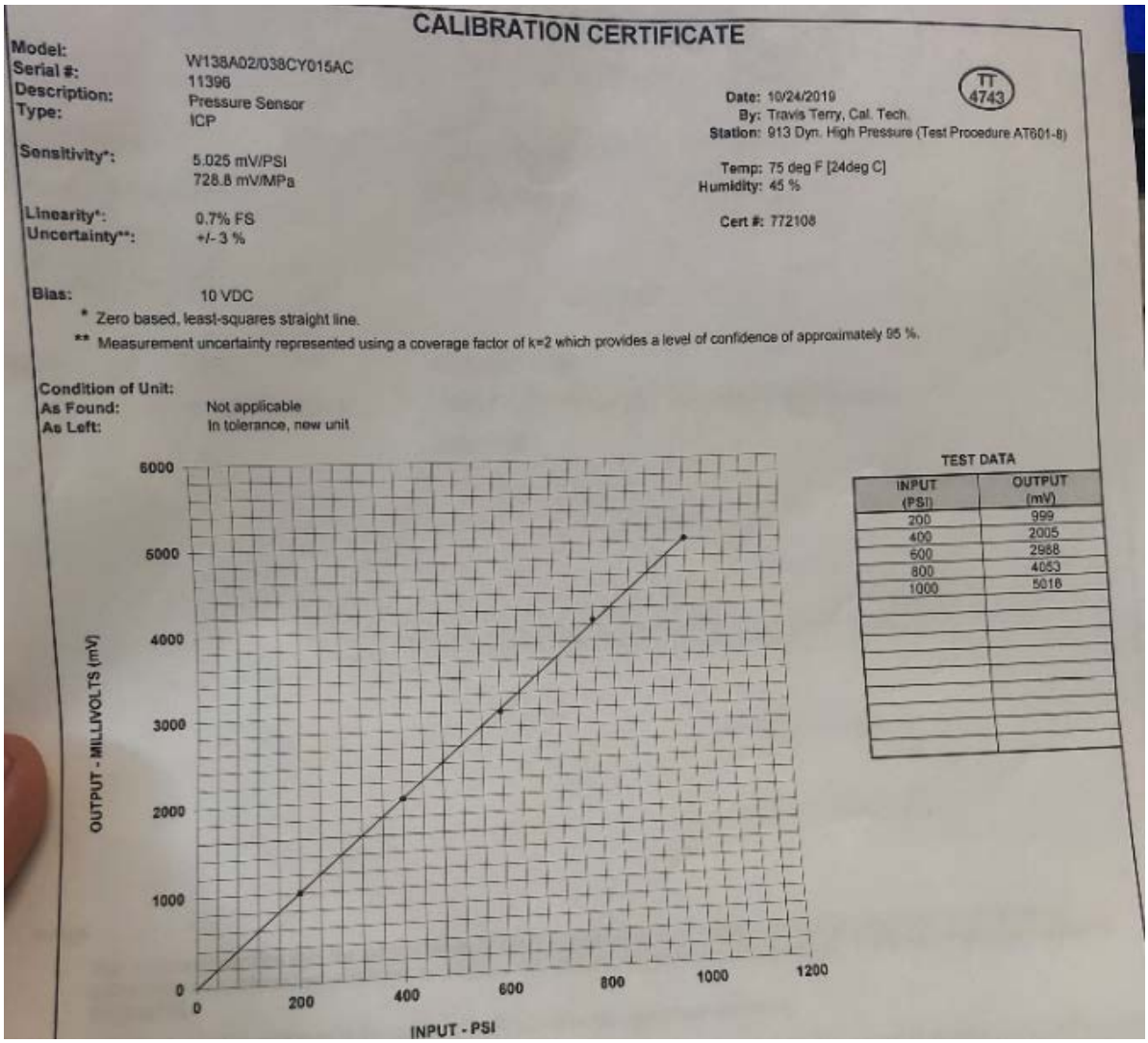

CALIBRATION CERTIFICATE

Model: W138A02/038CY015AC
Serial #: 11396
Description: Pressure Sensor
Type: ICP

TT 4743

Date: 10/24/2019
By: Travis Terry, Cal. Tech.
Station: 913 Dyn. High Pressure (Test Procedure AT601-8)

Sensitivity*: 5.025 mV/PSI
728.8 mV/MPa

Temp: 75 deg F [24deg C]
Humidity: 45 %

Linearity*: 0.7% FS
Uncertainty**: +/- 3 %

Cert #: 772108

Bias: 10 VDC

* Zero based, least-squares straight line.

** Measurement uncertainty represented using a coverage factor of k=2 which provides a level of confidence of approximately 95 %.

Condition of Unit:
As Found: Not applicable
As Left: In tolerance, new unit

TEST DATA

INPUT (PSI)	OUTPUT (mV)
200	999
400	2005
600	2988
800	4053
1000	5016

OUTPUT - MILLIVOLTS (mV)

6000
5000
4000
3000
2000
1000
0

0 200 400 600 800 1000 1200

INPUT - PSI

Figure 97. Calibration certificate pressure sensor 2

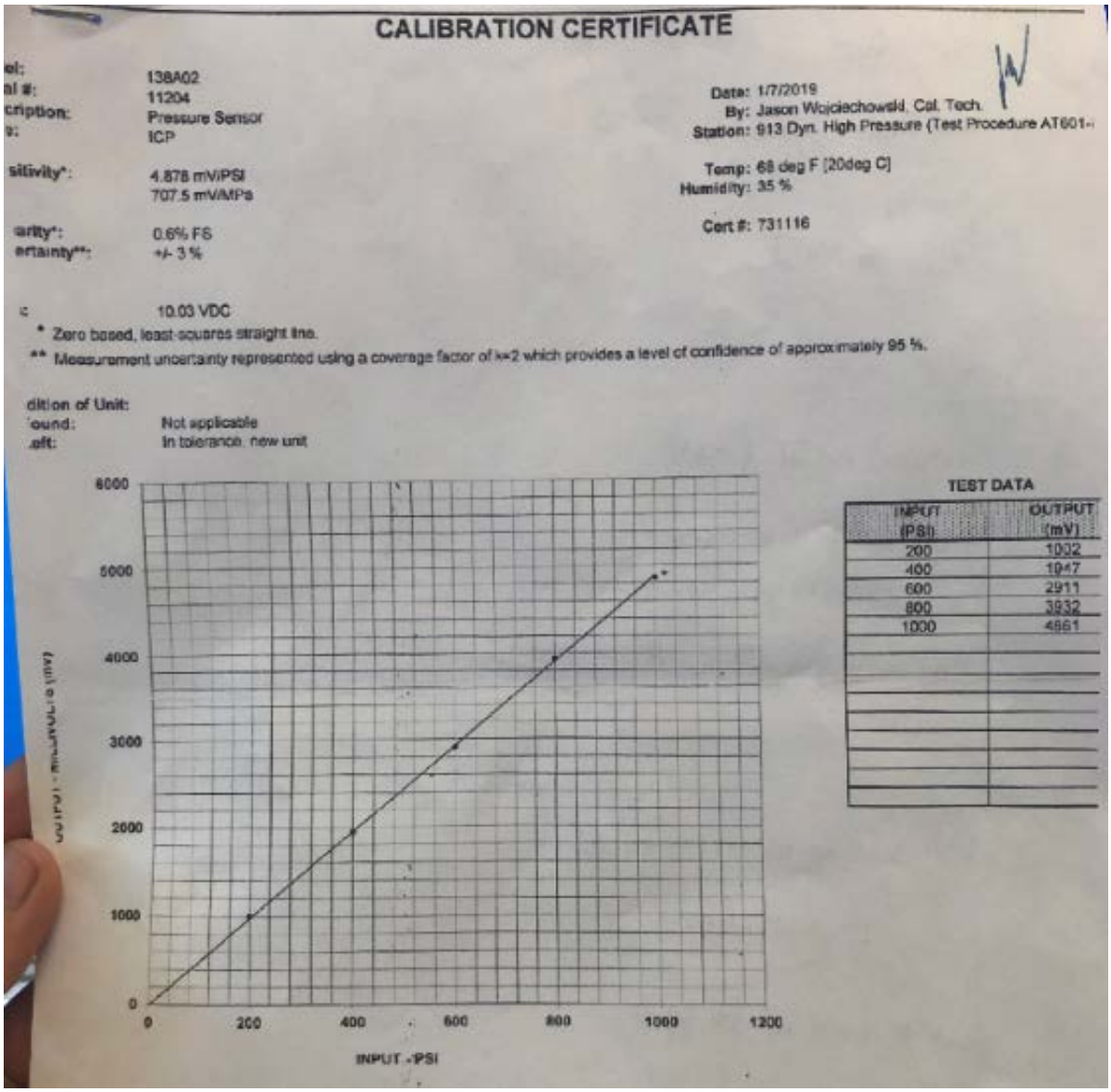

Figure 98. Calibration certificate pressure sensor 3

THIS PAGE INTENTIONALLY LEFT BLANK

APPENDIX B. PHASE 2 THIN PLATE PRESSURE FIGURES

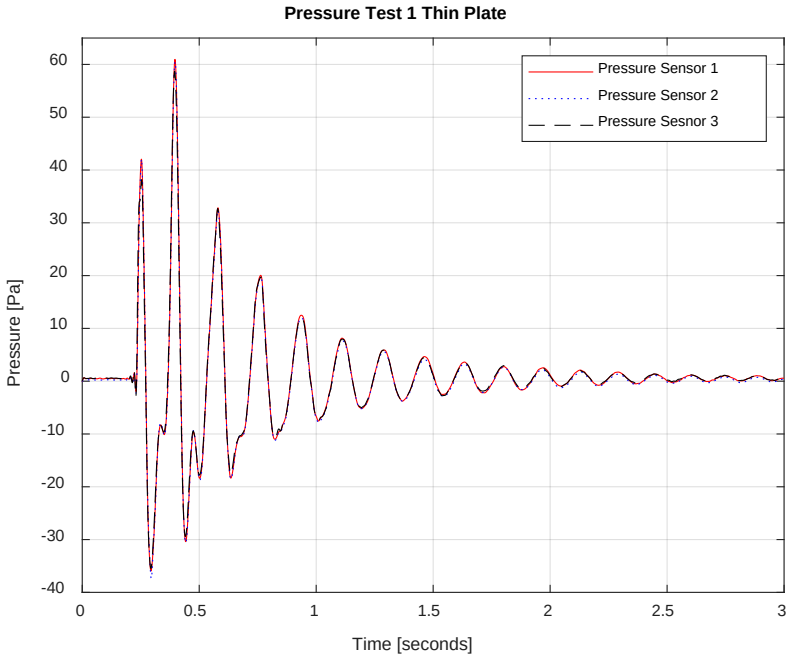

Figure 99. Pressure thin plate 1st blast

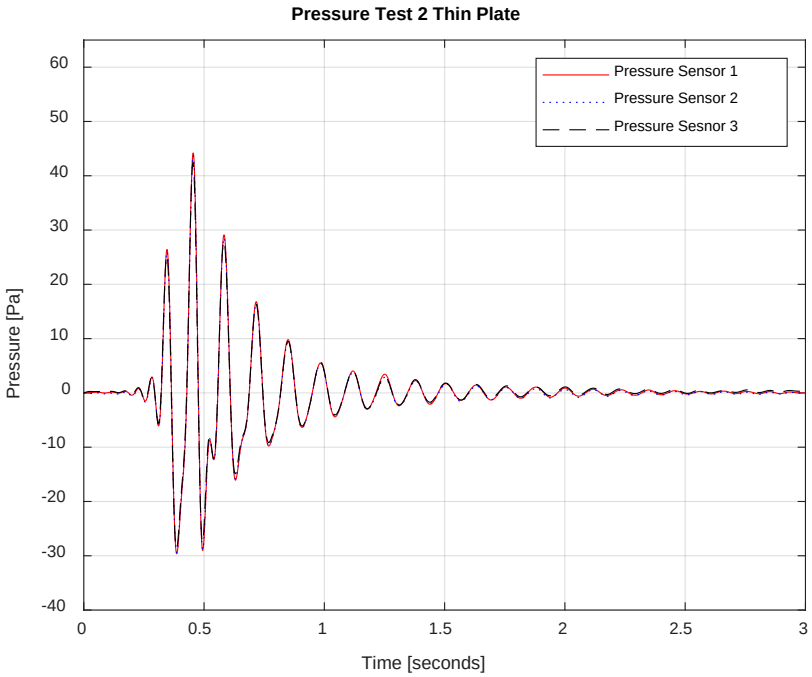

Figure 100. Pressure thin plate 2nd blast

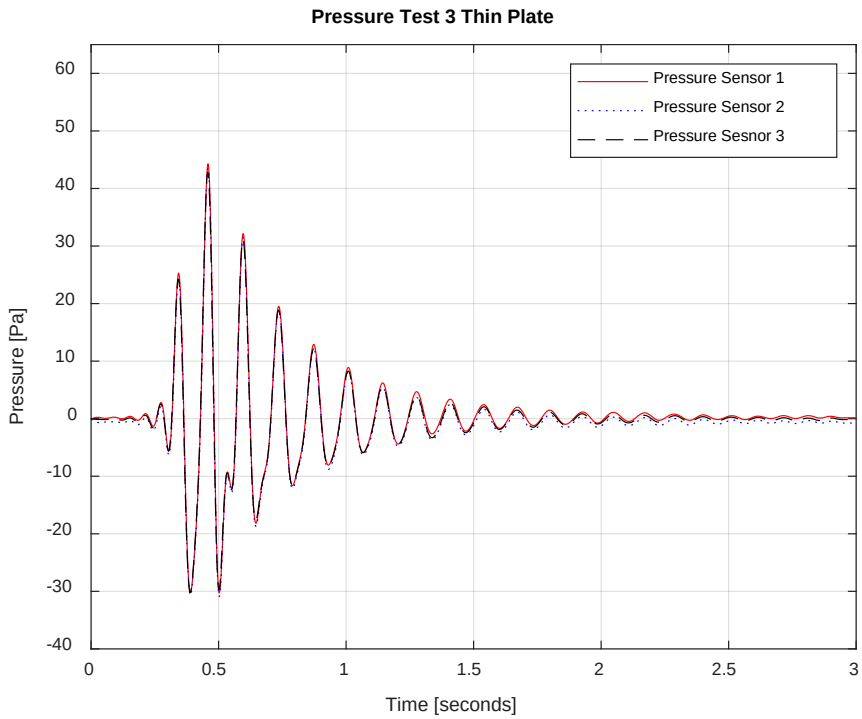

Figure 101. Pressure thin plate 3rd blast

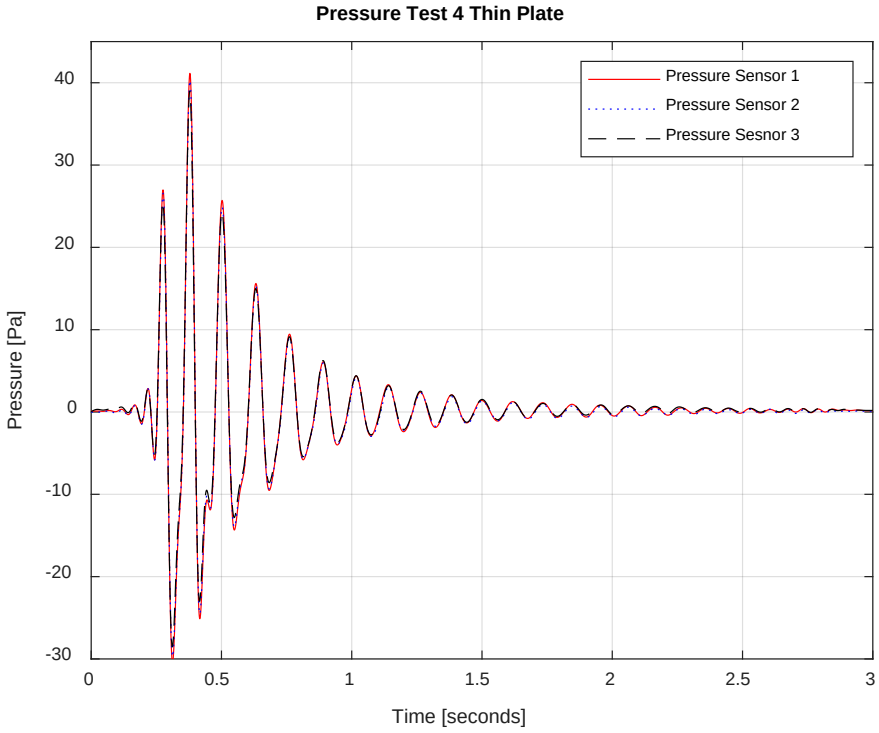

Figure 102. Pressure thin plate 4th blast

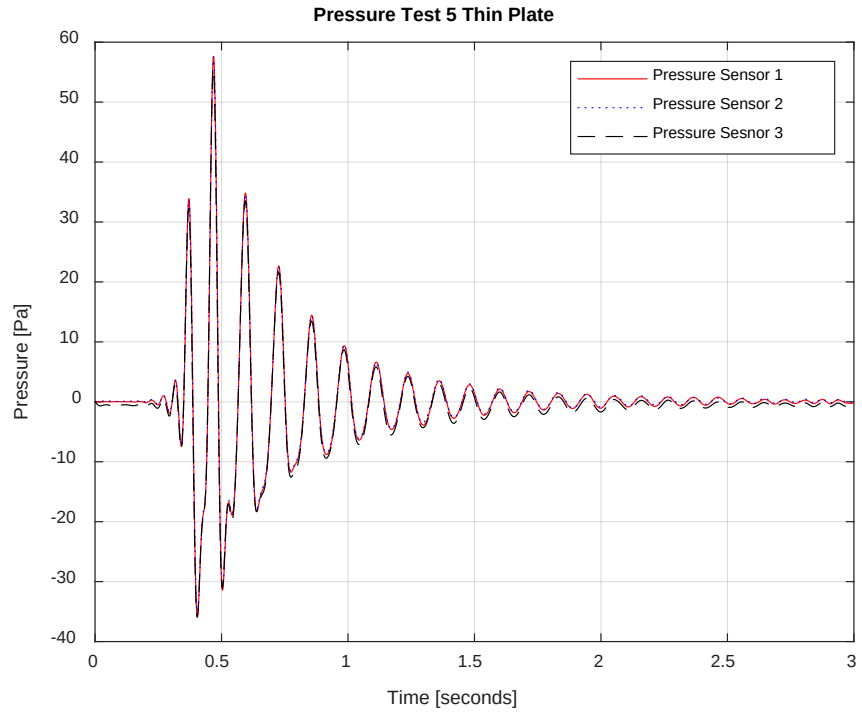

Figure 103. Pressure thin plate 5th blast

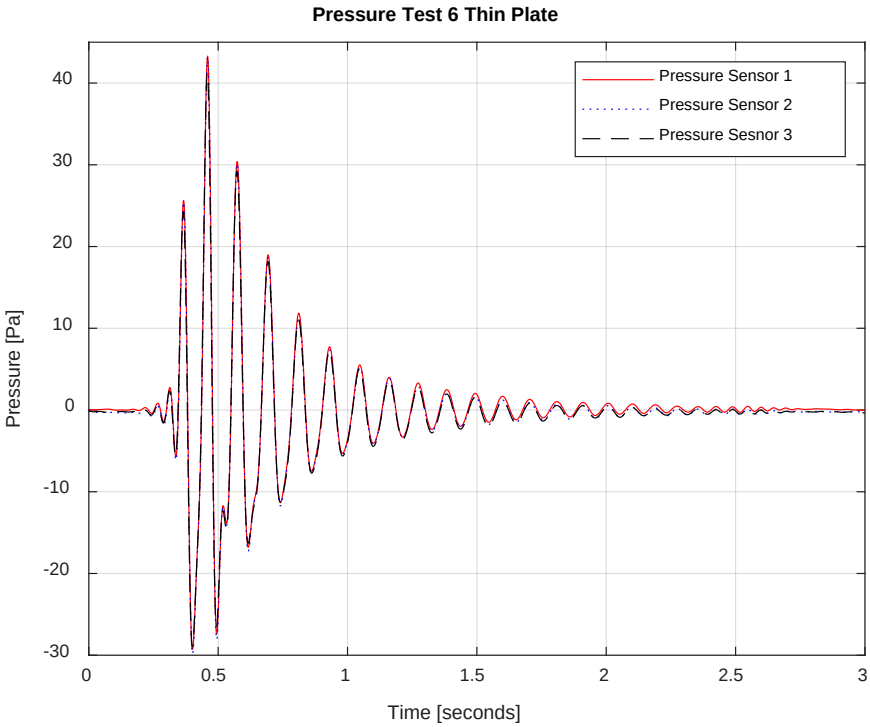

Figure 104. Pressure thin plate 6th blast

THIS PAGE INTENTIONALLY LEFT BLANK

APPENDIX C. PHASE 2 THICK PLATE PRESSURE FIGURES

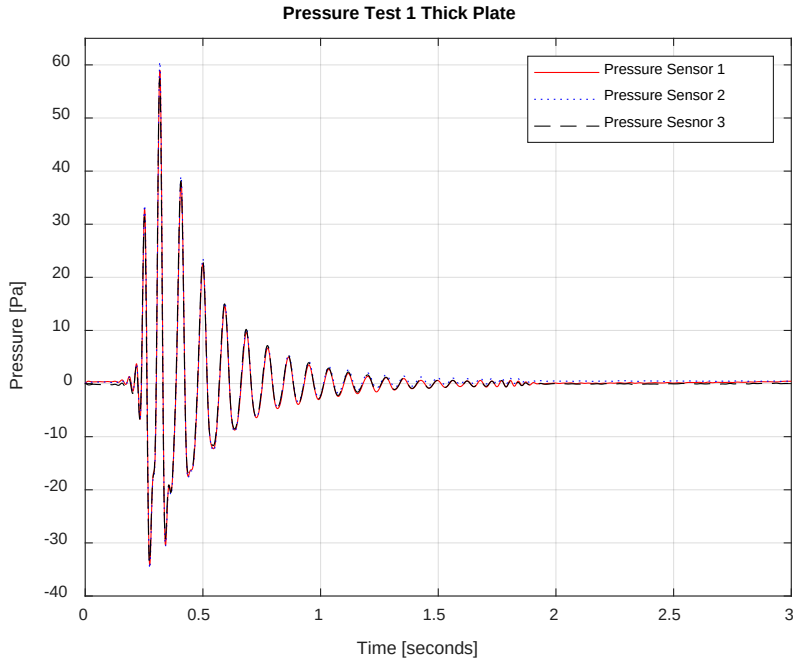

Figure 105. Pressure thick plate 1st blast

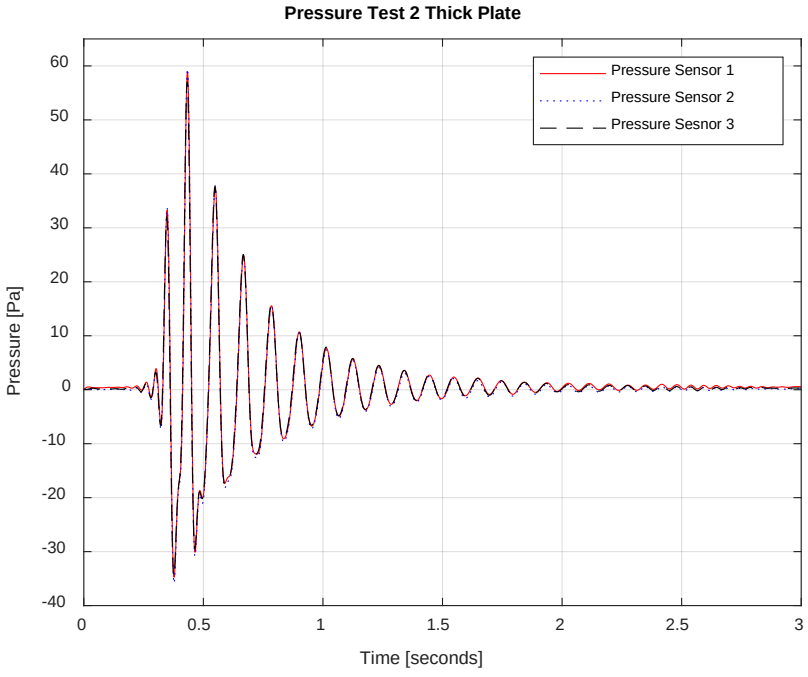

Figure 106. Pressure thick plate 2nd blast

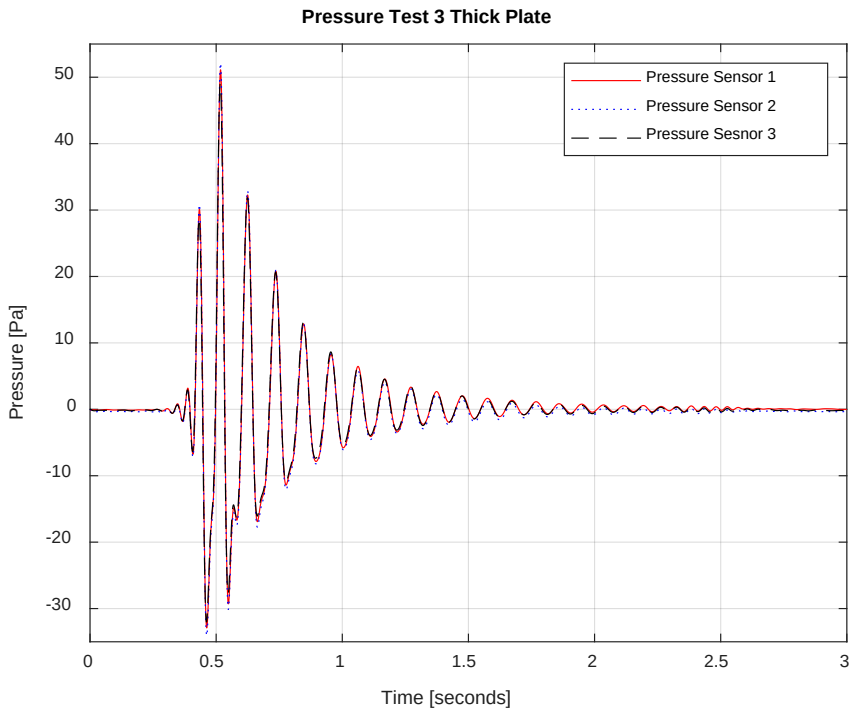

Figure 107. Pressure thick plate 3rd blast

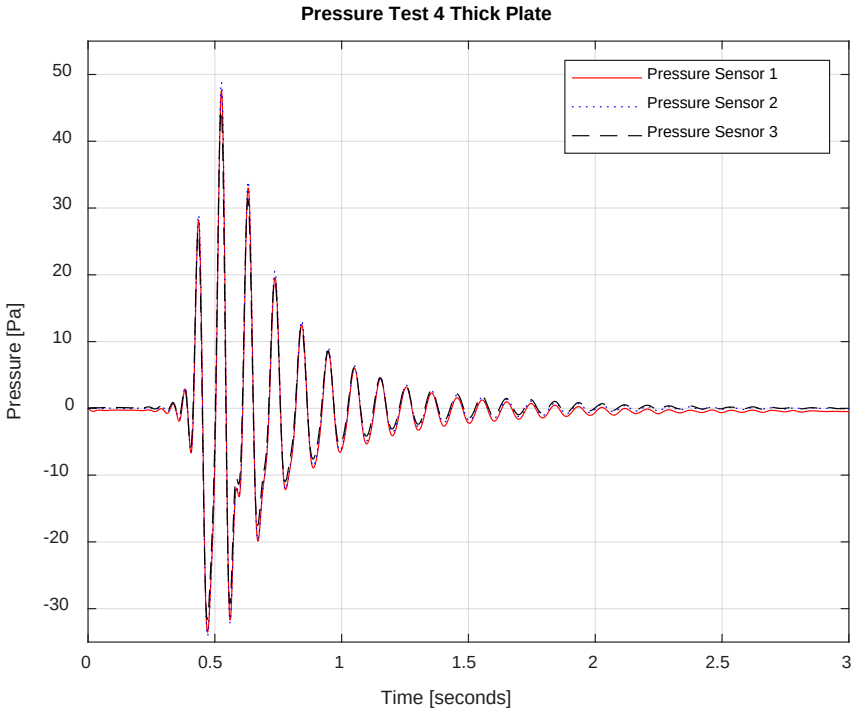

Figure 108. Pressure thick plate 4th blast

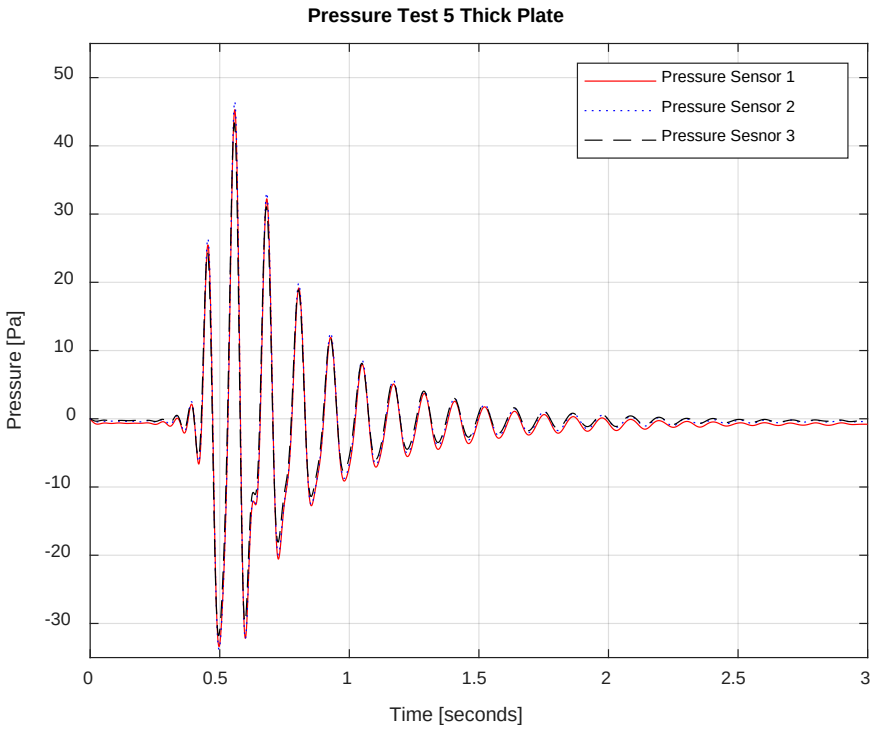

Figure 109. Pressure thick plate 5th blast

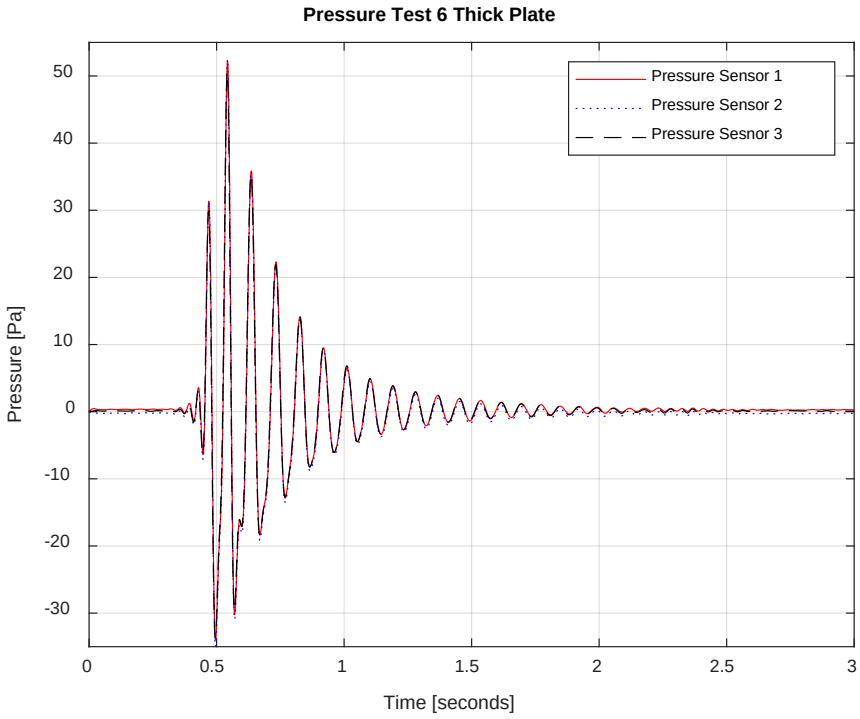

Figure 110. Pressure thick plate 6th blast

THIS PAGE INTENTIONALLY LEFT BLANK

APPENDIX D. PHASE 3 SAMPLE 3 SET-UP 2 PRESSURE AND STRESS FIGURES

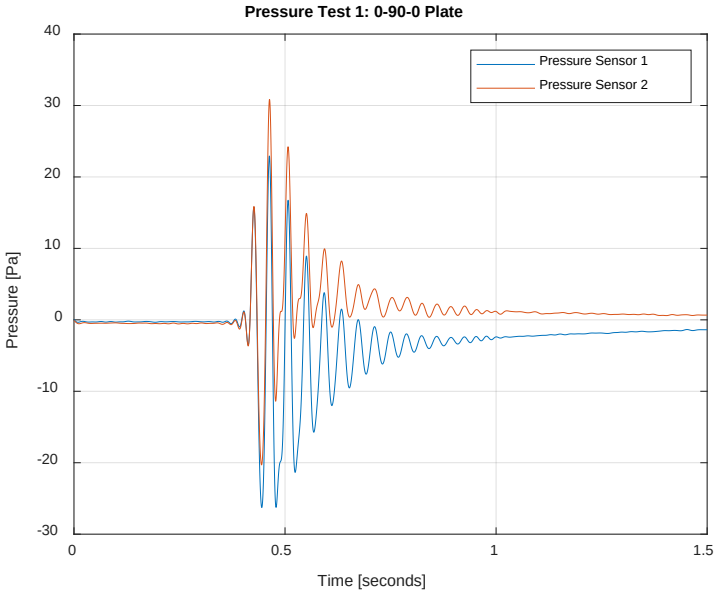

Figure 111. Sample 3 pressure 1st blast

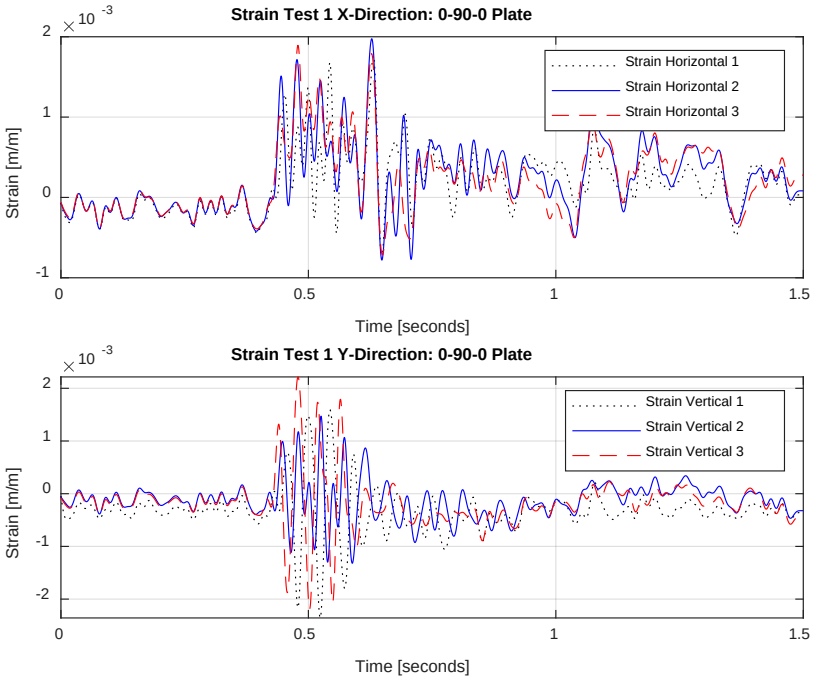

Figure 112. Sample 3 strain 1st blast

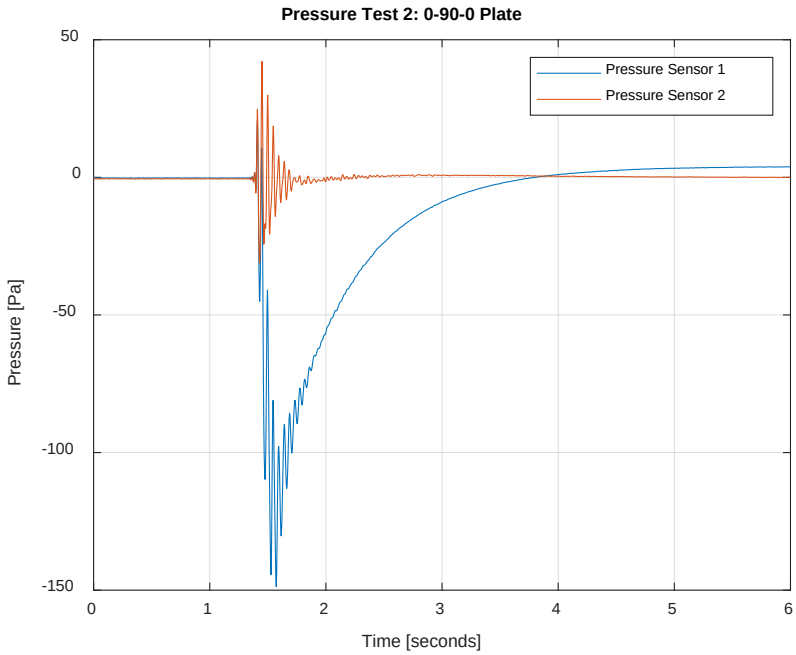

Figure 113. Sample 3 pressure 2nd blast

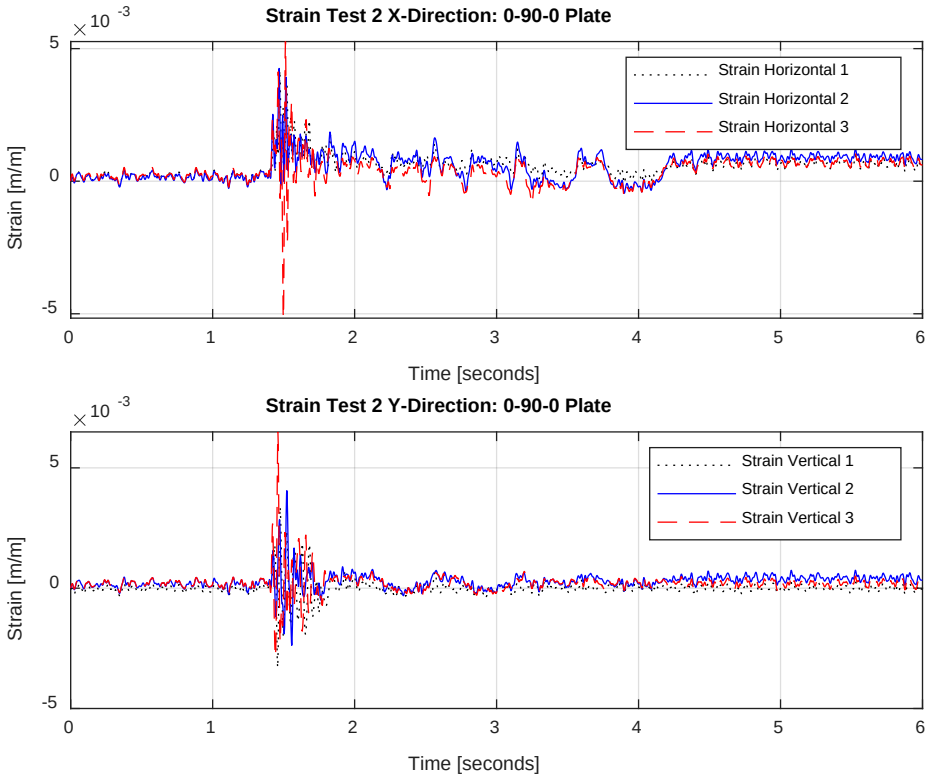

Figure 114. Sample 3 strain 2nd blast

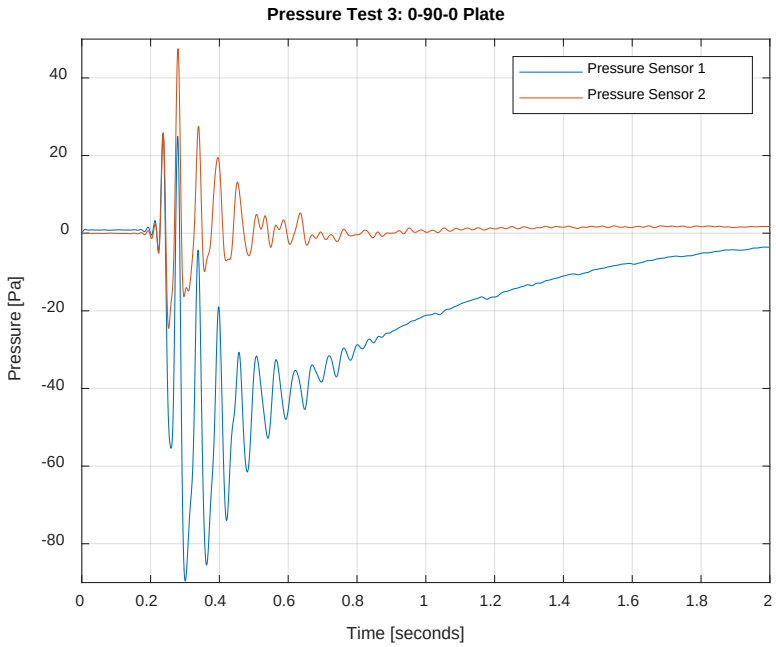

Figure 115. Sample 3 pressure 3rd blast

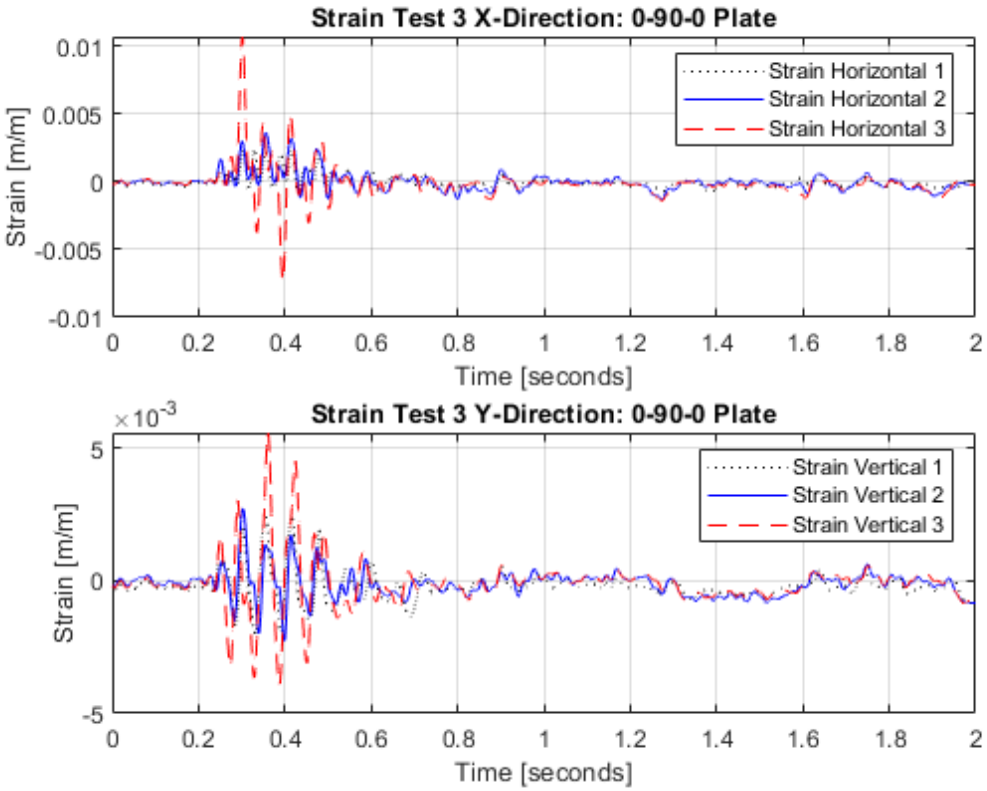

Figure 116. Sample 3 strain 3rd blast

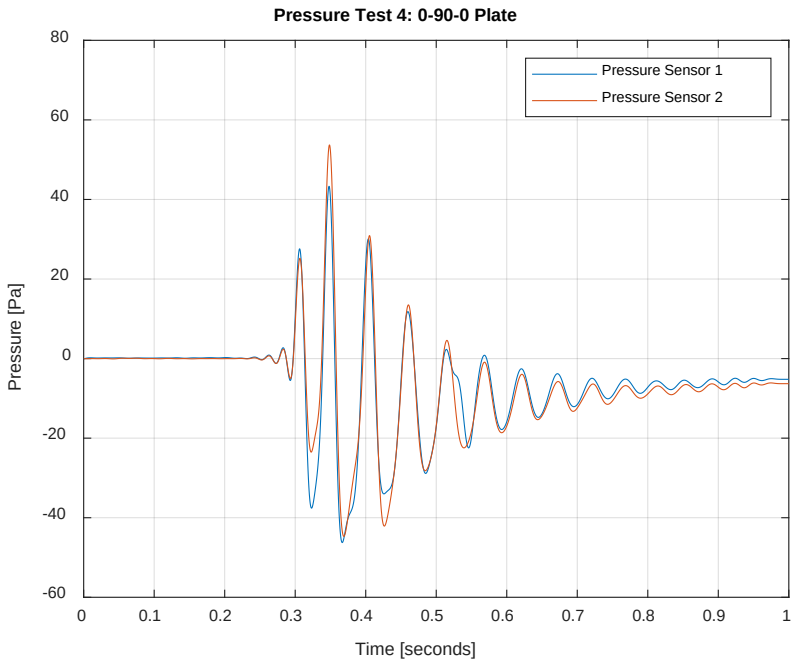

Figure 117. Sample 3 pressure 4th blast

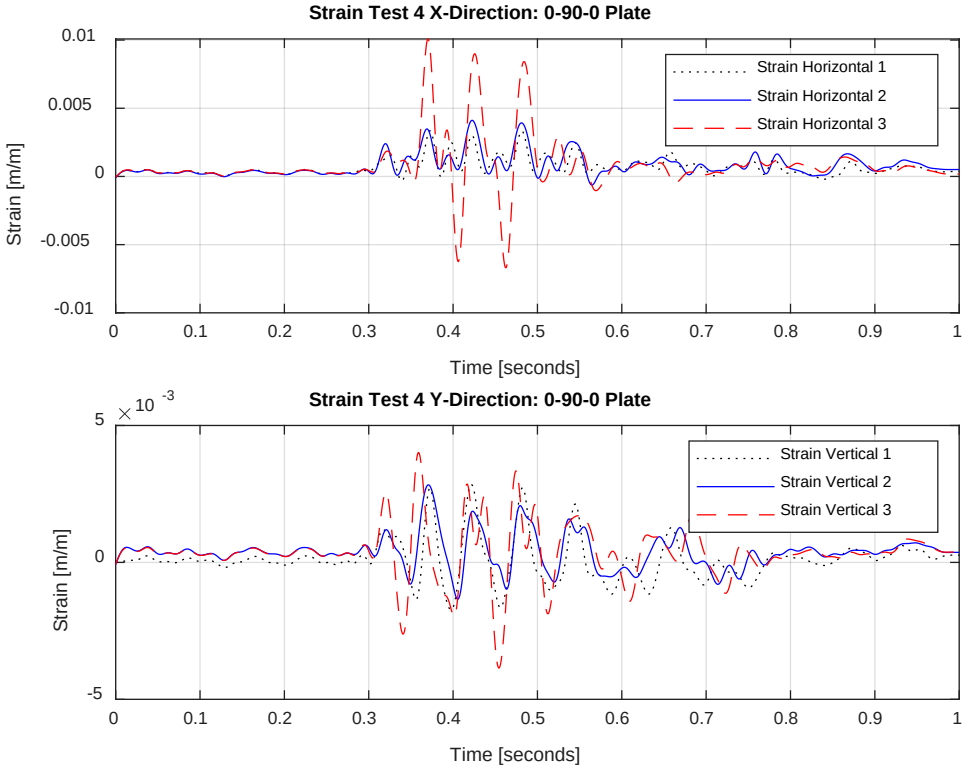

Figure 118. Sample 3 strain 4th blast

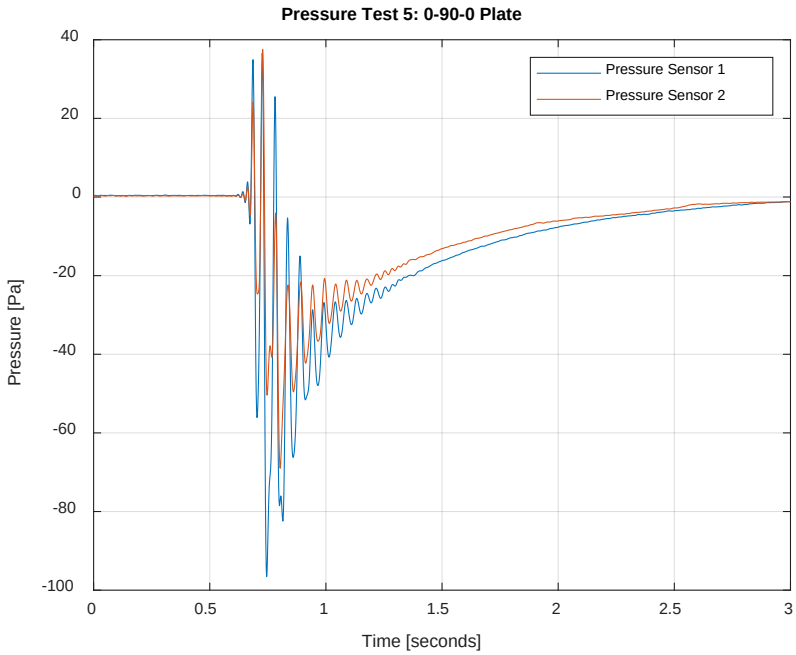

Figure 119. Sample 3 pressure 5th blast

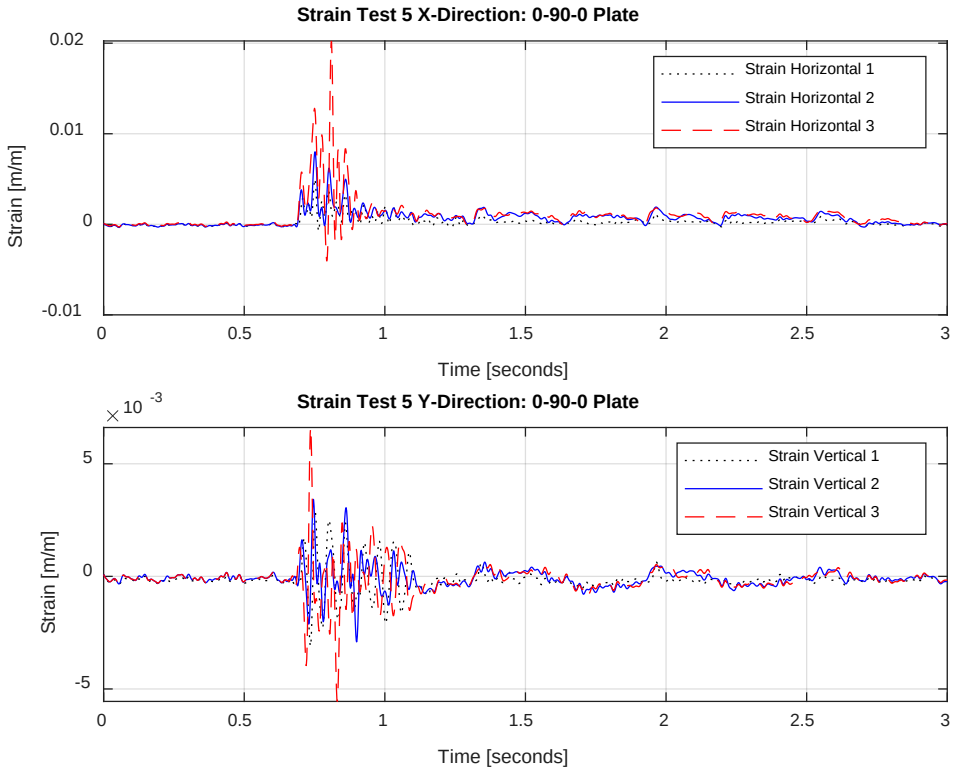

Figure 120. Sample 3 strain 5th blast

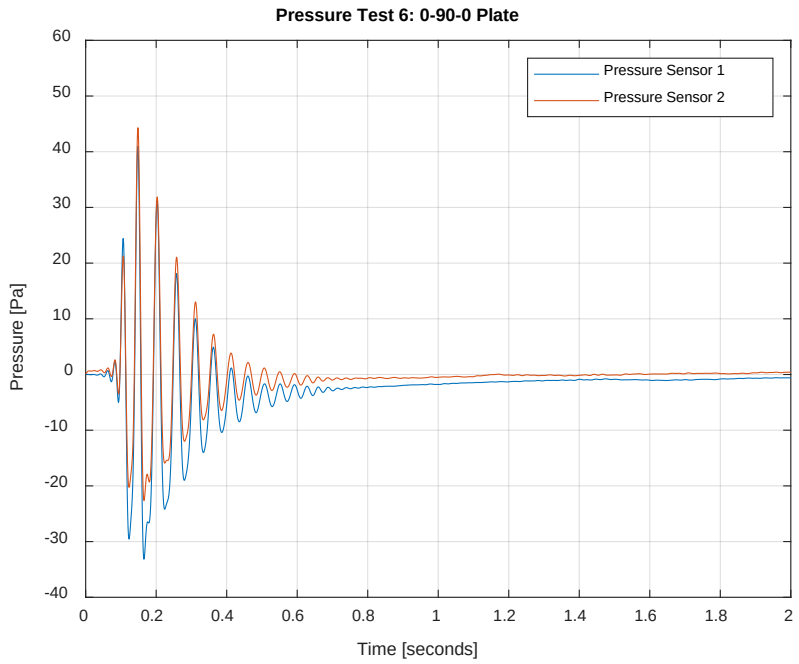

Figure 121. Sample 3 pressure 6th blast

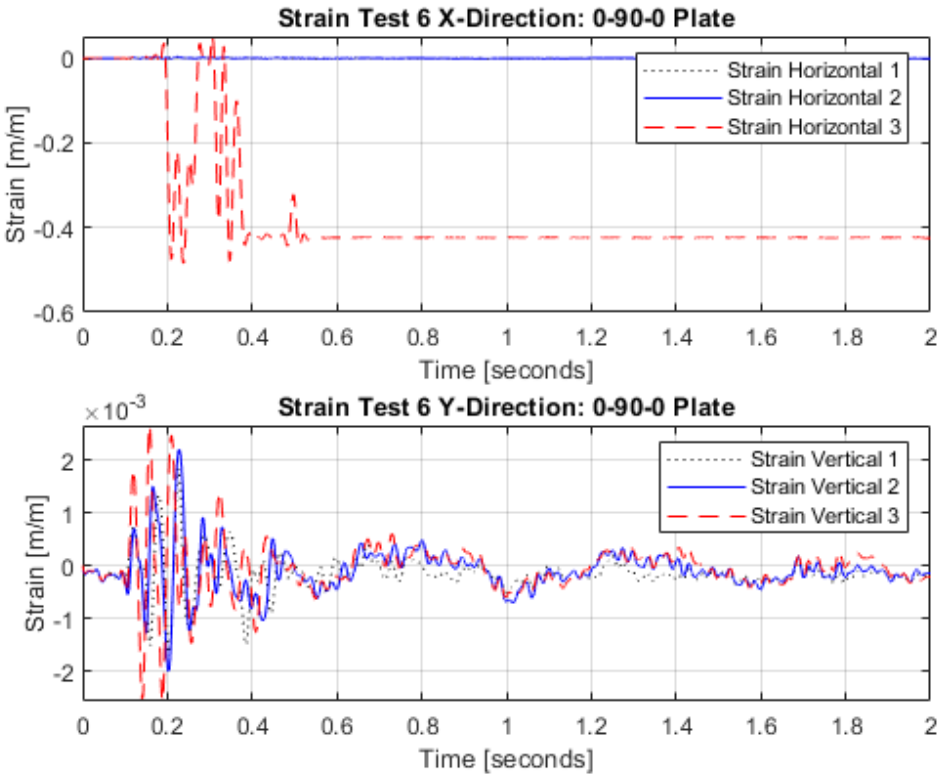

Figure 122. Sample 3 strain 6th blast

APPENDIX E. PHASE 3 SAMPLE 3 SET-UP 3 PRESSURE AND STRAIN FIGURES

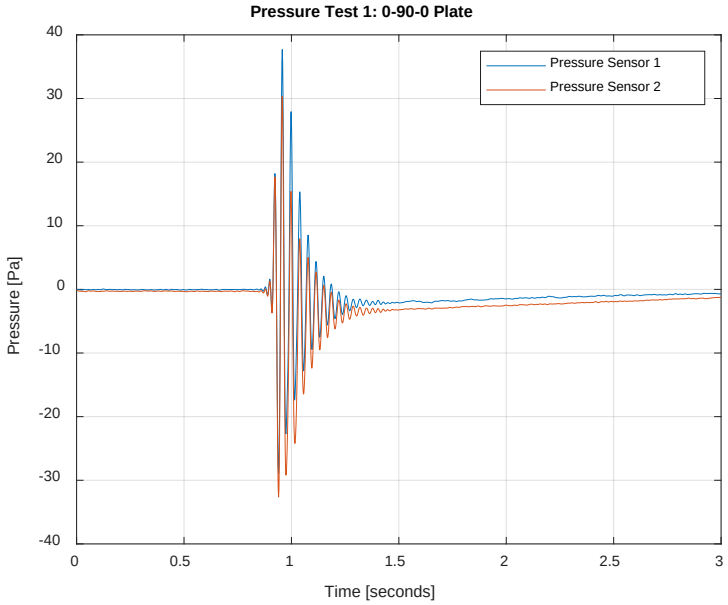

Figure 123. Sample 3 pressure 1st blast

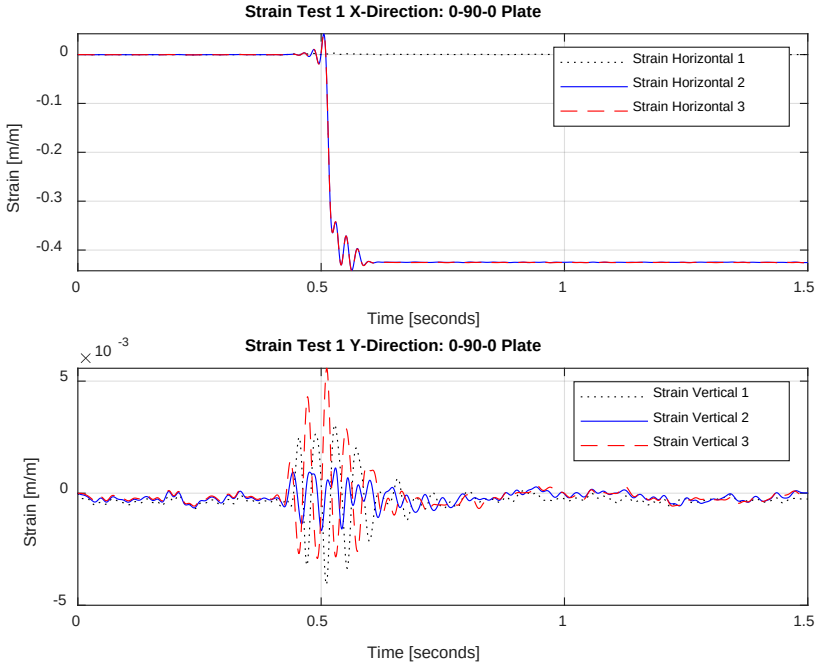

Figure 124. Sample 3 strain 1st blast

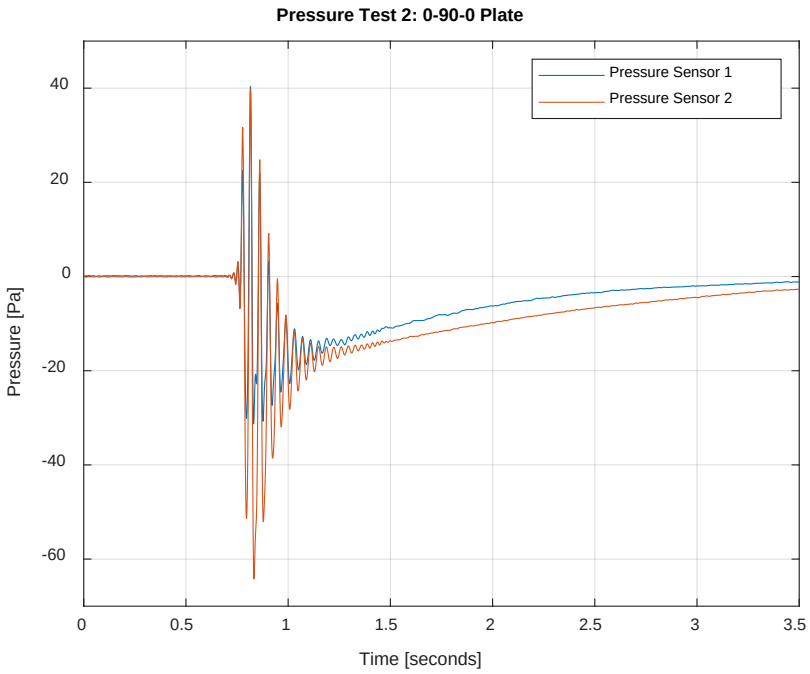

Figure 125. Sample 3 pressure 2nd blast

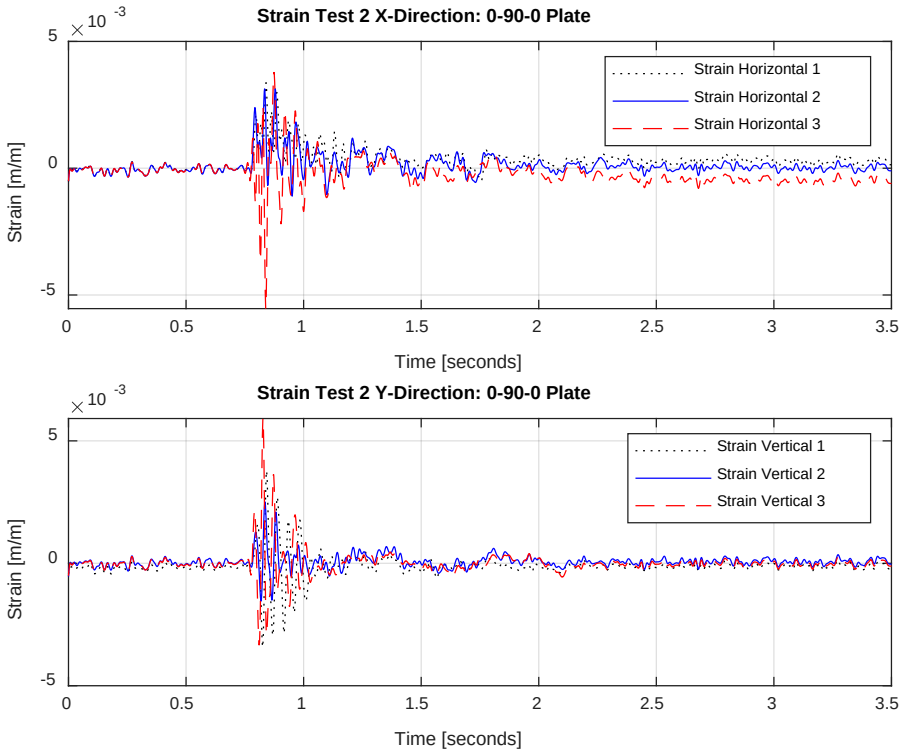

Figure 126. Sample 3 strain 2nd blast

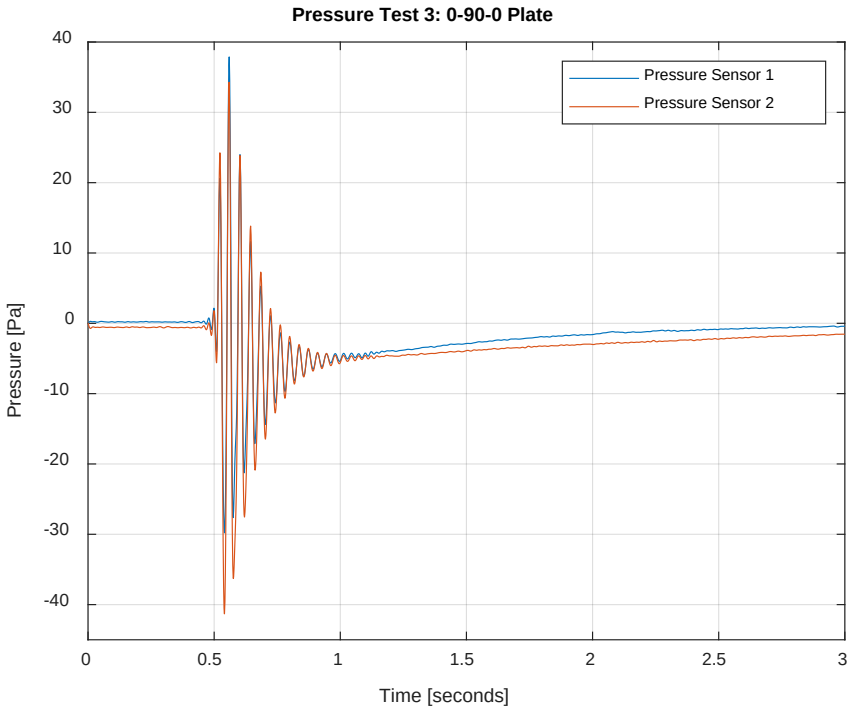

Figure 127. Sample 3 pressure 3rd blast

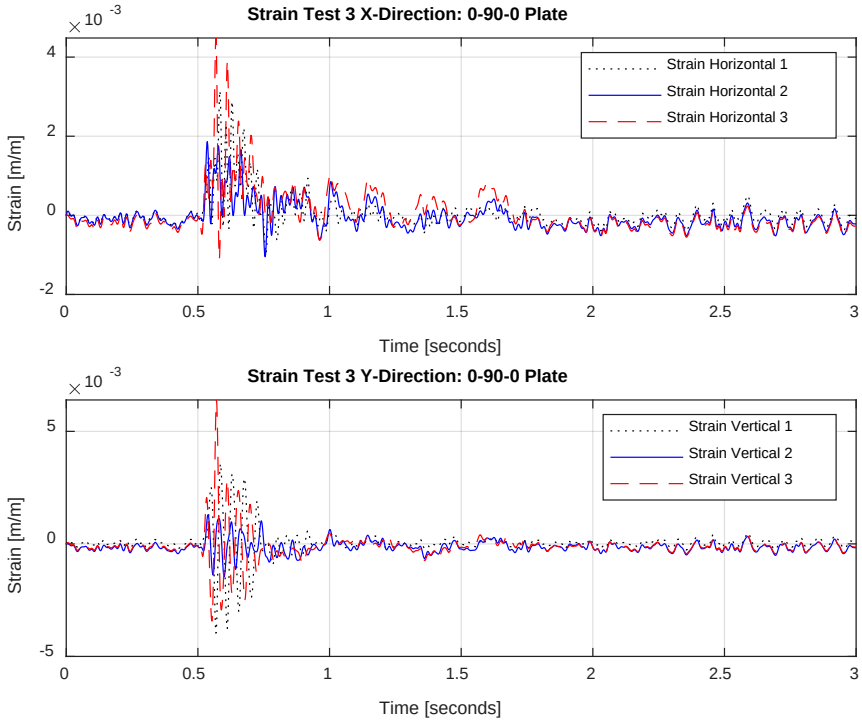

Figure 128. Sample 3 strain 3rd blast

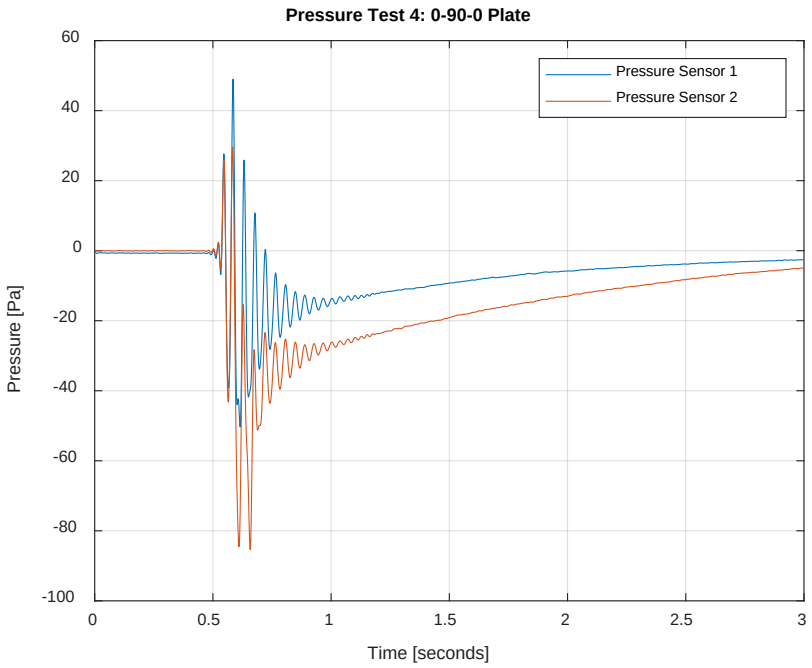

Figure 129. Sample 3 pressure 4th blast

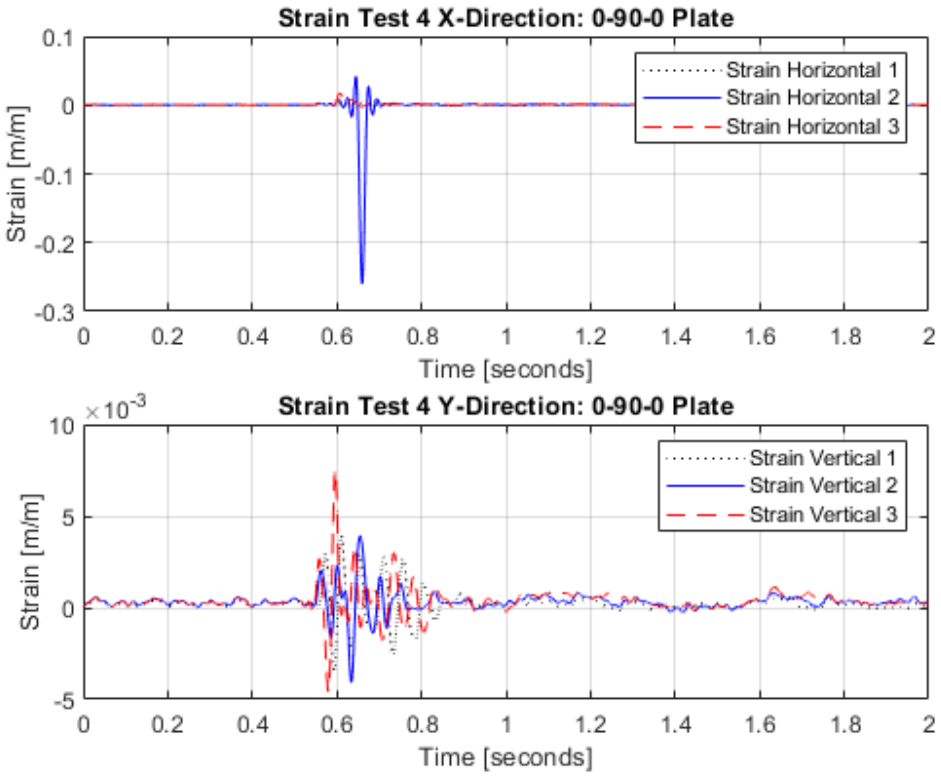

Figure 130. Sample 3 strain 4th blast

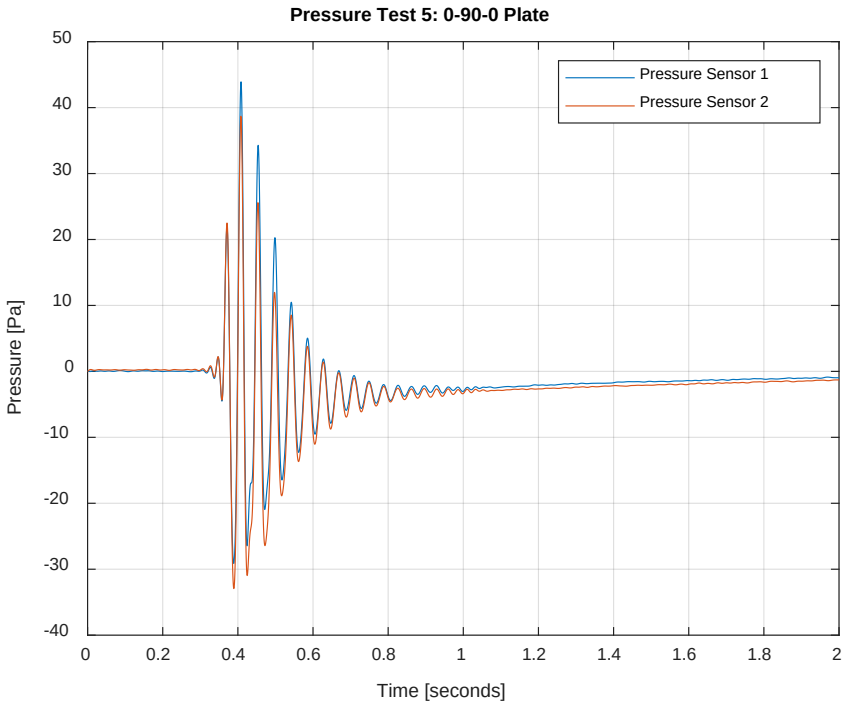

Figure 131. Sample 3 pressure 5th blast

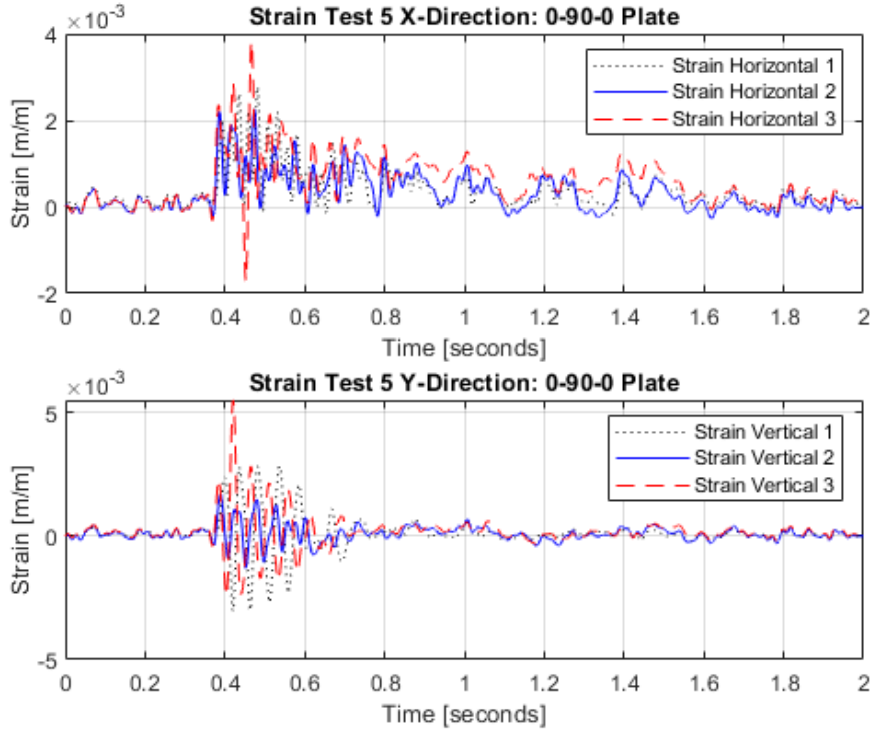

Figure 132. Sample 3 strain 5th blast

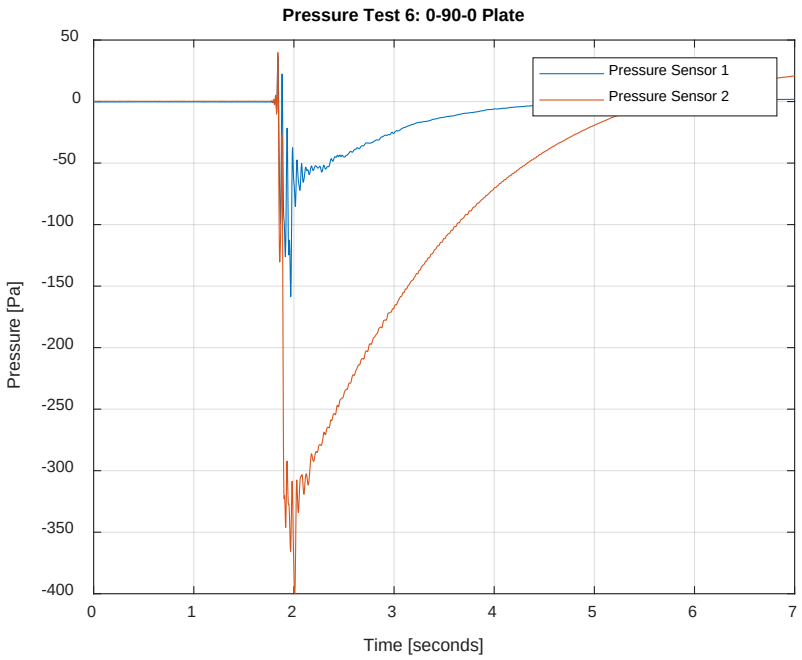

Figure 133. Sample 3 pressure 6th blast

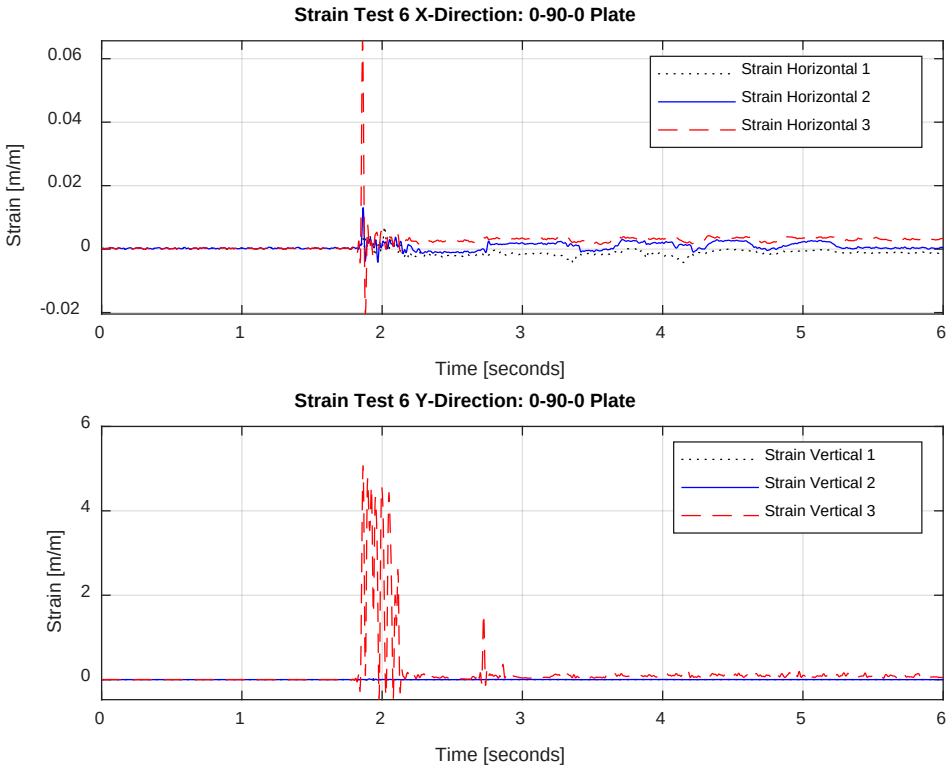

Figure 134. Sample 3 strain 6th blast

APPENDIX F. PHASE 3 SAMPLE 4 SET-UP 1 PRESSURE FIGURES

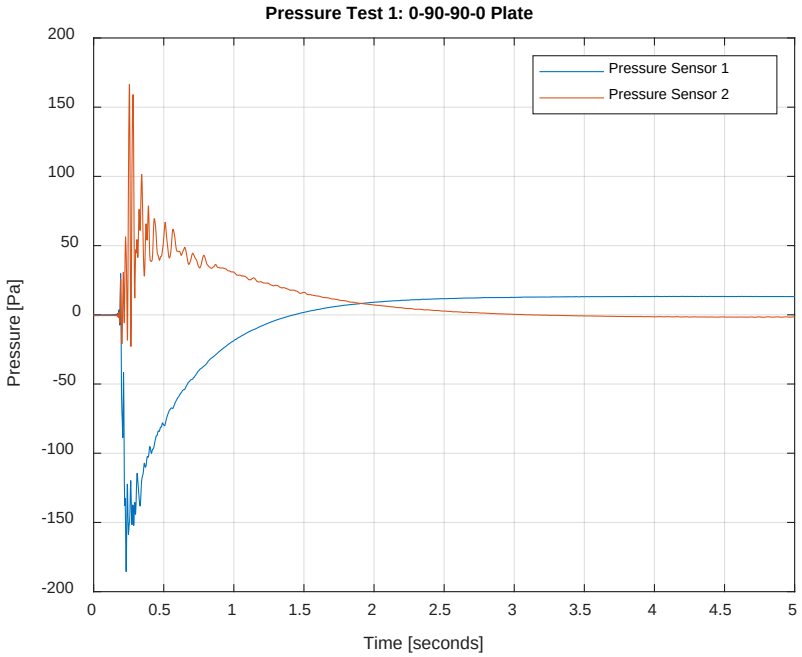

Figure 135. Sample 4 pressure 1st blast

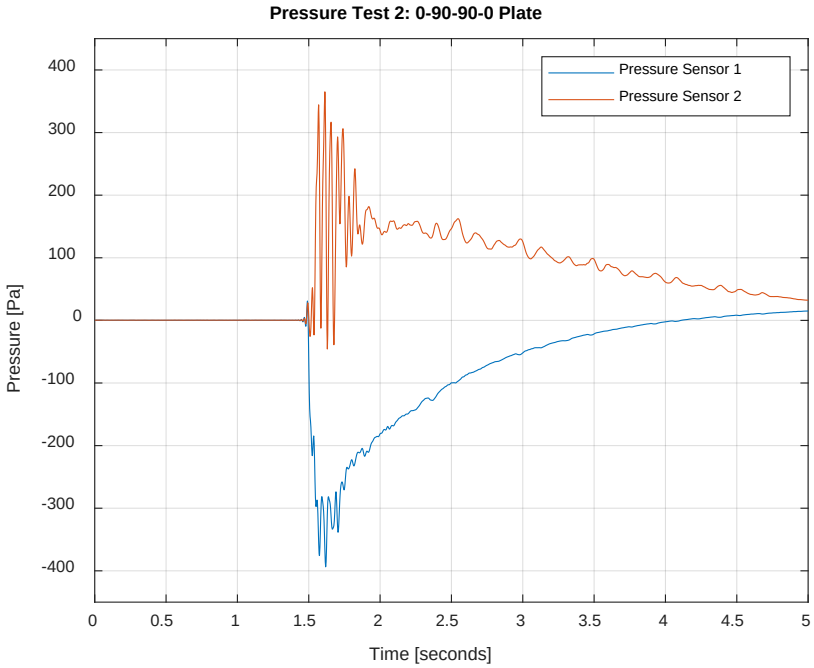

Figure 136. Sample 4 pressure 2nd blast

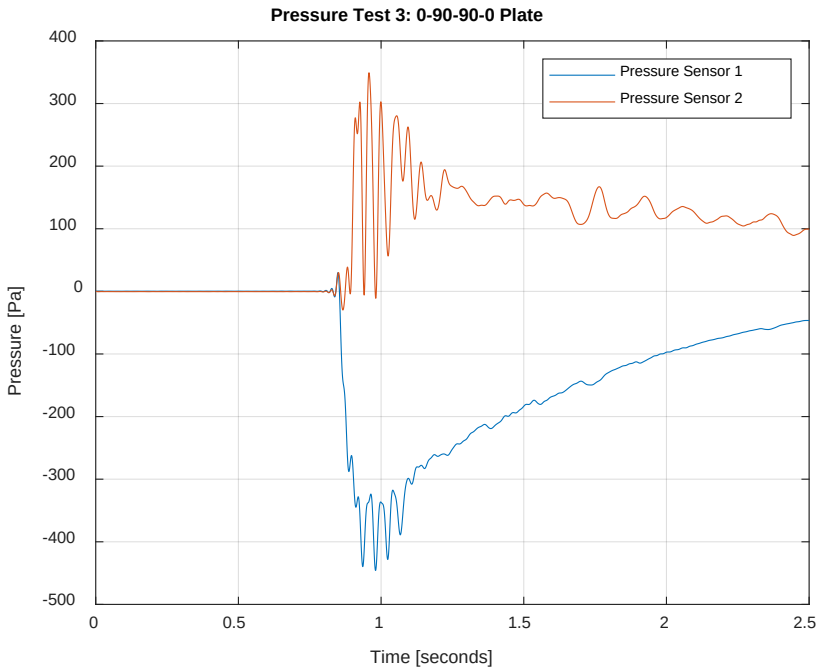

Figure 137. Sample 4 pressure 3rd blast

APPENDIX G. PHASE 3 SAMPLE 4 SET-UP 2 PRESSURE AND STRAIN FIGURES

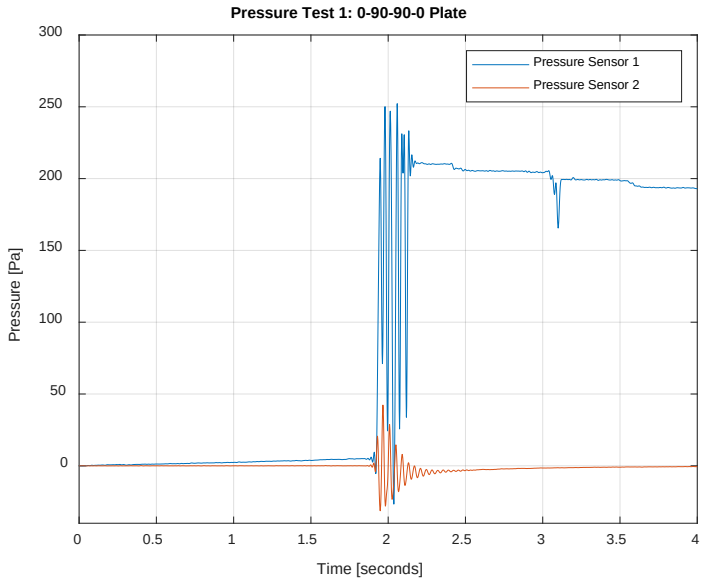

Figure 138. Sample 4 pressure 1st blast

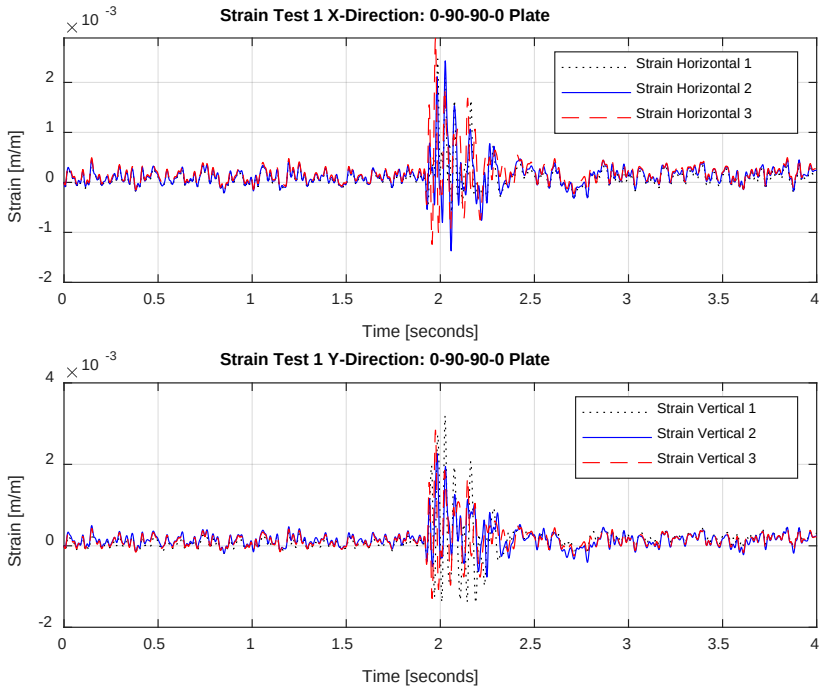

Figure 139. Sample 4 strain 1st blast

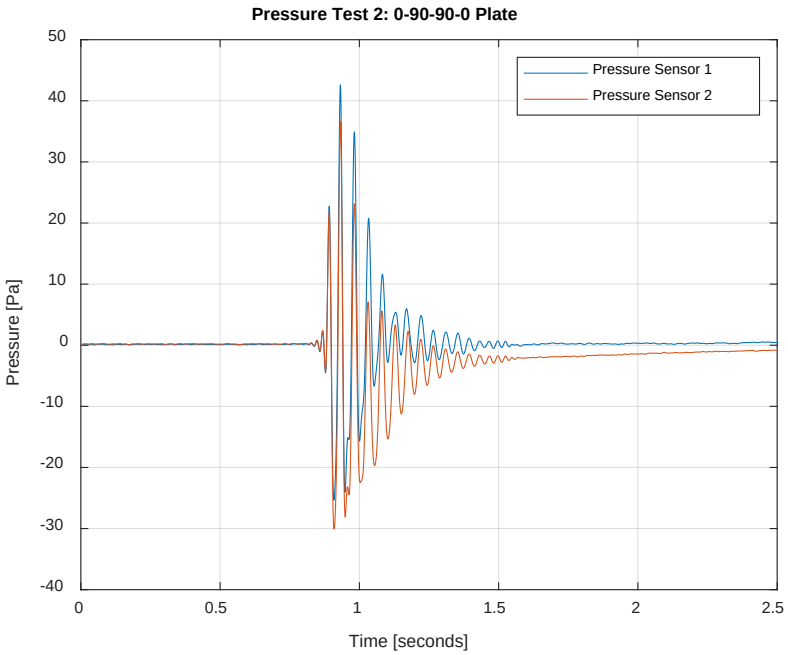

Figure 140. Sample 4 pressure 2nd blast

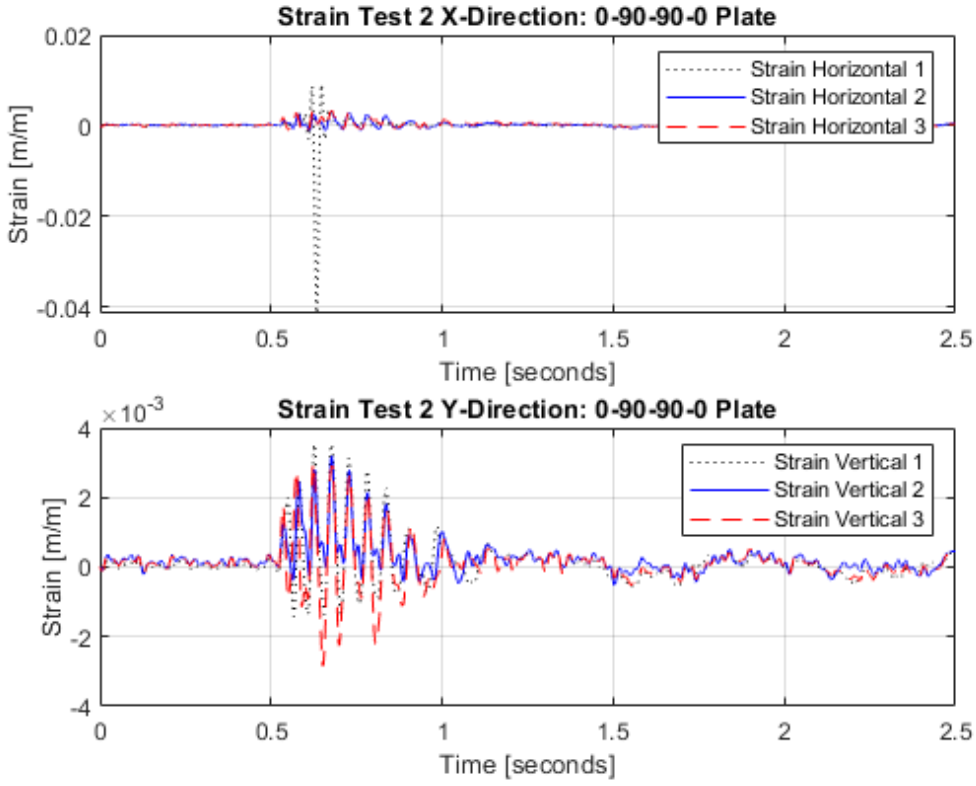

Figure 141. Sample 4 strain 2nd blast

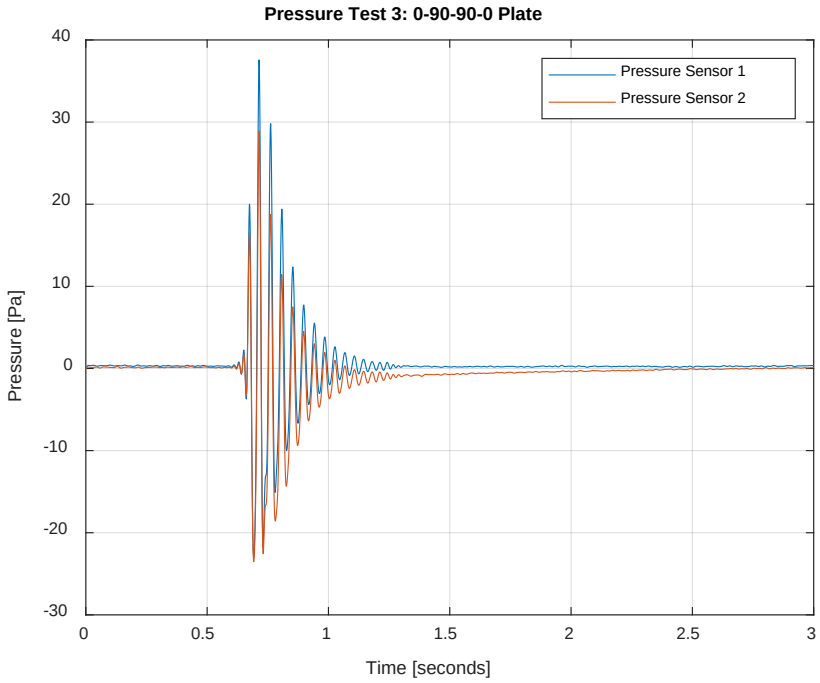

Figure 142. Sample 4 pressure 3rd blast

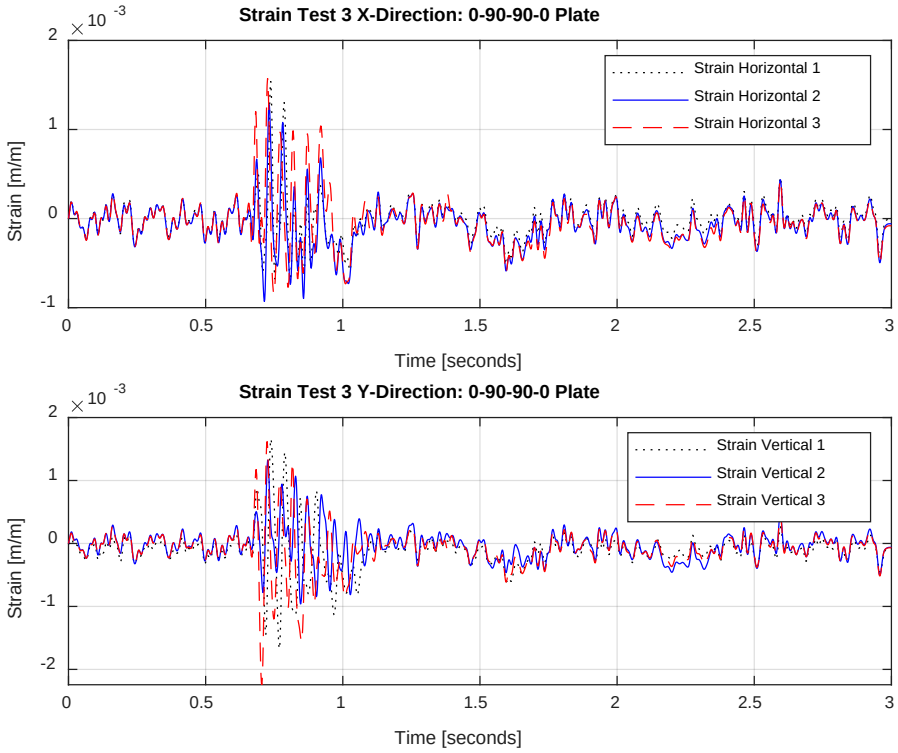

Figure 143. Sample 4 strain 3rd blast

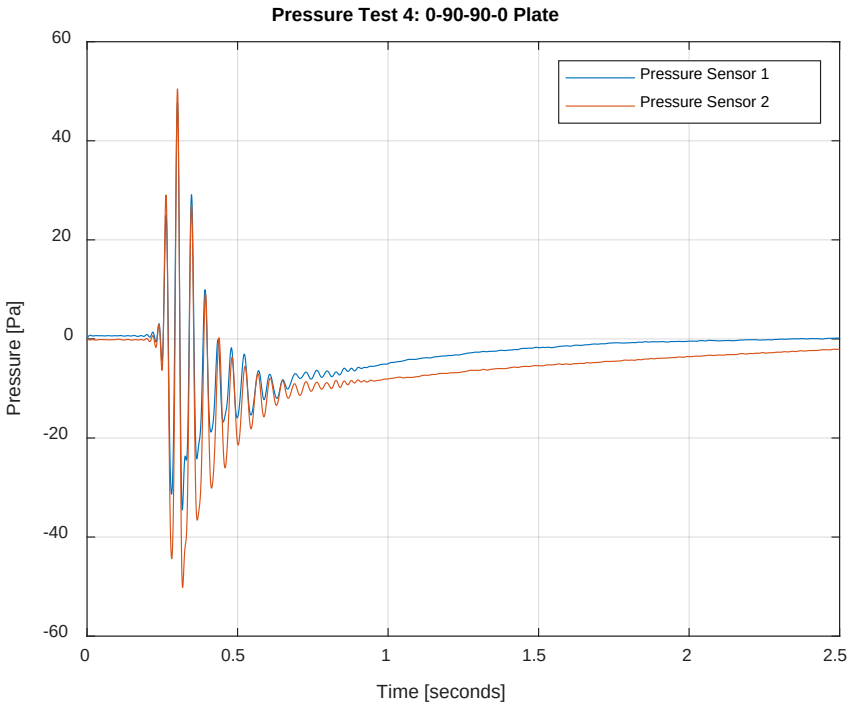

Figure 144. Sample 4 pressure 4th blast

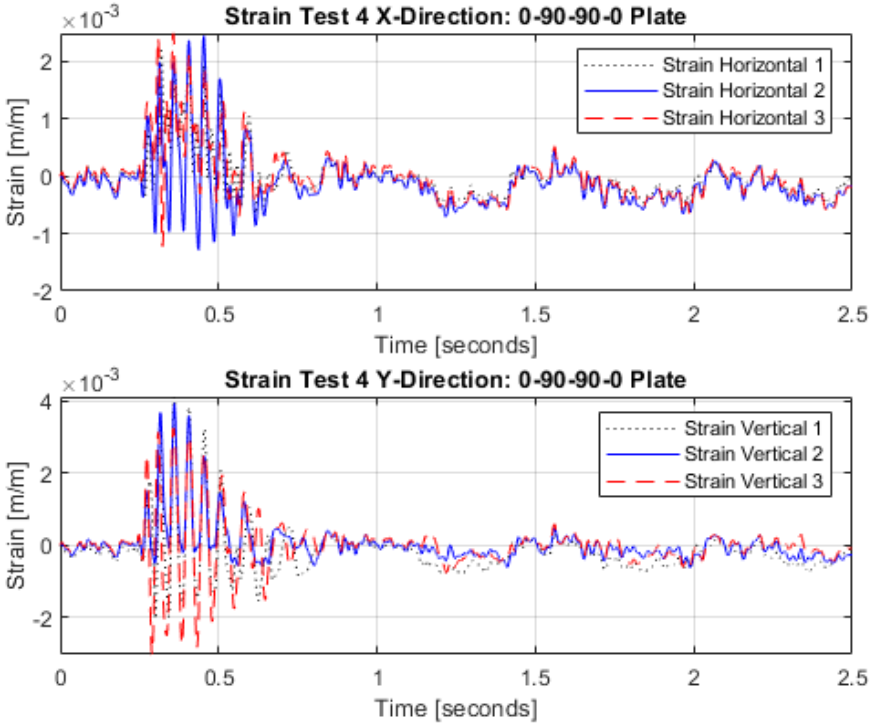

Figure 145. Sample 4 strain 4th blast

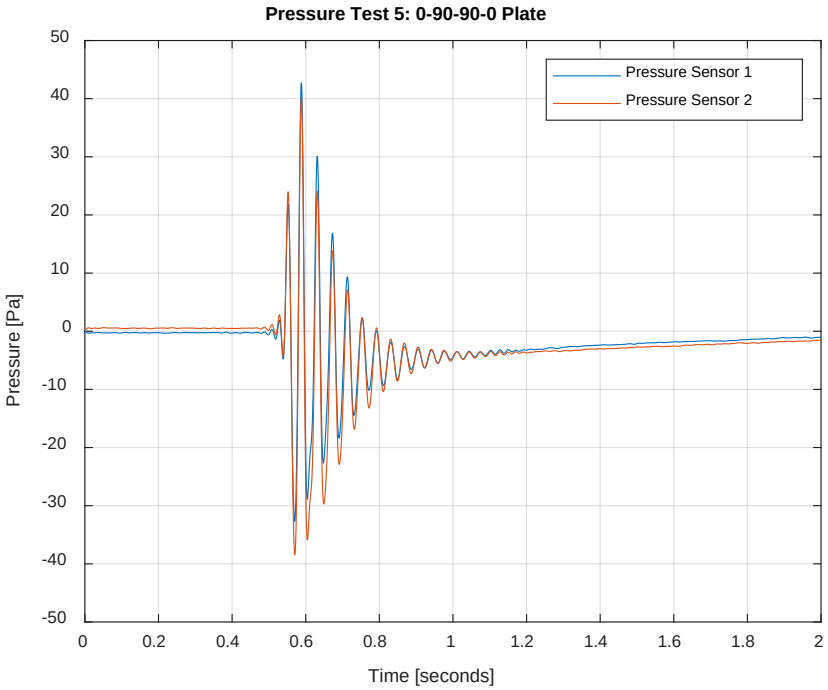

Figure 146. Sample 4 pressure 5th blast

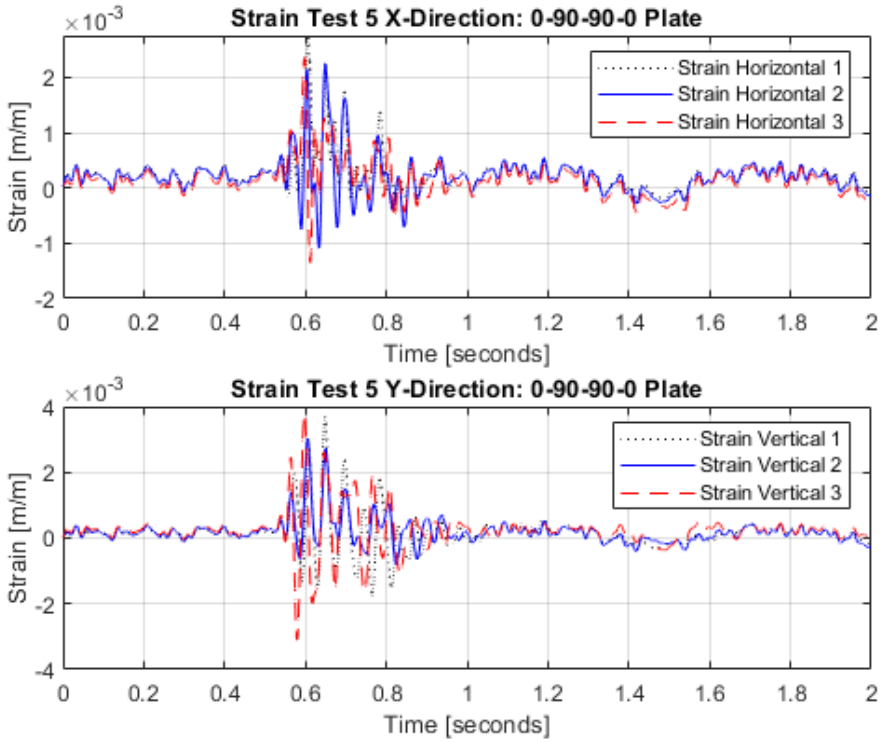

Figure 147. Sample 4 strain 5th blast

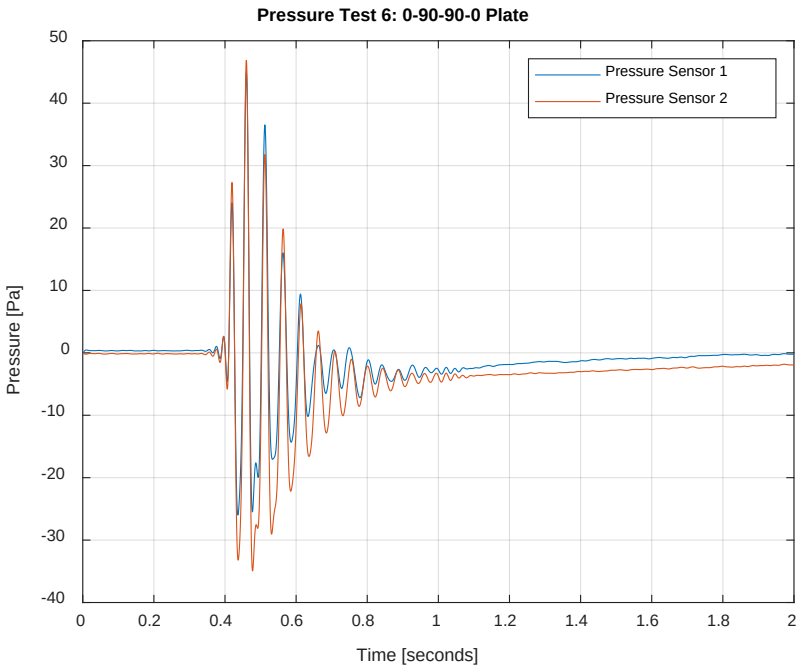

Figure 148. Sample 4 pressure 6th blast

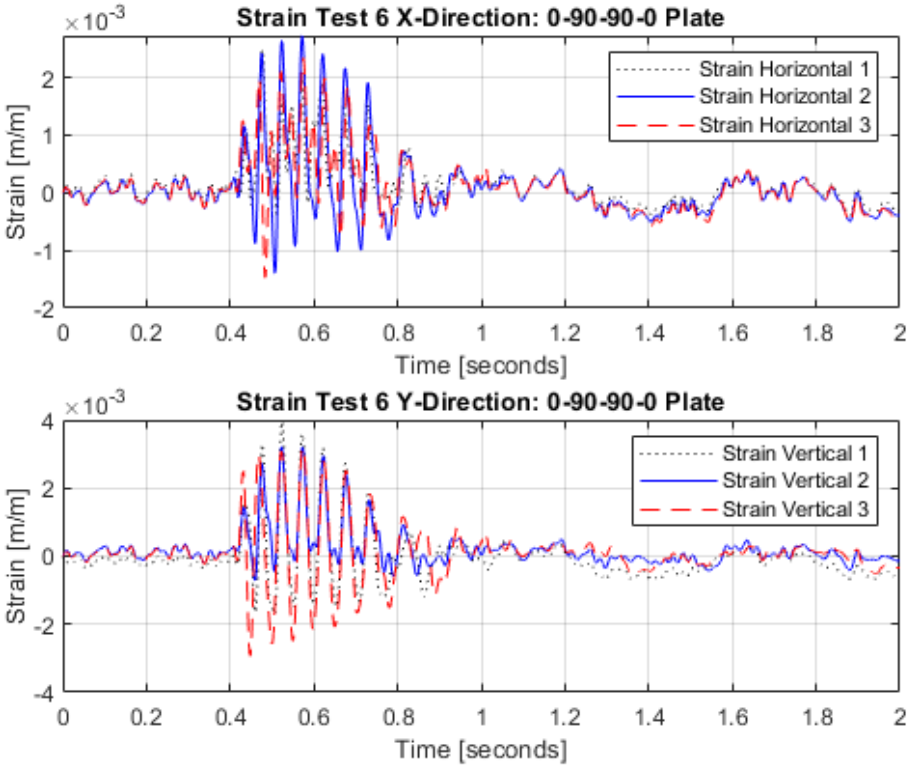

Figure 149. Sample 4 strain 6th blast

APPENDIX H. PHASE 3 SAMPLE 4 SET-UP 3 PRESSURE AND STRAIN FIGURES

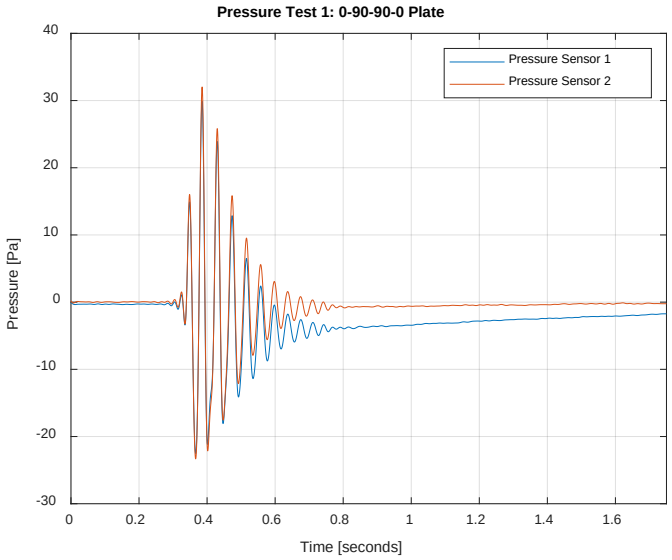

Figure 150. Sample 4 pressure 1st blast

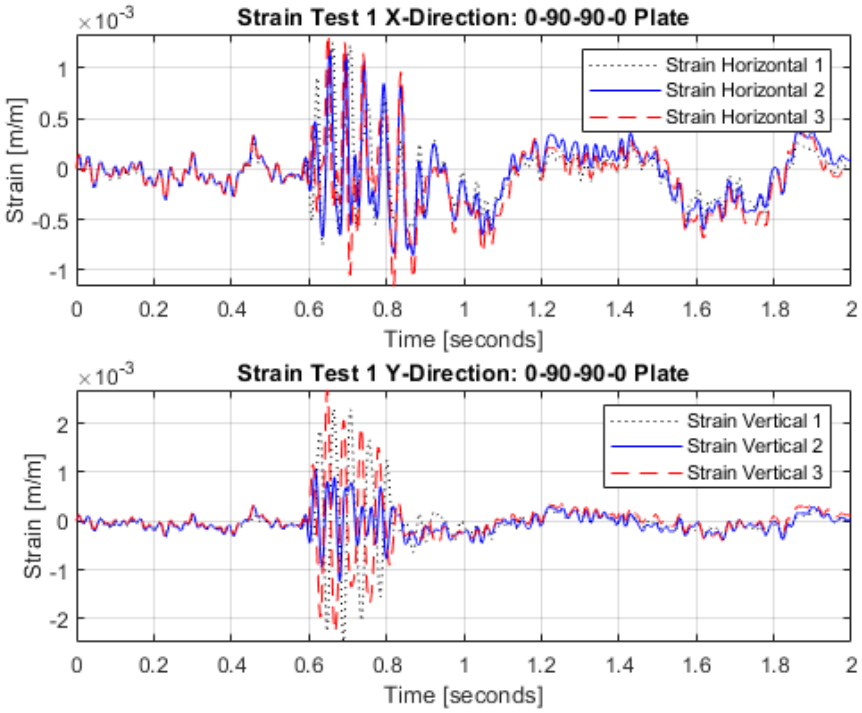

Figure 151. Sample 4 strain 1st blast

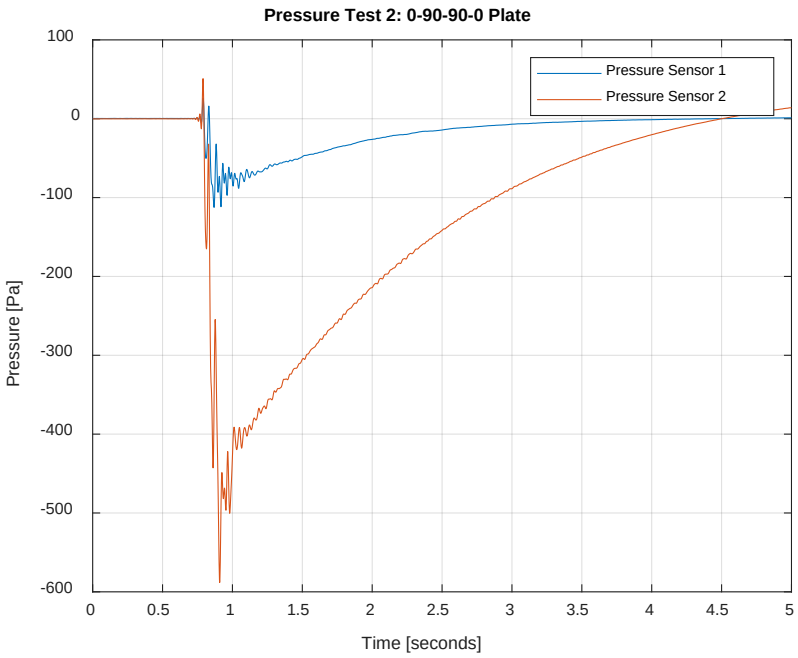

Figure 152. Sample 4 pressure 2nd blast

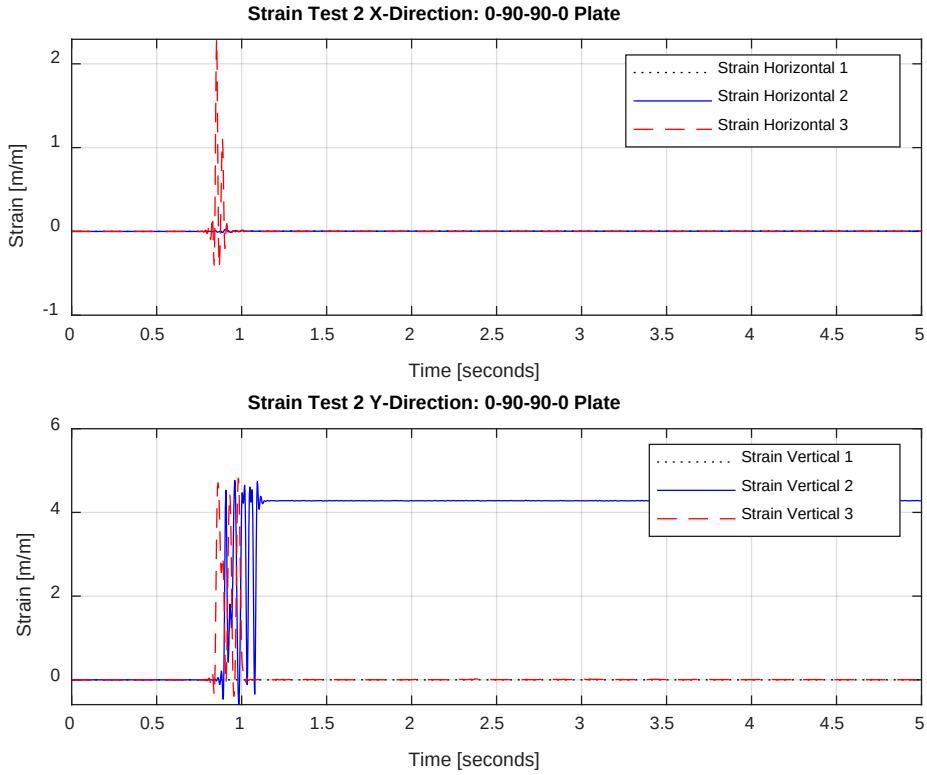

Figure 153. Sample 4 strain 2nd blast

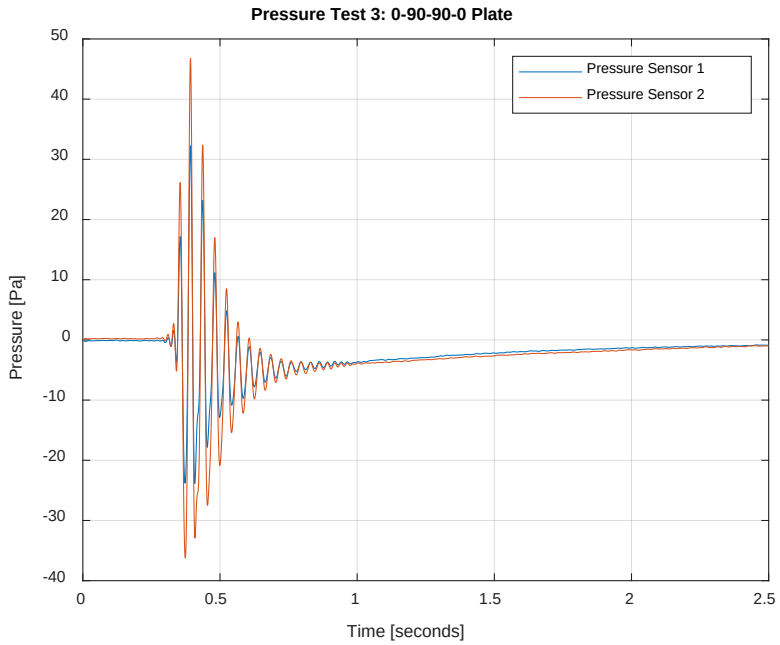

Figure 154. Sample 4 pressure 3rd blast

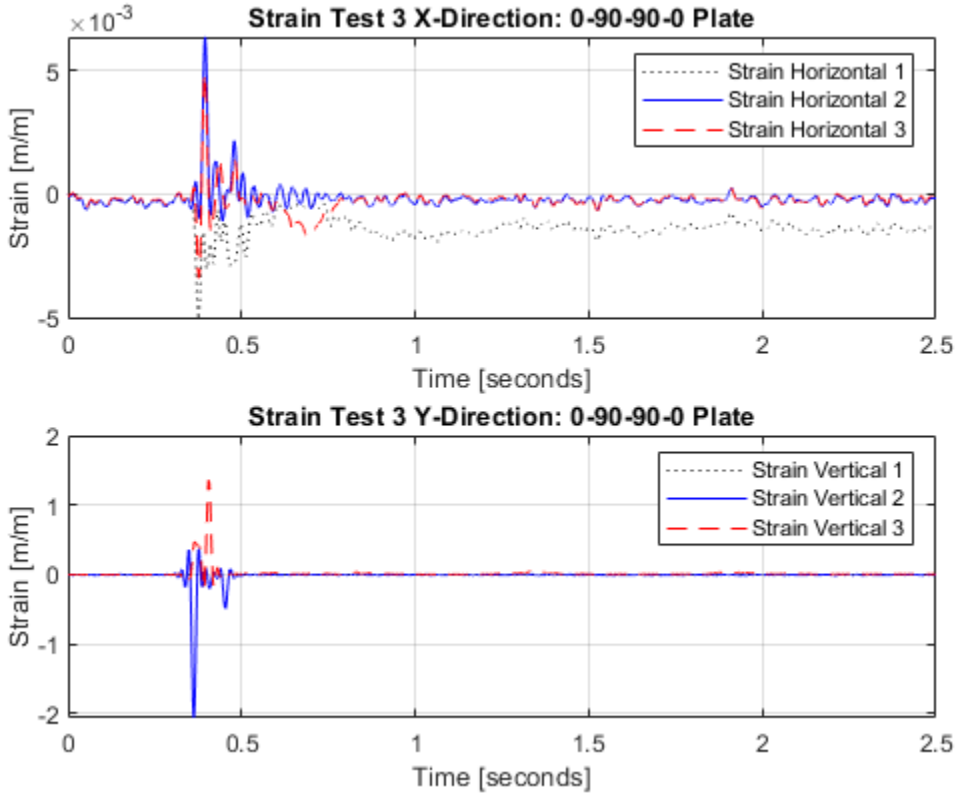

Figure 155. Sample 4 strain 3rd blast

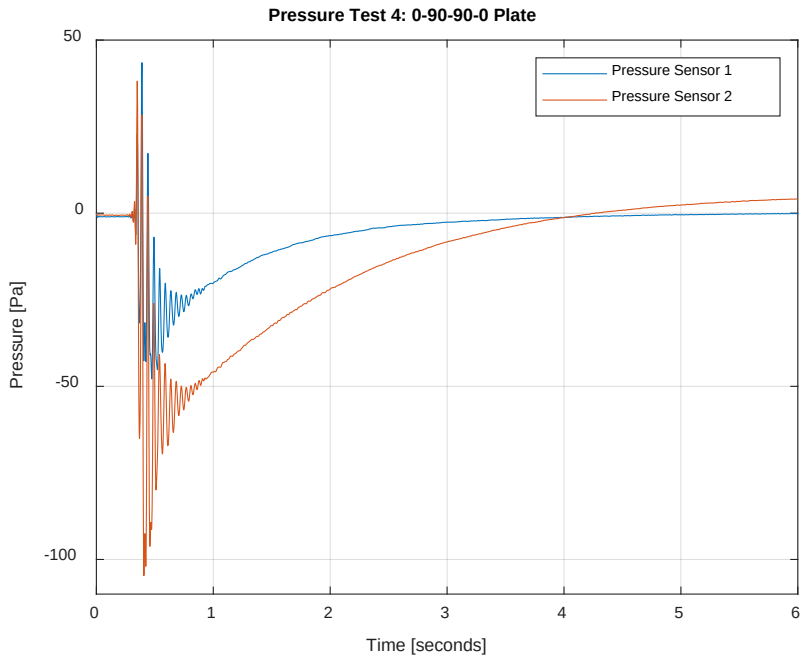

Figure 156. Sample 4 pressure 4th blast

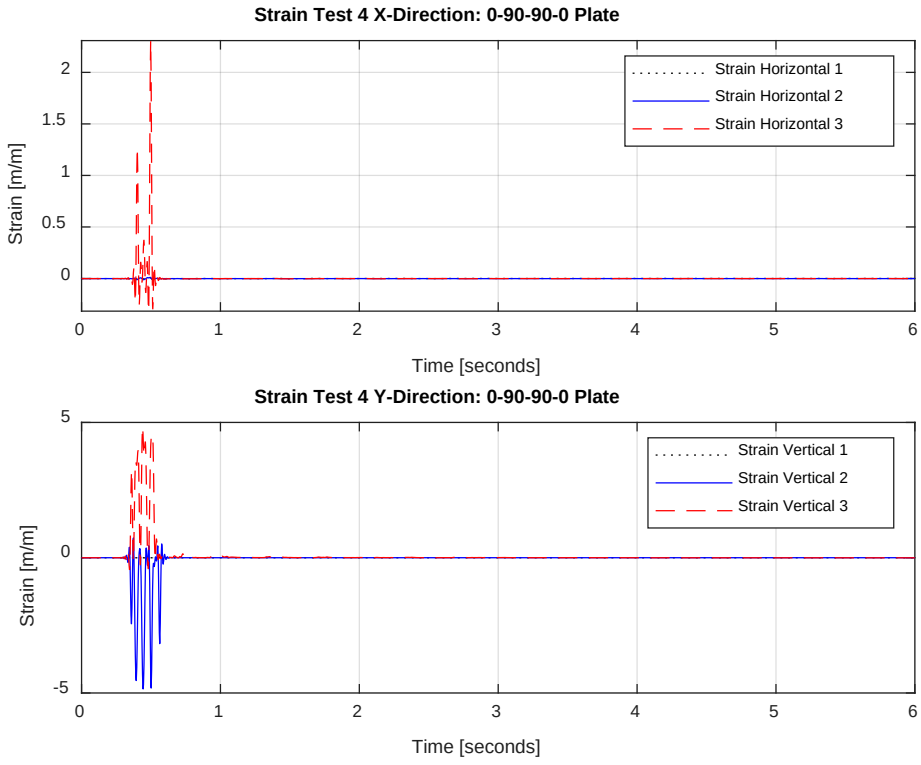

Figure 157. Sample 4 strain 4th blast

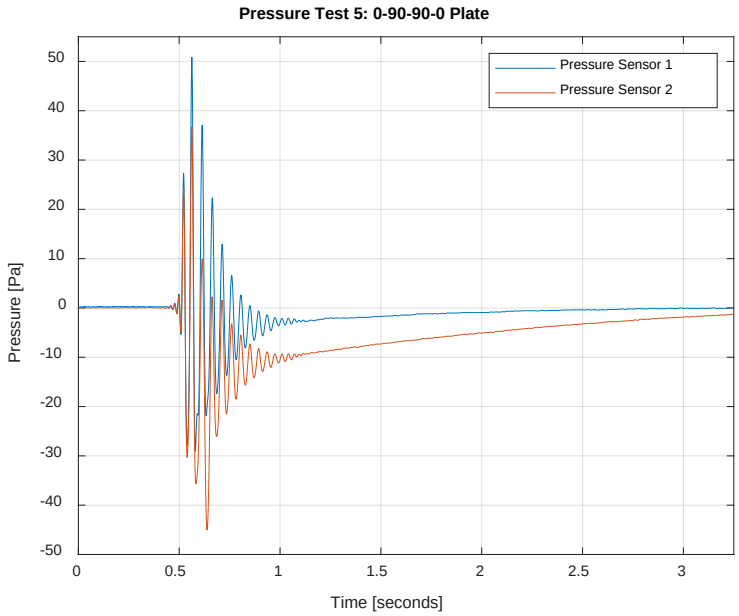

Figure 158. Sample 4 pressure 5th blast

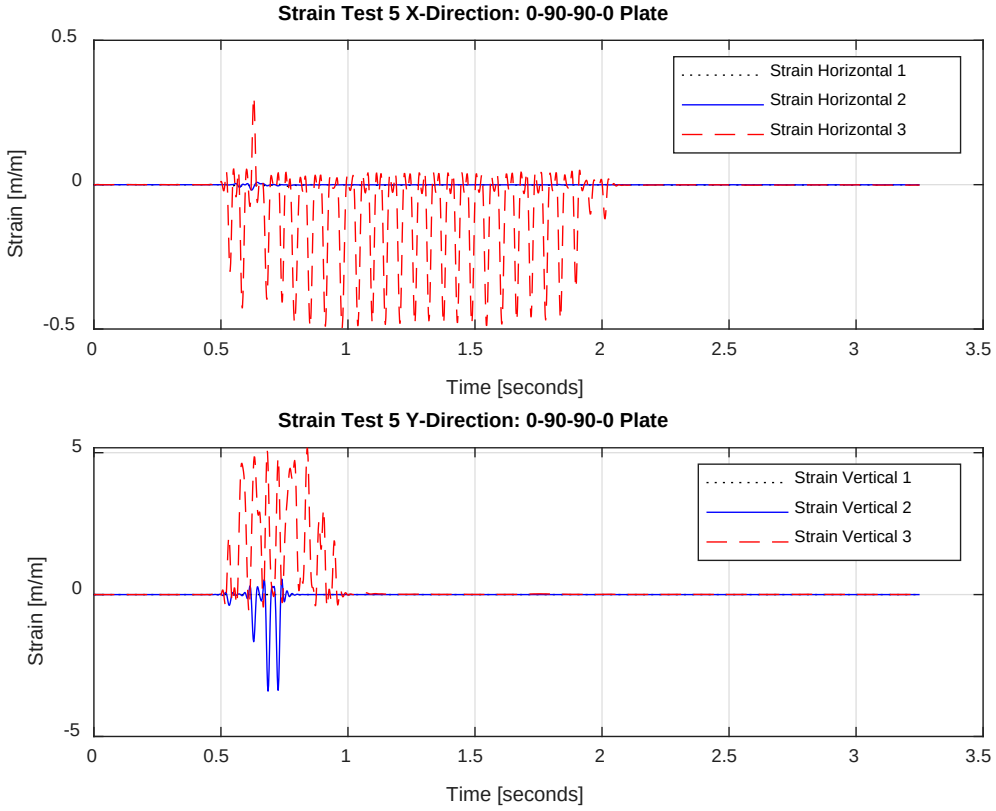

Figure 159. Sample 4 strain 5th blast

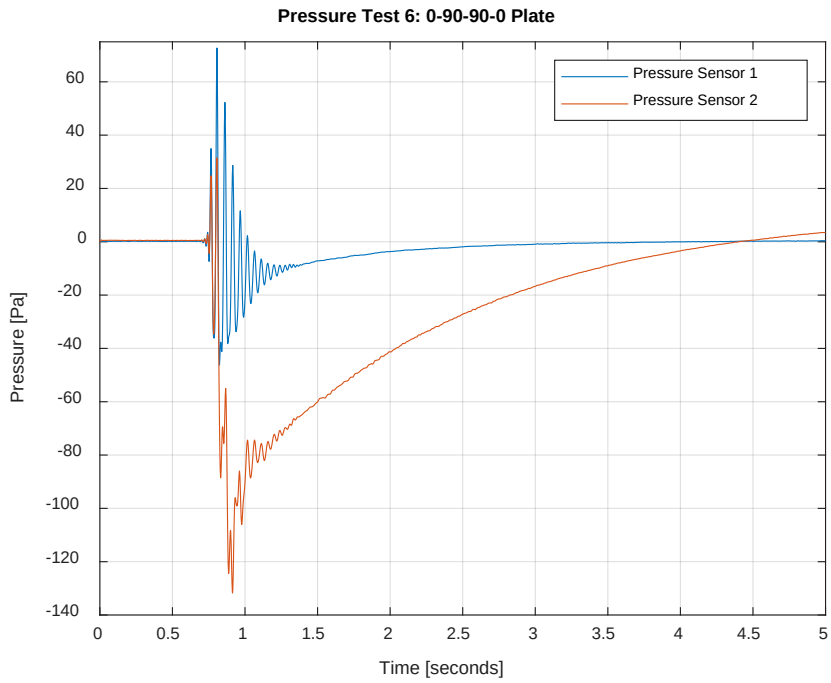

Figure 160. Sample 4 pressure 6th blast

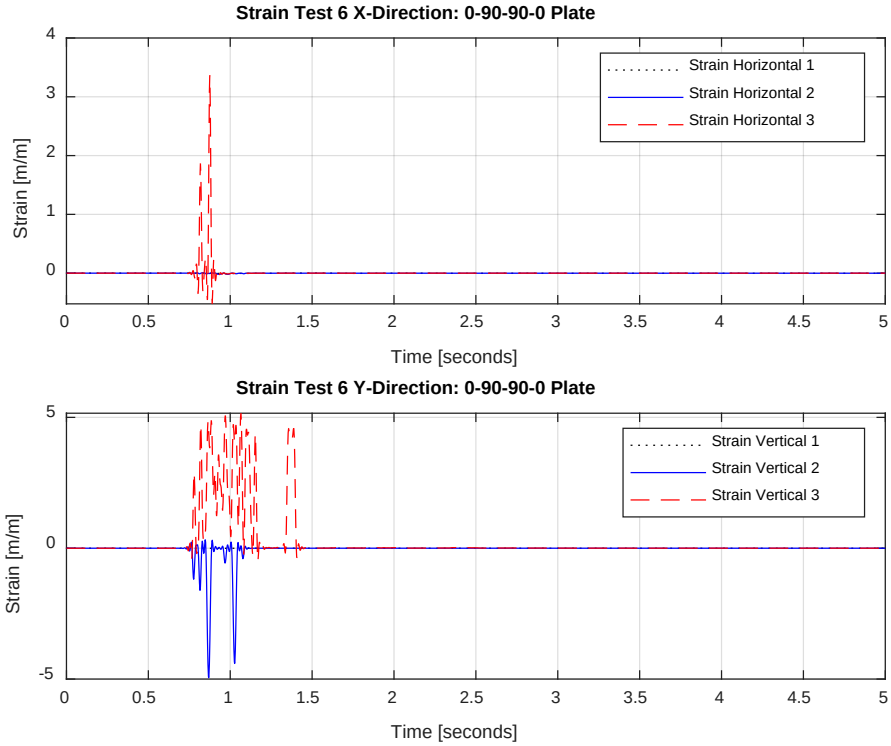

Figure 161. Sample 4 strain 6th blast

LIST OF REFERENCES

[1] *Shock Hardening of Surface Ships*, OPNAVINST 9072.2, Department of the Navy, Washington, DC, USA, 1987.

[2] G.J. Ohara, "Background for mechanical shock design of surface ships," Naval Research Laboratory, Washington, DC, 1965.

[3] A.P. Mouritz, E. Gellert, P. Burchill, K. Challis, Review of Advanced Composite Structures for Naval Ships and Submarines, *Composite Structures*, vol. 53, pp. 21–42, 2001.

[4] D. Middleton, *Composite Materials in Aircraft Structures*. U.K.: Longman Group, 1990.

[5] L.H. Strait, M.L. Karasek, and M.F. Amateau, "Effects of stacking sequence on the impact resistance of carbon fiber reinforced thermoplastic toughened epoxy laminates," *Journal of Composite Materials*, vol. 26, no. 12, pp. 1725–1740, 1992.

[6] DragonPlate Composite Manufacturer, "What is carbon fiber?" [Online]. Available: www.dragonplate.com/what-is-carbon-fiber.

[7] K. Galanis, "Hull construction with composite materials for ships over 100 m in length," M.S. thesis, Dept. of Ocean Eng., Massachusetts Institute of Technology, Cambridge, MA, 2002.

[8] Dexcraft Carbon Fiber Composites, "Aluminum vs carbon fiber-comparison of materials," [Online]. Available: www.dexcraft.com/articles/carbon-fiber-composites/aluminium-vs-carbon-fiber-comparison-of-materials.

[9] PCB Piezotronics MTS Company, "Tourmalin underwater blast." Accessed September 15, 2020. [Online]. Available: https://www.pcb.com/sensors-for-test-measurement/pressure-transducers/blast-transducers/tourmaline-underwater-blast

[10] S. Mannan, *Lees' Loss Prevention in the Prcoess Industries: Hazard Identification, Assessment and Control*. Kidlington, Oxford, UK: Elsevier Inc., 2012.

[11] S. Wang and A. Zhang, "Bubble dynamics and its applications," Journal of *Hydrodynamics*, vol. 30, pp. 975–991, Nov. 23, 2018.

[12] Y. Kwon, private communication, Nov. 2020.

THIS PAGE INTENTIONALLY LEFT BLANK

INITIAL DISTRIBUTION LIST

1. Defense Technical Information Center
   Ft. Belvoir, Virginia

2. Dudley Knox Library
   Naval Postgraduate School
   Monterey, California